Phytoavailability, Mobility, and Solid-phase Speciation of Antimony (Sb) and Lead (Pb) in Brunisolic Soils Surrounding a Pb-Zn Smelting Complex, Trail, British Columbia, Canada

by

Jaime Nicole Caplette

A thesis submitted in partial fulfillment
of the requirements for the degree of
Master of Science (MSc) in Geology

The Faculty of Graduate Studies
Laurentian University
Sudbury, Ontario, Canada

THESIS DEFENCE COMMITTEE/COMITÉ DE SOUTENANCE DE THÈSE
Laurentian Université/Université Laurentienne
Faculty of Graduate Studies/Faculté des études supérieures

Title of Thesis Titre de la thèse	Phytoavailability, Mobility, and Solid-phase Speciation of Antimony (Sb) and Lead (Pb) in Brunisolic Soils Surrounding a Pb-Zn Smelting Complex, Trail, British Columbia, Canada
Name of Candidate Nom du candidat	Caplette, Jaime
Degree Diplôme	Master of Science
Department/Program Département/Programme	Geology
Date of Defence Date de la soutenance	January 13, 2017

APPROVED/APPROUVÉ

Thesis Examiners/Examinateurs de thèse:

Dr. Graeme Spiers
(Supervisor/Directeur(trice) de thèse)

Dr. Nelson Belzile
(Committee member/Membre du comité)

Dr. Murray McBride
(External Examiner/Examinateur externe)

Approved for the Faculty of Graduate Studies
Approuvé pour la Faculté des études supérieures
Dr. David Lesbarrères
Monsieur David Lesbarrères
Dean, Faculty of Graduate Studies
Doyen, Faculté des études supérieures

ACCESSIBILITY CLAUSE AND PERMISSION TO USE

I, **Jaime Caplette**, hereby grant to Laurentian University and/or its agents the non-exclusive license to archive and make accessible my thesis, dissertation, or project report in whole or in part in all forms of media, now or for the duration of my copyright ownership. I retain all other ownership rights to the copyright of the thesis, dissertation or project report. I also reserve the right to use in future works (such as articles or books) all or part of this thesis, dissertation, or project report. I further agree that permission for copying of this thesis in any manner, in whole or in part, for scholarly purposes may be granted by the professor or professors who supervised my thesis work or, in their absence, by the Head of the Department in which my thesis work was done. It is understood that any copying or publication or use of this thesis or parts thereof for financial gain shall not be allowed without my written permission. It is also understood that this copy is being made available in this form by the authority of the copyright owner solely for the purpose of private study and research and may not be copied or reproduced except as permitted by the copyright laws without written authority from the copyright owner.

Abstract

Smelting activities in the Trail, British Columbia region since the late 1890's has emitted metal(loid) contamination in the region (Pb, Zn, Cu, As, and Cd). The objective of this study was to determine the potential availability, mobility and operationally defined speciation of Sb and Pb in contaminated soils. Total Sb and Pb are strongly enriched in surface horizons in the profile (maximum of 737 and 26 376 mg kg^{-1}), with concentrations decreasing with depth. Sequential extractions on soils indicate an enrichment of Sb in the operationally-defined residual > reducible > oxidizable > easily extractable fractions (< below detection limits), whereas Pb shows residual > oxidizable > reducible > easily extractable fractions. Electron optical and microchemical analysis of selected magnetic grains from LFH horizons indicate the anthropogenically derived Sb- and Pb particles to be present as discrete oxide- and sulfide/sulfate particles. The mineralogical and morphological nature of Sb- and Pb- particulate matter is diverse, ranging from angular massive Sn- bearing Sb- Pb oxides, euhedral and subrounded Sb-oxides, and Pb-sulfides and sulfates. These results indicate that, although soils are highly enriched in Sb and Pb relative to soil quality guidelines, minimal biological uptake and mobility should exist for both elements.

Key Words: Trail, British Columbia, Antimony, Lead, Smelter, Emissions, Sequential extraction, Soils, Mobile, Phytoavailable, Rosiaite, Anglesite, metal oxide

Acknowledgements

I would like to start by thanking my supervisor, Dr. Graeme Spiers, for his patience, guidance, friendship, and passing-on of knowledge throughout the last 1.5 years. It's been quite an uphill battle, but I honestly cannot express my gratitude enough for helping me become the independent, "stubborn" researcher I am today. Thank you! Thank you for the support throughout the year(s) and helping me to find my passion and realize that soils are, in fact, very important.

Next, I would like to thank my committee member Dr. Nelson Belzile and external reviewer Dr. Murray McBride for their very helpful insight and comments with this thesis. I would like to thank Mark Tinholt at Teck Resources for his assistance with sampling in Trail and very helpful constructive input and feedback on this research. Additionally, a "whole-hearted" thank you to researchers and technicians who have worked endless, tiresome hours to help me accomplish my goals throughout the years, their mentorship and friendship. Thank you, Dr. Matt Leybourne for your support with my degree, conferences, input on grant applications and abstracts, and mentorship. Thank you, Dr. William Zhe at CAF for being a friend and a very helpful researcher. Thank you, Troy Maki, at ELRFS for being a great mentor and friend. Lizane Pamer and John Hechler at the GeoLabs for working so hard to be able to give me data on time for conferences, I know this was a pain but thank you! Thank you Cyndy Desjardins at LWL for training me on the TOC, your patience and guidance with the instrument. I would like to thank the students who volunteered their time to help me do analysis in the lab: Andrew Hall, Serge Levesque, Anna Beckett, and Emilia Principe.

Lastly, I am so lucky to have the support system that I have had through this degree. I'd like to

thank my cheerleading team who have shared my triumphs and sorrows throughout this degree with me and have always constantly reminded me of the finish line when things were hard. I couldn't have made it throughout without the love and support from my dad (thank you!!), grandfather (thank you!!), MJ, JJ, AF, CL, HC, SD, MD, HB, NN, VG, and SL (thank-you for answering all my "silly" chemistry questions!).

Table of Contents

List of Tables

List of Figures

List of Appendices

Chapter 1

1.0 Introduction

Trail, British Columbia, is located in the Southern Kootenay Mountains in the Columbia River Valley bounded by the Moonashee Mountains to the west and the Selkirk Mountains to the east (Goodarzi et al. 2001a, 2001b, 2002a, 2002c, 2003, Abollino et al. 2003, Agg 2004, Sanei et al. 2007). The inter-montane region is dominated by a mildly continental climate and mean annual temperature of 8.1ºC, with common droughts during the summer months (Archibold 1978, Goodarzi et al. 2001a, 2001b, 2002a, 2002c, Abollino et al. 2003, Agg 2004, Sanei et al. 2007). The prevailing wind direction in the region is north-northwest and south-southeast and is strongly controlled locally by the approximate north-south orientation of the Columbia River (Goodarzi et al. 2003). The Columbia River Valley controls the dispersion of smelter emissions (Goodarzi et al. 2003).

Vegetation in the region is controlled by elevation with lower elevations being dominated by mixed dry coniferous forest (ponderosa pine, lodgepole pine, douglas fir, and western larch) and higher elevations by coniferous species (western red cedar, western hemlock, white spruce, and balsam fir) (Agg 2004).

The exploitation of ore deposits discovered in the Rossland area led to the construction of a smelter in Trail in 1896, initially designed for copper-gold recovery, and then later expanded in 1905 to produce lead and zinc (Goodarzi et al. 2001a, 2001b, 2002a, 2002c, 2003, Abollino et al. 2003, Sanei et al. 2007). Currently, the Trail smelting complex produces elemental lead, zinc,

cadmium, silver, gold, bismuth, indium, germanium, copper and sulfur, and manufactured products including fertilizers, sulphuric acid, liquid SO_2 (blackening agent in the pulp and paper industry), and other compounds such as copper (copper sulfate, copper arsenate, and sodium antimonate) and ferrous granules (product-grade furnace slag) (Goodarzi et al. 2001a, 2001b, 2002a, 2002c, 2003, Abollino et al. 2003, Agg 2004, Sanei et al. 2007).

The sulfur dioxide emissions between 1926 to 1930 exceeded 1.1×10^5 t $year^{-1}$ and caused extensive damage to the vegetation and soils in the region (Archibold 1978, Fox and Tarnocai 2011). Prior to the 1930's, the southern region of Trail has sparse vegetation, soils were eroded, and landscapes were defined by sand dunes (Archibold 1978). With a lack of vegetation cover in the region caused by a combination of extensive logging, fires, and SO_2 emissions, soils of the landscapes south of the Trail smelter were occupied by immature Regosols with Ah/C horizons in the late 1970's (Archibold 1978, Agg 2004).

Reclamation activities post 1950's included the use of fertilizer and lime, tree planting, with associated planting of native and non-native grasses (Agg 2004). Terrestrial Environmental Risk Assessments showed regions impacted by SO_2 and metal emissions have low biodiversity, but will likely equilibrate with time, although some areas may require remedial intervention (Agg 2004). Monitoring of aquatic species such as periphyton and invertebrates indicated increasing biodiversity, with numbers of species sensitive to metals increasing in importance in the Columbia River and tributaries (Agg 2004).

Chapter 2

2.0 Study Region Background

2.1 Previous Studies in the Region

Extensive work was done in the Trail, British Columbia region by the Geological Survey of Canada Metals in the Environment Project (GSC-MITE) to evaluate the extent and impact of regional deposition and accumulation of trace elements in the surficial soils surrounding the Teck-Cominco smelter, with the use of moss bags as active monitoring stations (Goodarzi et al. 2001a, 2001b, 2002b, 2002c, 2003, Sanei et al. 2007). The two-year long study reported a high concentration of trace elements in surface soils, a decrease in trace element distribution with distance from the smelter, and showed trace element concentration to be strongly influenced by meteorological controls, physiography of the region and smelting activities (Goodarzi et al. 2001a).

The studies concluded secondary sources of metal(loid)s are of concern, and are the major contributor to Pb and Zn levels observed in the region (Goodarzi et al. 2001a, 2002b, 2003). The chemistry and mineralogy of Pb and Zn particles evaluated using SEM-EDS collected with the moss monitoring stations was shown to consist of angular fragments of sulfide ore (ZnS (potentially sphalerite)) provenance, and fine subangular to rounded, “fluffy” particles with a chemical composition of PbO, suggesting potential oxidation, and is consistent with smelter-derived compounds (Goodarzi et al. 2001a). Strong correlations between Pb, Zn, Cd and Cu deposition rates at moss monitoring stations and total soil concentrations indicate that these elements are airborne derived, whereas weak correlations between As and Hg suggest a probable

geogenic source of these metal(loid)s (Goodarzi et al. 2001a, 2002b). Lynch et al. (1980) assessed the association of airborne particulate matter and soil metal concentrations adjacent to the Trail smelter and concluded that airborne particulate matter was enriched in smelter-derived Pb, Zn, Cu, Cd, As and Sb relative to soil total-metal concentrations.

In 2002, the Trail Ecological Risk Study Team, conjoined with Technical and Public Advisory committees conducted a Risk Assessment to determine the impact of previous, present, and potential future smelting emissions on human and ecological health (Agg 2004). The study region was a 800 km^2 region including the entire Columbia River Valley, from the international boundary 15 km south of Trail to Mt. Sentinel and Ladybird Mountain north of Castlegar with the region being subsequently decreased after further evaluation based on elevated metal concentrations (Agg 2004). The ERA evaluated three groups of elements based on: chemical concentrations within environmental media measured in the study region (soil, air and water), chemical distributions associated with the smelter operations, and potential chemical toxicity. The ERA focus emphasized probable smelter-derived metal(loid)s, with 17 chemicals of concern in the soil environment: Sb, As, Ba, Be, Cd, Cr, Co, Cu, F, Hg Se, S, Th, Sn and Zn (Agg 2004). Twelve (12) chemicals of concern were identified in regional waters: As, Cd, Cr, Co, Cu, Pb, Hg, Se, Ag, Th, and Zn (Agg 2004). Nine (9) chemicals of concern were identified in sediments: As, Cd, Cr, Cu, Pb, Ni, Ag, Th, and Zn (Agg 2004). The selection of chemicals of concern was based on their enrichment relative to natural geogenic background levels as a consequence of regional emission zonation from the smelter complex. Antimony (Sb) was eliminated from the study based on modelled assessment of risk to wildlife, and potential to be present as Sb (V) in the natural environment (Agg 2004). The remaining metal(loid)s: As, Cd, Cu, Pb, Hg, and Zn

were evaluated (Agg 2004). Results of the study indicated that several terrestrial and aquatic species, including mammals such as river otters and shrews, benthic invertebrates and algae could be at risk (Agg 2004, Swanson 2007).

In 1975, Schmitt et al. (1979) discovered elevated blood Pb (PbB) levels in the blood of children. Lead levels as high as 22 μL dL^{-1} in children 1-3 years old in 1975 were measured (Schmitt et al. 1979, Hilts et al. 1998). The average for PbB in the late 1980's was 13 μL dL^{-1} for children 2–3 years old, with almost 40% of children being above the Canadian guidelines of 15 μL dL^{-1} (Hilts et al. 1998). The average PbB levels in the average pre-school aged child has decreased from 13 μL dL^{-1} in 1989 to 6 μL dL^{-1} more recently (Agg 2004). The implementation of the Trail Lead Task Force, educational programs, annual blood testing, research and community dust abatement programs have helped to significantly reduce the PbB levels in children (Hilts et al. 1998). Given the results of these human and environmental studies, the smelting complex has been equipped with electrostatic precipitators, scrub houses, and baghouses since the 1990's (Goodarzi et al. 2001a, 2001b, 2002a, 2002c, 2003).

2.2 Regional Geology

The well drained soils formed at lower valley elevations in the Columbia River valley have a relatively low organic matter content, and are dominated by sand and gravel textures, with higher elevations being dominated by clayey glacial tills (Agg 2004). The geology in Trail, B.C. is complex and consists of rock units of varying origin and ages ranging from surficial Pleistocene glacial sediments to Upper Jurassic to Lower Cretaceous plutonic rocks (the Nelson Intrusives

and Rossland Monzonite), Lower Jurassic metavolcanic and metasedimentary rocks (Elise Formation), upper Paleozoic sedimentary (Pennsylvanian) and metasedimentary rocks (Mount Roberts Formation) and the pre-Pennsylvanian Trail Gneiss (Simony 1979, Little 1982, Goodarzi et al. 2003, Simony et al. 2006).

The majority of the city area is over the lacolithic Trail Pluton, consisting of the Upper Jurassic Nelson Intrusives (Bonnington and Nelson Plutons) (Little 1982, Goodarzi et al. 2003). The Trail Pluton is dominated by granodiorite, quartz diorite, diorite, gabbro, and granitic rocks (Little 1982, Goodarzi et al. 2003). The Bonnington Pluton is composed of quartz gabbro to granite and potassic tonalite to granodiorite (Goodarzi et al. 2003). The Rossland Monzonite has been relatively dated older than the Late Jurassic and is composed of andesine, hornblende, orthoclase, augite, biotite, and quartz (Goodarzi et al. 2003). The Elise Formation is characterized by dominantly volcanic and pyroclastic rocks (flow breccia, volcanic breccia, tuffs, tuffaceous conglomerate, andesite, basalt and augite porphyry metamorphosed to greenschist facies) (Goodarzi et al. 2003). The Mount Roberts Formation consists of fine-grained siliciclastic rocks, argillite, carbonate and minor greenstone which are Pennsylvanian – Permian in age (Little 1982, Hoy and Andrew 1991, Goodarzi et al. 2003). The Trail Gneiss is composed of hornblende gneiss, granodioritic gneiss, folded aplite and pegmatite, massive pegmatite, quartzofeldspatic mica schist, and amphibolite and garnet mica schist, and marble (Goodarzi et al. 2003).

Molybdenum skarn and porphyry deposits exist at the margins of the Trail Pluton (Goodarzi et al. 2003). The Rossland Monzonite is known to host vein gold deposits (Goodarzi et al. 2003). The Elise Formation hosts the majority of the gold and copper deposits (pyrrhotite and chalcopyrite) in Rossland (Hoy and Andrew 1991, Goodarzi et al. 2003). Lead, zinc, and silver vein deposits are

also hosted in the Elise and Hall Formation contact, containing a mineral suite consisting of sphalerite, galena, arsenopyrite, pyrite, chalcopyrite and boulangerite (Goodarzi et al. 2003).

Chapter 3

3.0 Background on Antimony and Lead and Sequential Extraction Procedures at Contaminated sites

3.1 Antimony Uses, Characteristics, Toxicity, and Behaviour

Antimony, atomic number 51, is a metalloid in group 15 with atomic number 51 and is silvery white in colour (Sundar and Chakravarty 2010, Fu et al. 2016a). Naturally occurring in the environment, Sb ranges in abundance of 2 - 0.2 mg kg^{-1}, 8.4 - 0.3 mg kg^{-1}, and less than 0.1 µg L^{-1} in crustal, soil and aqueous environments, respectively (Filella et al. 2002, Wilson et al. 2010, Fu et al. 2016a). The industrial uses of Sb include the production of semiconductors, infrared detectors and diodes. Antimony is commonly blended with other metals in ammunition and explosives, lead storage batteries, solder, sheet and pipe metals, castings and pewter, also used as a fire retardant, and in medicines for parasitic diseases (Sundar and Chakravarty 2010, Wilson et al. 2010, Fu et al. 2016a). Mine production of antimony in the past 20 years is approximately 128 000 tonnes (Fu et al. 2016a), with the largest suppliers being China, India, and Mexico with 73, 11 and 5% of the global production of Sb, respectively.

With no known essential biological function, Sb has been shown to be a potential carcinogen, to cause respiratory issues such as pneumoconiosis, and to be a genotoxin (Sundar and Chakravarty 2010, Álvarez-Ayuso et al. 2013). Antimony is considered a priority pollutant of interest by the United States Environmental Protection Agency (USEPA) and European Union (EU) (Fu et al.

2016a). Canadian soil quality guidelines suggest antimony concentrations should be below 20 mg kg^{-1} in soils surrounding residential and parkland areas (Canadian Council of Ministers of the Environment 1998). Antimony has 4 valence states: 3^-, 0, 3^+, and 5^+, with the most common valence states in the environmental media being 3^+ and 5^+ (Wilson et al. 2010, Fu et al. 2016b). Antimony speciation is strongly dependent on oxidation and pH conditions in soils (Mitsunobu et al. 2006, Filella et al. 2009b, Wilson et al. 2010), and organoantimony species are generally considered less toxic than inorganic species following the order of: organoantimonals < antimonates (Sb(V)) < antimonites (Sb(III)) (Filella et al. 2002, Wilson et al. 2010). Differences in speciation and geometry of Sb causes variances in mobility and toxicity in the environment (Filella et al. 2002, Wilson et al. 2010).

Industrially impacted soils in Scotland and Italy demonstrated the association of Sb with the crystalline Fe-oxide and Al-silicate extractable fractions, with a lack of association with the bioavailable fraction (Gál et al. 2006). The Xikuangshan mine region in China had an average of 1315 mg kg^{-1} Sb in soils, with the bioaccumulation of Sb in organisms and plants being positively correlated with pH (Fu et al. 2016a). Antimony has been shown to be dominated by Sb(V) species (Wilson et al. 2004, 2010, Mitsunobu et al. 2006, Fu et al. 2016b) and strongly associated as inner-sphere complexes on Fe-oxyhydroxide surface functional groups in shooting range impacted soils (Scheinost et al. 2006) and tailings sediments (Okkenhaug et al. 2011, Fu et al. 2016b). Ferrihydrite and hydrous Al-oxide amendments added to soils were shown to be effective at reducing Sb leaching from soil horizons (Álvarez-Ayuso et al. 2013). Adsorption mechanisms for ferrihydrite were dominated by corner and edge sharing complexes, whereas

amorphous Al-oxides were shown to be dominated by both corner sharing and minor monodentate complexes (Álvarez-Ayuso et al. 2013).

3.2 Antimony Speciation as a Function of Reduction – Oxidation Potential and pH

Simplified Sb-O-H Pourbaix diagrams suggest Sb is present as an octahedrally coordinated *[6]* antimonate anion ($Sb(OH)_6^-$) under both acidic oxidizing conditions and moderately reducing alkaline conditions (Takeno 2005) (Figure 1). The Sb (III), antimonous acid ($Sb(OH)_3$). species is suggested to be dominant under moderately oxidizing acidic conditions to moderately reducing alkaline conditions (Takeno 2005) (Figure 1). Moderately reducing to highly reducing acidic and alkaline conditions, respectively, suggest the presence of metallic Sb species may be possible (Takeno 2005) (Figure 1).

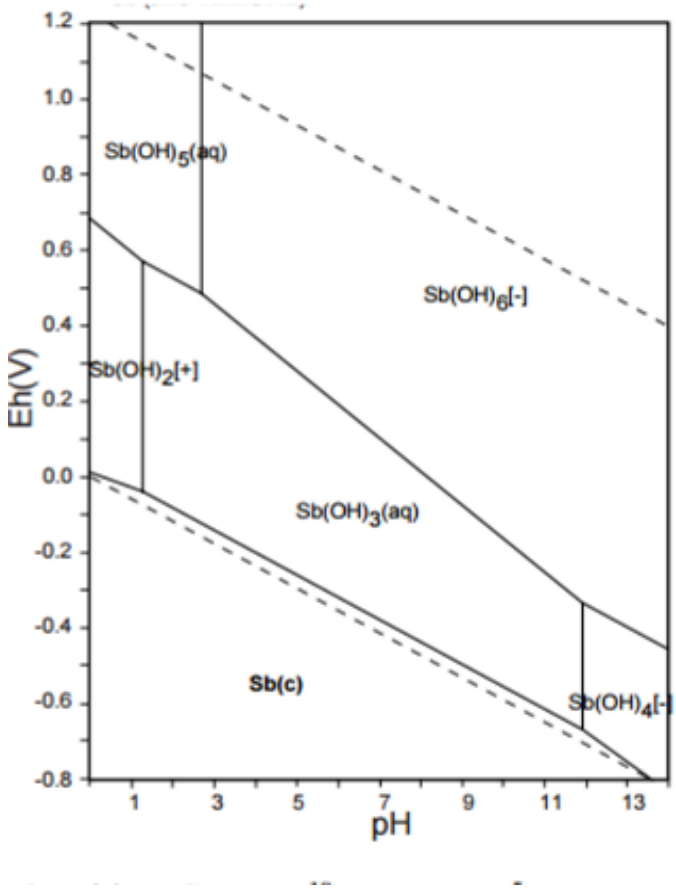

Figure 1. A Pourbaix diagram of a simplified Sb – H_2O system, where $\sum Sb = 10^{-10}$, 298.15 K, and 10^5 Pa (modified from (Takeno 2005)).

In systems containing sulfur, Sb is dominantly present in highly oxidizing reducing and alkaline conditions as an anionic pentavalent aqueous Sb oxide species (SbO_3^-), whereas under oxidizing acidic to moderately reducing alkaline conditions Sb is present as trivalent oxide species (senarmontite or valentinite, Sb_2O_3) (Vink 1996) (Figure 2). Under reducing-acidic conditions stibnite (Sb_2S_3) may be present, and under alkaline-reducing conditions an aqueous anionic

$Sb_2S_4^{2-}$ ligand may be present (Vink 1996). Metallic Sb may be present under highly reducing conditions (Vink 1996).

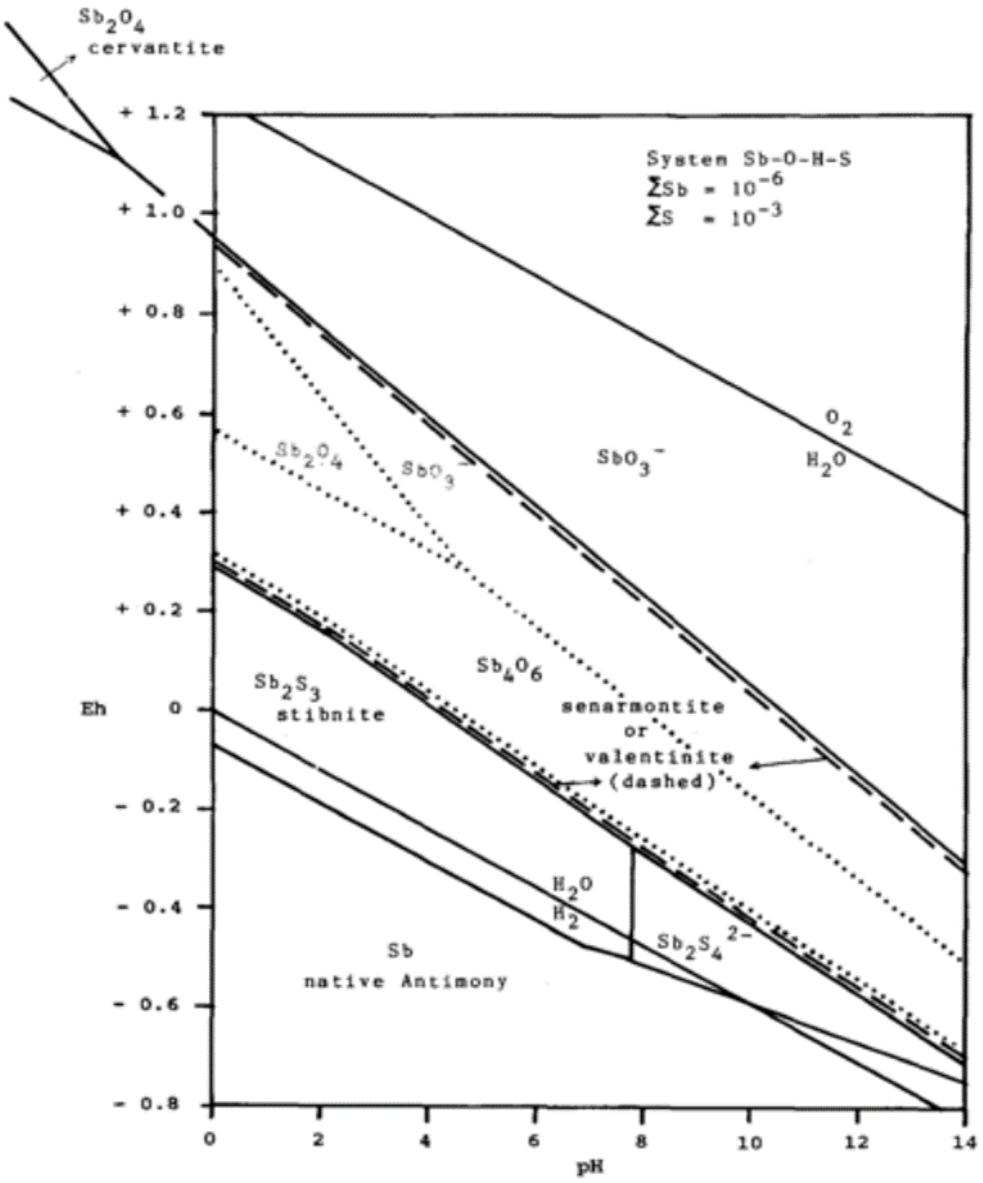

Figure 2. A Pourbaix diagram for the Sb – O – H – S system (modified from Vink 1996). Activities of ∑Sb = 10^{-6} m, and ∑S = 10^{-3} m.

3.3 Dominant Primary and Secondary Antimony Minerals

Antimony mineralogy is diverse, with over 200 documented mineral phases (Wilson et al. 2010, Roper et al. 2012). Antimony can be present as sulfosalts, sulfides, refractory oxides and silicate phases, with the most common being the tetrahedrite – tennantite series ($Cu_{12}Sb_4S_{13}$ – $Cu_{12}As_4S_{13}$), stibnite Sb_2S_3, and senarmontite (Sb_2O_3) (Wilson et al. 2004, Abdullah et al. 2008, Klimko et al. 2011, Roper et al. 2012). The most common refractory Sb oxide phases include: oxycalcioroméite ($Ca_2Sb_2O_7$), triphuyite ($FeSbO_4$), and bitikleite group minerals (e.g., $Ca_3SbSn(AlO_4)_3$) (Courtin-Nomade et al. 2012, Leverett et al. 2012, Roper et al. 2012). The latter two minerals are also found as secondary minerals surrounding Sb and Pb mines. The sulfide and sulfosalt minerals, unstable in oxidizing environments, react to form relatively soluble secondary minerals which oxidize to form oxides and follow the sequence from: stibnite → kermesite (Sb_2S_2O) → senarmontite/valentinite → cervantite (Sb_2O_4) → roméite group minerals (Roper et al. 2012). Roméite group minerals have the generalized mineral formula of $A_{2-m}B_2X_{6-w}Y_{1-n} \cdot pH_2O$ where *A* = predominately mono- and divalent cations, Ca^{2+}, Na^{+}, Ba^{2+}, Bi^{2+}, Pb^{2+}, trivalent cations (REE's and Sb^{3+}), and the tetravalent cations Zr^{4}+ and Th^{4+} (Brugger et al. 1997). The *B* site is dominantly occupied by pentavalent cations such as: Nb^{5+}, Ta^{5+}, Sb^{5+}, W^{5+}, trivalent cations including Al^{3+} and Fe^{3+}, and Ti^{4+} (Brugger et al. 1997). The *X* site is dominantly O, OH^{-} or F^{-}, and *Y* is O^{2-}, OH^{-}, F^{-} and alkali metals such as K^{+}, Rb^{+}, and Cs^{+} (Brugger et al. 1997). The common end-members of the group are hydroxycalcioroméite ($CaSb_2O_5(OH)_2$), oxycalcioroméite ($Ca_2Sb_2O_7$), and oxyplumboroméite ($Pb_2Sb_2O_7$) (Roper et al. 2012).

Under oxidizing conditions, as found in supergene environments, Sb appears to be dominated by immobile tripuhyite ($FeSbO_4$) and schafarzikite ($FeSb_2O_4$) (Mitsunobu et al. 2011, Courtin-Nomade et al. 2012, Leverett et al. 2012, Roper et al. 2015). Leverett et al. (2012) showed even under acidic conditions that these oxide phases are extremely insoluble, and can react at very low activities with goethite to form tripuhyite, which is acting as an important sink for Sb in the natural environment. Some authors have recognized the presence of nano-sized domains of tripuhyite in Fe-(oxyhydr)oxides (Mitsunobu et al. 2011, Courtin-Nomade et al. 2012, Leverett et al. 2012). Under acidic conditions, Fe^{2+} cations can be liberated with tripuhyite, decomposing to form senarmontite (Sb_2O_3) (Leverett et al. 2012). Three polymorphs of Sb_2O_3 exist, senarmontite (thermodynamically stable at 298.15 K) and valentinite which are cubic and orthorhombic, respectively, and an orthorhombic high-temperature polymorph, γ-Sb_2O_3 (Roper et al. 2012). Antimony (V) has also been observed to substitute in the jarosite ($KFe_3(SO4)_2(OH)_6$) mineral structure in tailings materials, likely on the octahedral site for Fe(III) (Courtin-Nomade et al. 2012). Roméite group minerals also appear to be an important sink for Sb in the environment (Scheinost et al. 2006, Filella et al. 2009b, Okkenhaug et al. 2011, Ettler et al. 2012, Roper et al. 2012, 2015).

3.4 Pb Toxicity and Behaviour in Soils

Lead, a group 14 element, is not known play any essential role in biological functions, and is considered a priority pollutant of interest by the USEPA (Magrisso et al. 2009). The effect of Pb on cognitive and neurological behaviour is of paramount concern in infants and young children (Goyer 1993, Hilts et al. 1998). Elevated levels lead to neurotoxicity, anemia, renal damage, and

can be fatal, for example, Pb can inhibit enzymatic processes responsible for heme synthesis (Barbosa et al. 2005). Lead can enter the body through a variety of pathways depending on the source materials, and, in turn, bioavailability (Barbosa et al. 2005). The amount of Pb absorbed by the human body is a function of both chemical and physical form, being controlled predominately by species solubility and particle size (Barbosa et al. 2005). The United States Centers for Disease Control and Prevention and the World Health Organization define a PbB value of 10 µg dL^{-1} as the threshold in young children (Hilts et al. 1998, Barbosa et al. 2005).

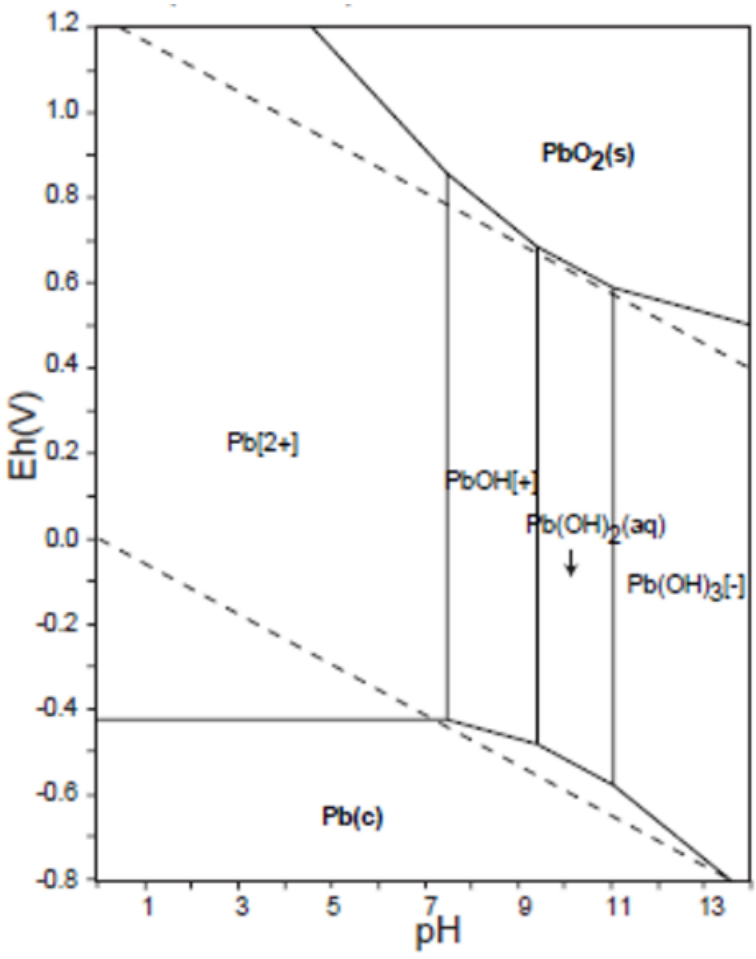

Figure 3. A simplified Pb-H_2O Pourbaix diagram for ∑Pb 10^{-10}, 298.15 K, and 10^5 Pa. Modified from (Takeno 2005).

The revised Eh – pH diagrams by Takeno (2005) suggest that in simplified Pb – H – O systems, the dominant Pb species in reducing to oxidizing, neutral and acidic environments is the Pb^{2+} cation (Figure 3). In highly reducing environments metallic Pb may be present, and in highly oxidizing acidic to basic environments the $Pb^{4+}O_{2(s)}$ species may be dominant (Figure 3). From a pH range of 7 – 9, in moderately reducing to oxidizing environments Pb is may be present as a $PbOH^{+}$ species (Figure 3). From pH 9 – 11, a $Pb(OH)_{2(aq)}$ species may be dominant, with $Pb(OH)_3^{-}$ possibly being dominant in the >11 pH in both reducing and oxidizing conditions (Figure 3).

Lead occurs in low abundances naturally in the environment, with average abundance of Pb in the earth being 15 mg kg^{-1}, ranging from 30 – 10 mg kg^{-1} in crustal materials and 67 – 10 mg kg^{-1} in soils (Patterson 1971). Anthropogenic activities such as mining and smelting activities, release of Pb-gasoline bi-products, dusts and/or breakdown of ammunition at shooting ranges, and emissions from battery processing plants, can strongly increase the concentration of Pb in the local environment (Patterson 1971, Zimdahl and Skogerboe 1977, Lin et al. 1995, Manceau et al. 1996, Ettler et al. 2001, 2005a, 2005b, Vitkova et al. 2009, Sanderson et al. 2010). The most common lead ore mineral is galena, PbS, which is commonly oxidized to anglesite ($PbSO_4$) in acidic conditions (Patterson 1971, Vitkova et al. 2009). At pH levels above 6 the mineral cerussite ($PbCO_3$) can commonly be present (Patterson 1971, Vitkova et al. 2009). Lead sulfates, oxides and silicates have been observed to be emitted from smelting processes (Ettler et al. 2001, 2005b, Goodarzi et al. 2003, Vitkova et al. 2009, Caplette et al. 2015). In neutral to mildly alkaline soils the solubility of Pb is low, being controlled by the presence of oxides, hydroxides,

carbonates and phosphates with any soluble Pb being strongly bound to organic matter and iron oxides (Hettiarachchi and Pierzynski 2004, Tai et al. 2013).

Lead has been observed to be complexed to salicylate and catechol-type functional groups on the surface of humic substances, to be associated with lead sulfates and silicate minerals in soils surrounding a battery reclamation facility, and to be present as divalent Pb with ligands (OH, O) surrounding smelting facilities (Manceau et al. 1996). In forested soils, Pb has been shown to have a strong affinity for the operationally-defined oxidizable organic matter fraction, whereas in cultivated soils Pb has been shown to 'prefer' operationally-defined reducible phases (e.g., hydrous Fe-oxides) (Ettler et al. 2007). Lead has also been shown to form stable, inner-sphere complexes with hydrous Fe- and Mn- oxides (Ettler et al. 2005b).

3.5 Uses of Sequential Extraction Procedures at Contaminated Sites

Sequential extraction procedures (SEP) have been used on environmental media (i.e., soils, sediments and sludges) to gain an understanding of operationally defined phase associations at contaminated sites (Tessier et al. 1979, Hall et al. 1996a, Rauret et al. 1999, Gleyzes et al. 2002, Bacon and Davidson 2008, Zimmerman and Weindorf 2010, Abedin et al. 2012, Tai et al. 2013). The extraction solutions enable an evaluation of the potential "phases" that metal(loid)s could be associated with in the medium, and enable a prediction of environmental conditions that could potentially induce liberation of these metal(loid)s of concern (Tessier et al. 1979, Maiz et al. 1997, Rauret et al. 1999, Gleyzes et al. 2002, Zimmerman and Weindorf 2010). Sequential extractions are chemical dissolution procedures applied to environmental matrices in order of

increasing strength to evaluate the most common operationally-defined fractions of metal(loid)s are associated with, ranging in availability or bonding strength from the labile and exchangeable fractions, acid soluble (carbonate bound), reducible (hydrous oxide bound), oxidizable (bound to organic matter and sulfides), and residual fraction (strong acid digestion) (Tessier et al. 1979, Hall et al. 1996a, Rauret et al. 1999, Gleyzes et al. 2002, Bacon and Davidson 2008, Zimmerman and Weindorf 2010, Abedin et al. 2012, Tai et al. 2013).

Bioavailable metals are considered the fraction potentially available for human, animal, and plant uptake, that may also cause deleterious effects in organisms (Hettiarachchi and Pierzynski 2004, van Gestel 2008). Additionally, metal bioavailability is dependent on a variety of factors including the physiological properties of the organism, exposure, and uptake pathways to organisms with variations between organisms and specific physiochemical soil properties (van Gestel 2008). Bioavailable and available fractions are evaluated commonly using water as an extractant, or by changing the ionic potential of the solution using a neutral salt (e.g., $CaCl_2$, $LiNO_3$, $MgCl_2$) (Tessier et al. 1979, Hall et al. 1996a, Maiz et al. 1997, Gleyzes et al. 2002, Ryan et al. 2002, Ettler et al. 2007, Zimmerman and Weindorf 2010, Van Vleek et al. 2011, Abedin et al. 2012). Generally, Sb shows very little bioavailability at anthropogenically contaminated sites (Lintschinger et al. 1998, Flynn et al. 2003, Smichowski 2008, Filella et al. 2009a, Van Vleek et al. 2011). Lead bioavailability in the environment tends to be strongly dependent upon the physical nature of the soil, Pb mineralogy and solubility (Hettiarachchi and Pierzynski 2004, Ettler et al. 2005b, Magrisso et al. 2009).

Hydrous oxides of Fe and Mn are well known sinks for trace elements in environmental media, and effectively scavenge metal(loid)s from soil solutions and natural waters (Tessier et al. 1979,

Hall et al. 1996a, Filgueiras et al. 2002, Gleyzes et al. 2002, Zimmerman and Weindorf 2010). Metal sequestration can be controlled by formation of surface coatings or presence of fine discrete particles, and by a combination of the following mechanisms: adsorption, co-precipitation, surface complex formation, ion exchange and/or incorporation structurally into the crystal lattice (Filgueiras et al. 2002). Hydrous oxides composed of oxidized Mn and Fe, or Al have been observed to control solid-phase speciation of Sb in soils through adsorption mechanisms (Lintschinger et al. 1998, Filella et al. 2002, 2009a, Wilson et al. 2010, Hernández-Nataren et al. 2011, Vithanage et al. 2013). The hydrous oxides therefore have the potential to facilitate solubilisation of trace elements through desorption processes and/or dissolution of the host phase (Tessier et al. 1979, Hall et al. 1996a, Rauret et al. 1999, Filgueiras et al. 2002, Zimmerman and Weindorf 2010). Metal(loid)s associated with these fractions require a reducing reagent such as acid oxalate, alkaline citrate dithionite, or hydroxylamine hydrochloride to reduce the Mn(IV) or Fe(III) phases to cause trace element liberation (Tessier et al. 1979, Hall et al. 1996a, Rauret et al. 1999, Zimmerman and Weindorf 2010).

Amorphous Fe-(oxyhydr)oxides have been shown to be effective soil amendments for the immobilization of Sb in soils (Álvarez-Ayuso et al. 2013). Antimony (V) adsorption in floodplain soils was shown to be strongly associated with amorphous $Fe(OH)_3$ (>95% adsorbed) and less strongly associated with soil humic acids (60%) under acidic conditions (Tighe et al. 2005), and to be negatively correlated with the sand content in the soils (Vithanage et al. 2013). Inner-sphere complexation has been observed with Pb, Sb (III) and (V) on Fe- and Al-(oxyhydr)oxides where Sb species were shown to be dominated by bidentate mononuclear,

mononuclear and binuclear complexation, in addition to multilayer adsorption (Smith 1999, Ettler et al. 2005b, Wilson et al. 2010, Vithanage et al. 2013).

The majority of organic matter in soils and surface waters is assumed to be represented as humic substances, 60 – 70%, and 30 – 50%, respectively (Jones and Bryan 1998). Soil organic matter is relatively stable unless oxidation or decomposition processes occur to potentially liberate large quantities of elements (Filgueiras et al. 2002). Humic substances are large macromolecular assemblies of covalently bonded aromatic and aliphatic residues carrying carboxyl, phenolic and alkoxy groups (Jones and Bryan 1998). Humic substances are believed to be formed in the environment by microbial and plant decay and have a strong ability to aggregate together and present behaviour similar to colloidal materials in the presence of metal cations in acidic environments (Jones and Bryan 1998). Given the heterogeneous nature of humic substances and their associated colloidal aggregation ability, a variety of potential binding sites are present on their surfaces (Jones and Bryan 1998). Humic substances show both pH and ionic strength dependent binding tendencies (Jones and Bryan 1998).

Humic substances have major and minor sites available for metal complexation with the majority of the binding sites composed of carboxylate and phenolate functional groups being weak (Ettler et al. 2005b). Minor sites form strong complexes with metals, being composed of a minority of the functional groups which include a variety of sulfur and nitrogen bearing sites (Ettler et al. 2005b). Under most natural pH ranges, organic matter has a negative charge and has the ability to bind to mineral surfaces which, in turn, changes their affinity for metals (Neagoe et al. 2012). Binding mechanisms are dominated by ligand exchange cation bridging, proton exchange, water bridging, hydrogen bonding, and van der Waals interactions (Neagoe et al. 2012).

Van Vleek et al. (2011) showed the association of Sb with humic acids in shooting range soils to be “tightly bound” in the upper 10 cm of the soil profile, with Dousova et al. (2015) also observing a bonding or complexation preference of Sb relative to As to organic matter in the organic-rich horizons of the soil profile. The preference for Pb to form strong complexes with soil organic matter is well documented, with the majority of Pb in the soil system, namely up to 50% in acidic soils and > 90 % in circumneutral conditions, being as organo-complexes (Sauve et al. 1997, Ettler et al. 2005b, Tai et al. 2013).

The purpose of this current study is to evaluate the association of Sb and Pb in selected Brunisolic pedons surrounding a Pb-Zn smelting complex with varying operationally defined physicochemical species using sequential extraction procedures (SEP) as little is known of Sb solid-phase speciation and toxicity in the soil environment, and Pb poses a potential risk for organisms in the region. The operationally-defined species will shed insight into the potential liberation and risk of Sb and Pb into the soil environment. This study evaluates the potentially phytoavailable, exchangeable, reducible, oxidizable and residual fractions of Sb and Pb in these soils, and uses the association to interpret potential mobility in the local soil environment. Solid-phase analysis using scanning electron microscopy coupled with energy dispersive spectroscopy (SEM-EDS) and powder X-Ray Diffraction (XRD) are also used in conjunction with the SEP results to interpret the origin and mineralogy of specific Sb- and Pb- bearing phases in the sola.

Chapter 4

4.0 Methods

4.1 Soil Field Sampling

Pedons in the Trail, B.C. vicinity at distances of 2 to 6 km from the Teck – Cominco Pb-Zn smelter were selected in June, 2015 following a detailed examination of a series of undisturbed sites with mature vegetation cover within the smelter airshed. The five (5) pedons selected for sampling for this study were all within Trail city limits, at least 50 m from road allowances to ensure minimal contamination from road dust, and formed on stable sites on level glaciofluvial or till terraces within 6 km of the smelter complex (Figure 4). The Brunisolic pedons were excavated to a depth of approximately 1 m to allow detailed pedological descriptions to be completed, with descriptions of pedon horizonation, soil structure, texture, root abundance, and colour obtained.

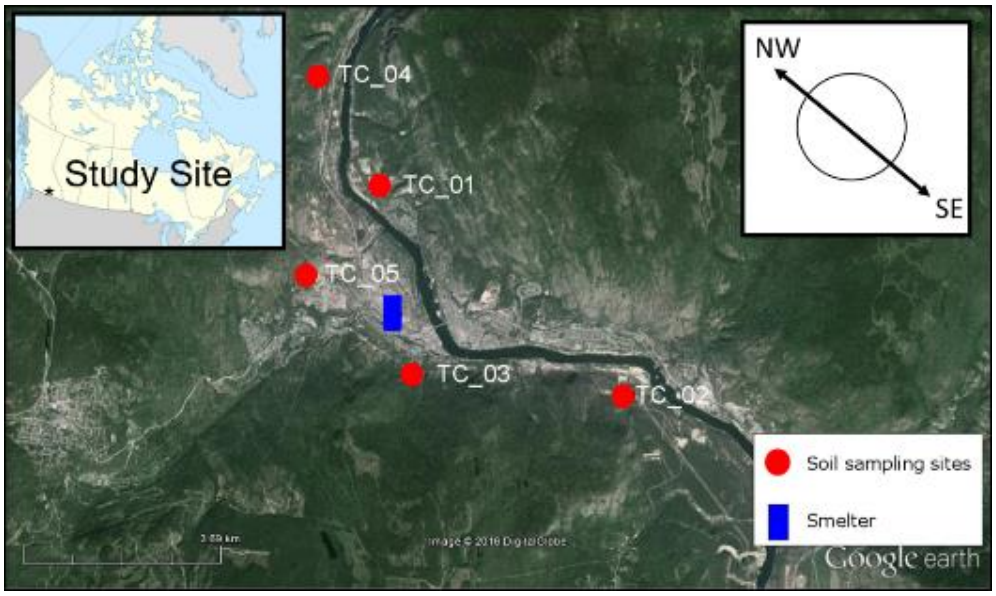

Figure 4. Location of the study region (black star on the map of Canada insert). Pedon sampling sites (2015) are indicated by red dots and the smelter is marked by the blue rectangle. The NNW-SE prevailing wind directions are indicated by the arrows in upper right box of the map

The soil parent material was sampled from the bottom of the soil pit (60 to ~94 cm) using a Dutch auger. The humus forms (LFH horizons) were sampled intact, with the mineral soil being sampled on a depth increment basis (Figure 5a-d). The upper mineral horizons were sampled in 2 cm intervals to the 30-cm depth (Figure 5e). The lower mineral horizons to ~60 cm depths were sampled in 10 cm increments (Figure 5e). Samples were carefully labelled, double bagged, and shipped to Laurentian University for subsequent research analysis.

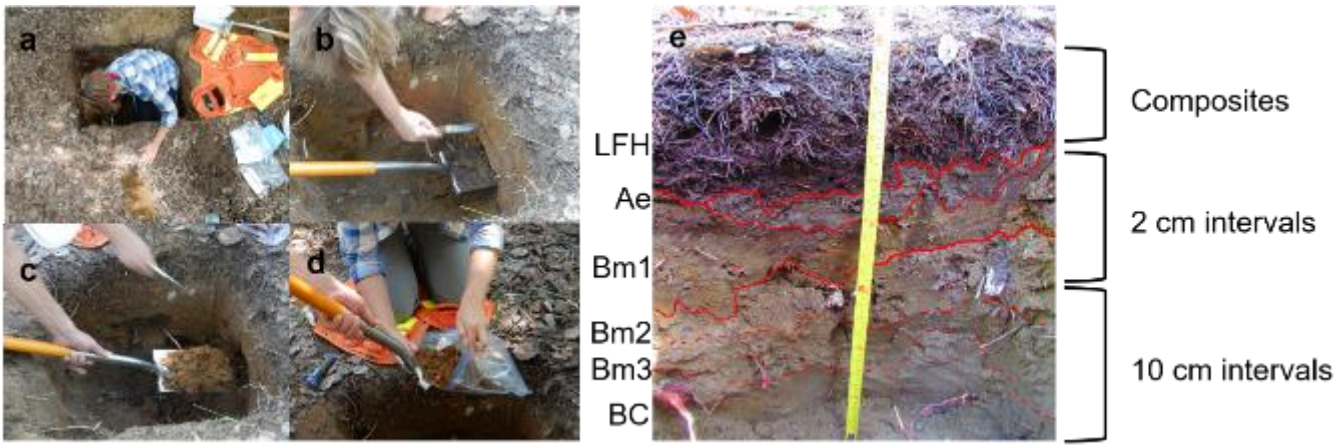

Figure 5. Composite photographs of field sampling protocols for the soil pedons.

4.2 Sample Preparation

All LFH and mineral horizon samples were oven dried at 105ºC for 24 hours and sieved to obtain the < 2 mm fraction prior to storage for further analysis. A 20 g representative split of each sample was ground to pass through a 200 mesh sieve using a ceramic pestle and mortar for further mineralogical and chemical analysis, with the balance of the sample being archived.

4.3 pH, Reduction-Oxidation Potential (Eh), and Conductivity

All pH, reduction-oxidation potential (Eh, mV) and electrical conductivity (µS cm^{-1}) measurements were completed at the Elliot Lake Field Research Station (ELRFS) at Laurentian University. The pH measurements were completed using a calibrated Denver Instrument pH meter, model 215, with soil pH measurements being completed using both a 1:2 and 1:4 soil:solution (m/v) ratio for mineral and organic soil samples, respectively. Soil pH was measured using both ultrapure water and 0.01 M $CaCl_2$, with soils suspensions being stirred intermittently for 30 minutes and then allowed to equilibrate for 30 minutes prior to

measurements. Soil Eh and conductivity measurements were completed on the ultrapure water supernatant using a PerpHecT LogR meter, model 370 and Accumet BASUC AB30 conductivity meter, respectively.

4.4 Loss on Ignition

Loss on ignition (LOI) determinations were completed for all soil samples to provide organic C content estimates. Approximately 1 g of ground sample was weighed into a ceramic crucible before combustion in a closed Themolyne Type 6000 Furnace muffle furnace over night at 650ºC, with the weight loss after heating and oxidation representing the loss on ignition as calculated (equation 1).

$$\text{LOI} = \frac{DW_{105} - DW_{650}}{DW_{105}} \text{ x } 100 \qquad [1]$$

LOI is the loss on ignition at 650ºC as a percentage, DW_{105} is the dry mass (g) of soil at 105ºC before combustion, DW_{650} is the mass (g) of soil after combustion at 650ºC.

4.5 Total Dissolved Organic Carbon

Total dissolved organic carbon (TOC) analysis of $CaCl_2$ and Na-Citrate – Dithionite extracted solutions were completed with SHIMADZU TOC-5000A analyzer equipped with an ASI-5000A auto sampler at the Living with Lakes Centre, Laurentian University, Sudbury, Ontario for the non-purgeable organic carbon (NPOC) method with a Pt catalyst (680ºC). Sample duplicates, blanks (degassed, acidified and sparged Milli-Q water) and a 10-ppm dissolved organic carbon standard analyzed approximately every 10 samples. Samples were acidified with 2 N HCl and

sparged with extra pure dry air for 5 minutes (300 mL min^{-1}) before analysis to remove dissolved $CO_{2(g)}$.

4.6 Particle Size Analysis

Textural analysis of mineral horizons from profiles 1 and 2, were completed by the Ontario Geoscience Laboratories (OGL) in Sudbury Ontario using a laser diffraction analyzer (S3500 Microtrac Analyzer) for particle size ranges of 0.024 to 2816 µm on sieved soils (< 2000 µm). The Microtrac Analyzer utilizes scattered light from multiple laser beams projected through the stream of particles (Ontario Geoscience Laboratories 2016). The amount and direction of scattered light is measured by photodetector arrays, with the quantity of light at specific angles measured using the photodetectors and is proportional to the measured light flux values (Ontario Geoscience Laboratories 2016). In house reference materials (PSA-B-#1) are used for quality control at the beginning and end of each analytical batch, with sample duplicates run every 10 samples.

4.7 Powder X-Ray Diffraction

Samples for Powder XRD were finely ground and mounted as smear mounts on glass disks mounted in stainless steel sample holders for analysis at the Central Analytical Facility (CAF) at Laurentian University, Sudbury Ontario. Magnetic fractions from LFH horizons of two profiles with high Sb concentrations were analyzed. Additionally, Powder XRD analysis of selected samples from profiles 1 and 2 (extraction 1), and 3 and 5 (extraction 2) was completed on both

untreated and residual soils from the sequential extraction processes to assess the mineralogical selectivity of the extraction techniques.

The diffractograms were collected between 5 or 10^0 - 75^0 2θ using a 0.02^0 step size and a 2 second integration time using a Philips PW 1729 instrument equipped with Co Kα (1.79 Å) radiation at 40 kV and 30 mA, or a Scintag automated theta-2theta PW1820 X-Ray diffractometer with Cu Kα (1.54 Å) radiation at 40 kV and 30 mA. All diffractograms were processed using HighScore Plus 3.0 software to facilitate identification of major phases based on the presence of matching 3 or more of the most intense peaks as documented in the COD and PDF2 databases. Phases in low abundance were initially identified based on the presence of major peaks (e.g., amphibole at 8.45 Å).

4.8 Optical Microscopy

Particles from two soil humus forms (profiles 1 and 2), separated initially using a hand magnet, were examined optically, with grains of interest showing morphological characteristics (i.e., smelter particles, angular reddish and black particles, etc.) being mounted on double sided tape on a glass thin section slide. The grains were examined using a LEICA MZ75, Meyer Instruments binocular microscope. Grains of interest were photographed, and the images and samples were stored for SEM-EDS analysis.

4.9 Scanning Electron Microscopy and Energy Dispersive Spectroscopy

Scanning electron microscopy (SEM) and energy dispersive spectroscopy (EDS) was conducted at the CAF, Laurentian University using a JEOL 6400 equipped with a W filament, at 20 kV and

6 Ma. Both backscatter electron (BSE) and secondary electron (SEI) images were obtained. Selected grain mounts of soils were examined by SEI to allow morphological observation. A beam current of 0.08 nA was employed to minimize particle charging effects and to ensure image quality, and BSE using a higher beam current (0.20 nA) for semi-quantitative chemical analysis. Selected magnetic grain mounts from soil profiles of interest (Profiles 1 and 2) were Au coated for electron optical and energy dispersive analysis. All imaging and chemical data was processed using INCA 4.15 software.

4.10 Geochemical Analysis

Finely ground samples were digested for geochemical analysis using a three acid digest protocol mixture of concentrated trace metal grade (Fisher Scientific) HF:HCl:HNO_3 at ELRFS. The digestion of 1 g of oven dried, finely ground soil and extraction residues was completed in flat bottomed polypropylene tubes on a programmable digestion block (Questron Technologies Corp). Process quality control was ensured by use of 10 ppm Re-Ru spikes in every sample, with sample duplicates added every 10 samples, certified reference materials (LKSD-2 (lake sediment from Calabogie Lake, Ontario) and TILL-2 (till from Scission's Brook, New Brunswick)) were added to the digestion series every 25 samples. Additionally, 0.5 g of the MONII (Montana River II) certified reference material was added every 40 samples.

The multistep digestion procedure was initiated using 10 mL of 10:1 HF:HCl being heated at 110ºC and evaporated to dryness (270 min), followed with a 1:1 HCl:HNO_3 step using 7.5 mL of each acid, heated to 110ºC for 250 min. The final step required the addition of 0.5 mL HF, 2 mL

HCl, and 10 mL of HNO_3, with heating to 50ºC for 110 minutes to dissolve all materials. On completion, all samples were diluted to 50 mL with ultrapure water and stored prior to analysis.

Prior to ICP-MS and ICP-AES analysis at the Ontario Geoscience Laboratories (OGL) a 4.0 mL aliquot of the digestion solutions were spiked with 0.4 mL of 10 ppm Re-Ru solution, and diluted to 10 mL. The solutions were then analyzed by the OGL using a Perkin Elmer ELAN 9000 (ICP-MS) and Thermo iCAP 6500 (ICP-AES). Analytical detection limits for ICP-MS and ICP-AES are method dependent, being calculated for total digests and extractions ($LiNO_3$, $Na_4P_2O_7$ (explained below)) using the following equation:

$$DL = Avg + (3SD)DF \quad [2]$$

Where DL is the limit of detection, the Avg is the average of the element concentration in the method blank, SD is the standard deviation of the method blank and DF is the dilution factor. Analytical precision was calculated using sample duplicates data for both ICP-AES and ICP-MS analysis as the relative percent difference (RPD):

$$RPD = \frac{(sample\ result - duplicate\ result)}{(sample\ result - duplicate\ result)/2} \times 100 \quad [3]$$

where sample result is the original sample concentration in mg kg^{-1} and duplicate result is the concentration in mg kg^{-1} of the duplicate sample for analysis. Analytical precision was determined to be ≤ 10% for ICP-MS minor and trace element analysis, but more commonly ≤ 5%, and ≤ 10% for ICP-AES major, minor, and trace element analysis.

4.11 Single and Sequential Extractions

All single and sequential extraction procedures (SEP) were conducted at ELRFS. All extractions involved the use of approximately 1.0 and 0.5 g of finely ground mineral and organic soil, respectively, weighed into 50 mL centrifuge tubes. Quality control measures included matrix method blanks, duplicates every 10 samples, method specific calibration and sample matrix solutions. Three extraction approaches were performed, with two of the three being sequential extractions, and the third was a single extraction to assess the phytoavailable fraction of metal(loid)s in the soils. Calcium chloride, hydrogen peroxide and sodium citrate-dithonite (CD) extractions were analyzed using a Varian Red Top 810 ICP-MS with SPS 3 auto-sampler, and ICP-MS data was analyzed using ICP-MS Expert software (version 2.3, build 301). Lithium nitrate and sodium pyrophosphate extractions were analyzed at the OGL using a Thermo iCAP 6500 ICP-AES.

The first SEP evaluated the exchangeable fractions, followed by the reducible and lastly the oxidizable fractions (Figure 6a). The exchangeable fraction was estimated by extraction with a 0.1 M $CaCl_2$ solution at 1:10 soil:$CaCl_2$ (m/v). Samples were shaken for 1 hour at 200 rpm on an orbital shaker, and centrifuged for 15 minutes at 2000 rpm. The supernatant was filtered gravimetrically through 0.45 µm cellulose filters and collected in 10 mL centrifuge tubes and stored at 3.5 – 4.5ºC for analysis. Samples were rinsed with approximately 20 mL of ultrapure water, centrifuged for 5 minutes at 2000 rpm and the supernatant was discarded. Samples were oven dried at 50ºC after rinsing for 24 hr to drive off excess extraction solution. The reducible fractions were extracted using 50 mL of 0.68 M Na-Citrate solution and 0.80 g ± 0.05 g

dithionite (United States Department of Agriculture 1996). Samples were shaken for 16 hrs at 200 rpm, centrifuged at 2000 rpm for 15 min, and the supernatant was filtered as above. Samples were double rinsed and centrifuged with ultrapure water for 5 min at 2000 rpm, decanted and residue was oven dried at 50ºC for 24 hr. The oxidizable fraction extraction followed procedures outlined by Tessier et al. (1979). An initial 0.02 M HNO_3 and 5 mL of 30% H_2O_2 solution was added to the residue and adjusted to a pH 2 with HNO_3 in a hot water bath (85 ± 2ºC), and was occasional agitated for 2 hrs. This step was repeated, with the sample being agitated in the hot water bath for 3 hrs. The samples were cooled to room temperature and 5 mL of 3.2 M NH_4OAc in 20% (v/v) HNO_3 is added to the sample which was then diluted with ultrapure water to 20 mL and continuously agitated at room temperature for 30 min. Samples were treated as above: centrifuged, filtered, single rinse with ultrapure water and the residues are oven dried.

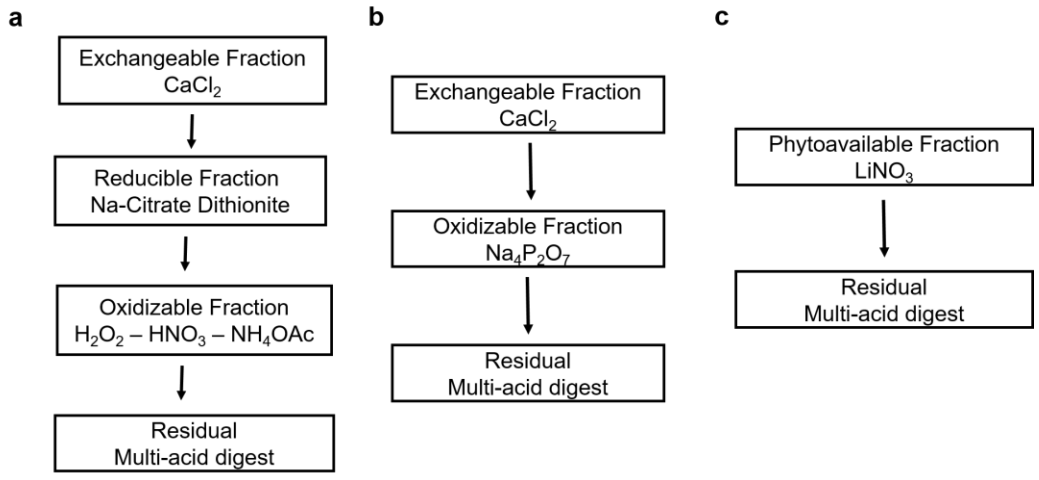

Figure 6. a) Extraction method 1 (exchangeable, reducible, oxidizable and residual fractions), b) extraction method 2 (exchangeable, oxidizable and residual fractions) and c) extraction 3 (phytoavailable and residual fractions).

The second SEP first step included the exchangeable fraction using the same protocol as mentioned for extraction 1 (Figure 6b). The oxidizable fraction was evaluated using methods proposed by Hall et al. (1996) using 30 mL 0.1 M $Na_4P_2O_7$ extraction at pH 10 shaken at room temperature for 1.5 hr (Figure 6b). Samples were centrifuged, filtered, rinsed, centrifuged, dried and stored as above.

The phytoavailable fraction was determined using a single 0.01 M $LiNO_3$ extraction procedure outlined by Abedin et al. (2012) (Figure 6c). A 1:10 (m/v) soil : extractant was used and the extraction was shaken for 20 hr. Samples were centrifuged, filtered, rinsed, centrifuged, dried and stored as above.

Chapter 5

5.0 Results

5.1 Morphological Properties

The five representative pedons sampled at stable, undisturbed sites in this study are illustrated in Figure 7. The dominant vegetation was either birch or pine trees. The well drained and developed soils are classified as Eluviated Dystric Brunisols, with the common horizon sequence of LFH, Ae/Ahe, Bm, BC and C (Sanborn et al. 2011) (Figure 7) formed on the upper till or glaciofluvial benches of the Columbia River.

The LFH horizons (top of the litter layer is designated as the 0 cm depth) were composed of partially to well decomposed litter materials The moist and dry soil colours are dominantly of 10 YR hue, with chroma ranging from the 7 to 5 (Appendix A). The friable soil structural units range from fine to medium subangular blocky in structure, breaking to a single grain for the mineral horizons.

Roots are present to a maximum depth of ~50 cm and are dominated by fine to medium roots with a sub-horizontal orientation in the Ae horizon, fining in size and abundance deeper in the profile. Profile 4 is cumulic, with multiple re-deposition events from fluvial and/or erosional processes depositing new materials on top of the previously developing soils (Figure 7d). The soils range in texture from sand to loamy sand, (Appendix B and Figure 8). Soil texture ranges

from sand fractions of 72 – 96 %, and silt fractions range from 28 to 3.7 % in profiles 1 and 2.

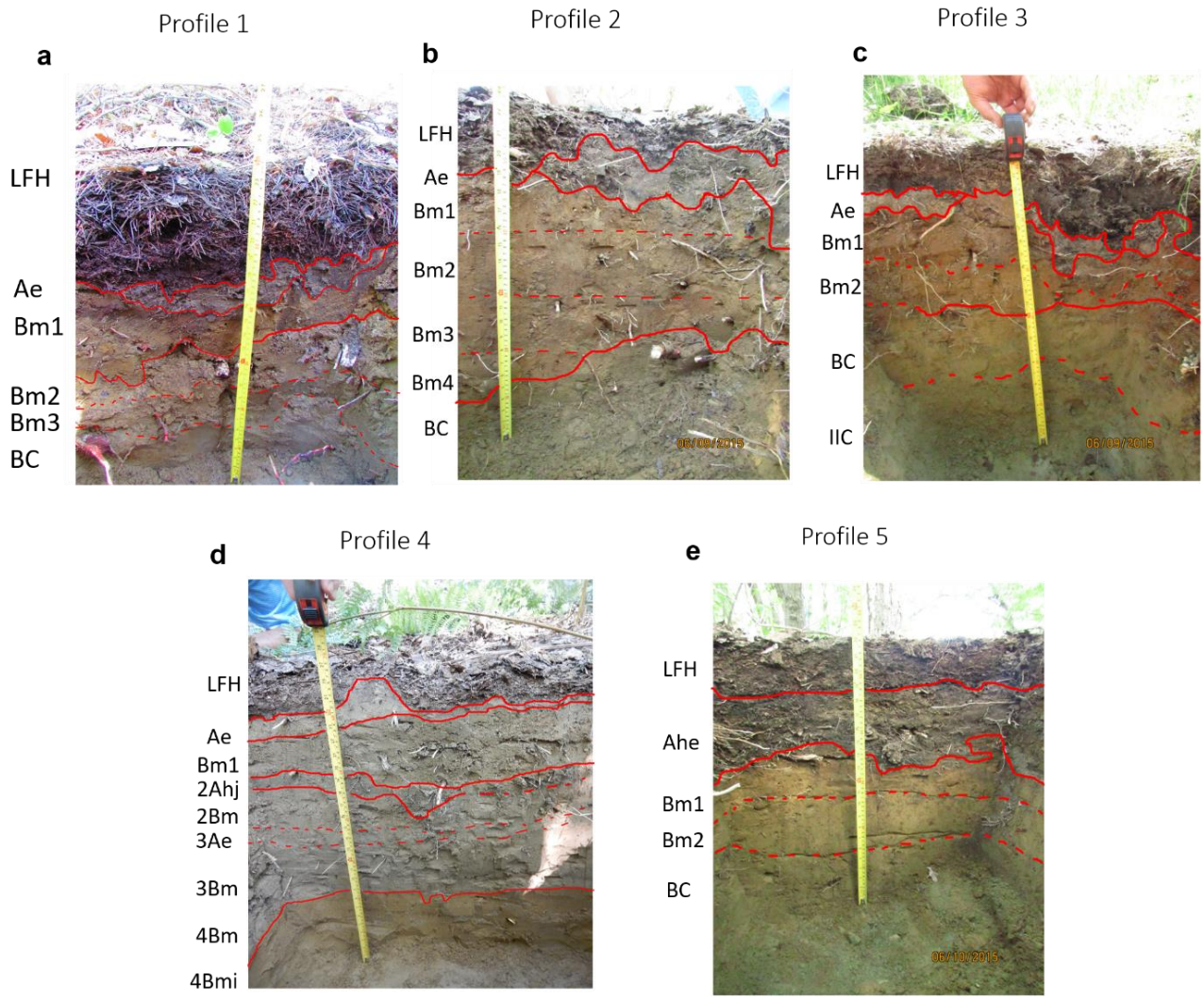

Figure 7. a-e) soil profiles and distinguishing horizons for each sampling site. Horizons are designated with master horizon and suffixes on the vertical axis. Solid red lines indicate sharp boundaries between horizons whereas dashed red lines indicate diffuse boundaries.

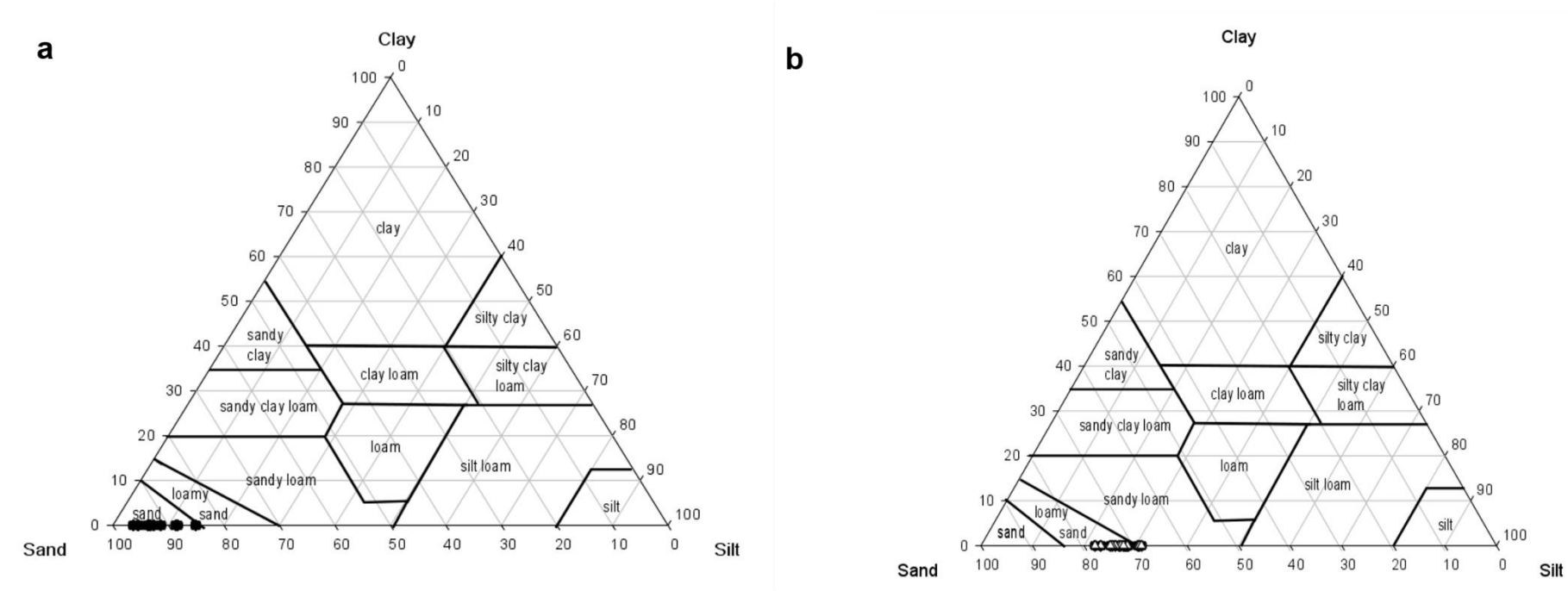

Figure 8. Ternary diagrams for soil texture measured using Laser Diffraction for PSA showing the distribution of clay, silt and sand represented as a % for the < 2 mm size fraction for a) profile 1, and b) profile 2.

5.2 pH, Reduction-Oxidation (Eh) Potential and Electrical Conductivity (EC) Results

All pH measurements (0.01 M $CaCl_2$ and H_2O) were conducted on oven dried soil samples. The soils are acidic, with a pH range between 4.9 – 3.1 and 5.6 - 3.6 for $CaCl_2$ and H_2O (Appendix C), respectively, suggestive of minimal buffering capacity of the underlying dominantly gravel – sand glacial sediment comprising the parental material (Little 1982). The average acidity of the soils was highest in the LFH and Ae horizons (Table 1), and generally increased with depth. The Eh of the water supernatant ranged from +735 to +488 mV, being highest in profile 2. Conductivity ranged from 669 – 19.5 µS cm^{-1} (Appendix C), with profile 2, the furthest downstream from the smelter complex having the highest EC values in the LFH and Ae horizons.

Table 1. Average: pH in H_2O and $CaCl_2$ for soil horizons, reduction – oxidation potential (Eh in mV), electrical conductivity (EC) (µS cm^{-1}). Some horizons were grouped together due to overlap in depth interval sampling.

Sample ID	Depth		pH_{avg}		Eh_{avg}	EC_{avg}	LOI_{avg}
	start	end	H_2O	$CaCl_2$	mV (+)	µS cm^{-1}	(% OM)
Profile 1							
LFH	0	13	4.97	3.92	558	66.8	39.33
Ae	13	19	4.61	4.27	635	60.5	4.06
Bm1	19	27	5.01	4.54	605	44.7	2.11
Bm2-Bm3	30	40	4.46	3.94	594	31.2	1.59
Bm3-BC	40	50	4.66	4.03	596	26.8	1.06

BC	50	60	4.60	4.14	592	36.1	1.02
BC-C	60	94	5.28	4.52	586	29.1	1.00

Profile 2

LFH	0	9	3.77	3.13	670	669	58.67
Ae	2	12	4.41	3.96	503	130	8.91
Bm1	10	20	4.87	4.46	629	72.5	5.42
Bm2	20	30	4.85	4.60	568	67.6	4.09
Bm3	30	40	5.2	4.88	542	65.5	3.48
Bm4	40	50	5.03	4.83	546	59.4	3.07
BC	50	60	4.58	4.23	735	51.2	2.88
IIC	60	94	4.37	3.79	733	53.5	1.82

Profile 3

LFH	0	9	4.07	4	631	556	45.04
Ae	9	14	4.2`	4	524	74.2	2.94
Bm1	14	24	4.55	4	520	73.8	2.68
Bm2	24	33	4.70	4	526	59.9	1.89
BC	33	39	4.72	4	524	47.7	1.30
IIC	39	60	4.94	4	546	34.9	0.94
	60	94	5.56	5	531	29.9	0.86

Profile 4

LFH	0	8	4.14	3.92	630	130	25.61
Ae	8	12	4.42	3.80	509	54.0	1.86

Bm1	12	20	4.52	3.91	512	39.9	1.92
Ahj	20	23	4.48	3.91	508	43.4	1.66
2Bm	23	33	4.42	3.87	708	34.7	1.22
3Ae&3Bm	33	42	4.83	4.08	704	24.9	1.15
3Bm	42	52	4.75	4.11	682	19.5	1.32
4Bm	52	60	4.83	4.68	696	53.7	2.04
4Bmi	60	67	5.00	4.50	672	57.8	1.83
4C	67	101	5.24	4.40	648	24.1	0.71

Profile 5

LFH	0	8	3.75	3.30	661	264	84.89
Ahe	8	21	3.75	3.29	544	152	20.04
Bm1	21	31	4.16	3.76	569	79.0	5.63
Bm2	31	43	4.31	4.11	586	65.9	3.35
C	43	60	4.42	3.92	593	71.0	1.82
C	60	94	4.84	3.96	610	42.0	2.06

5.3 Organic Matter Content: Loss on Ignition and Total Organic Carbon

Loss on ignition, an estimate for total organic matter content, was obtained by sample combustion at 600ºC. The measured soil pH generally being less than 5 in the C horizons indicated absence of carbonates which do not decomposed and release CO_2 until temperatures ≥ 900ºC (Heiri et al. 2001). Organic matter content (LOI) of the surface forms (LFH) ranged from

25 to 85% with the highest organic matter content associated with Profile 5, and the lowest with Profile 4.

Dissolved total organic carbon on all supernatants of the extracts for the exchangeable ($CaCl_2$) (Appendix I) and reducible (CD) (Appendix J) extracts were obtained to enable an evaluation of Pb and Sb levels associated with the soluble and fine colloidal organic carbon components. Total organic carbon analysis was not conducted on $LiNO_3$ extractions as Pb and Sb were generally only detectable in the extraction solutions from the LFH horizons.

The exchangeable ($CaCl_2$) fraction has TOC values ranging from 0.17 – 8.12 mg kg^{-1}. The lowest value was associated with the 4Bm horizon in Profile 4 and highest value was associated with the 19 – 21 cm depth in Profile 1. Except for Profile 1, extractable TOC values were highest in LFH horizons and decreased with depth in the profile. The thin charcoal layers in profile 2 relative to the corresponding Bm horizons had approximately 1.5 times the amount of extractable TOC.

The reducible fraction ranged from 38 – 7018 mg kg^{-1} TOC in the extracts. The lowest value was associated with the 17 – 19 cm depth in profile 1, whereas the highest value was associated with profile 2 at the 21 – 23 cm depth. The extractable TOC values associated with the charcoal layer were lower relative to the corresponding Bm1 horizon at the same sample depths (Appendix J). Profiles 1 and 2 had higher extractable organic carbon content associated around the 19 – 27 cm depths (Figure 9).

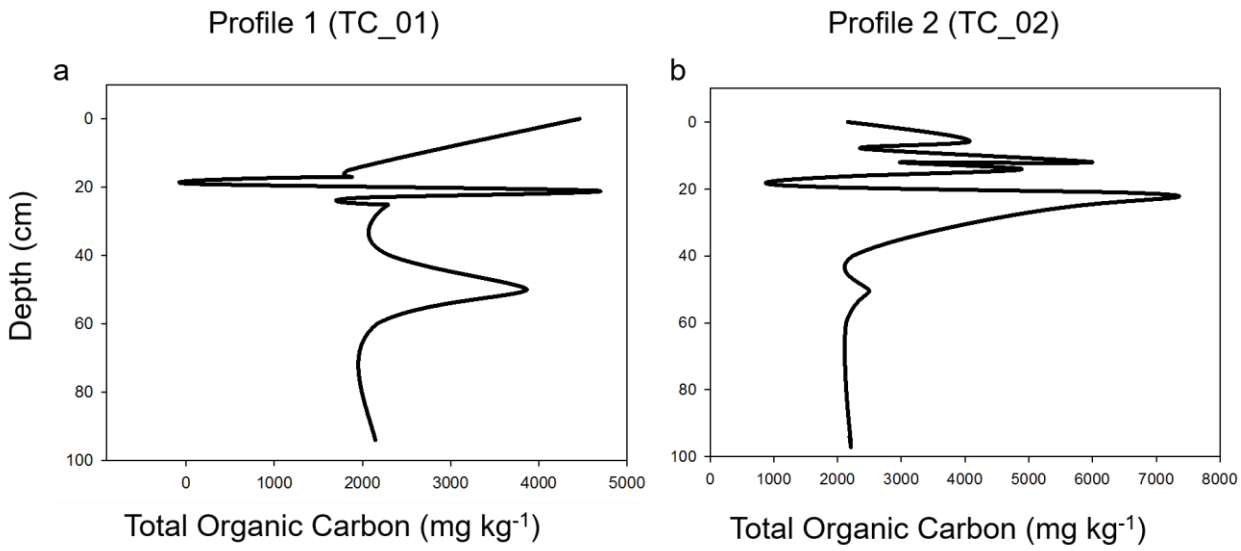

Figure 9. Total organic carbon content in mg kg^{-1} vs depth (cm) for profiles 1 and 2 in the Na-Citrate – Dithionite extractions.

The highest extractable organic carbon content, associated with the 21 – 23 cm (7018 mg kg^{-1}) depths in Profile 2, decreased with depth and then increased with depth around the 19 – 27 cm (max = 7018 mg kg^{-1} at 21 – 23 cm) depths. Profiles 4 and 5 show an extractable TOC range of 1905 – 5026 mg kg^{-1} and 1552 – 4858 mg kg^{-1}, respectively (Appendix J).

5.4 Total Digest Results

The concentrations of both Sb and Pb in the upper 20 cm of the soil profiles exceed the acceptable levels documented in the Canadian Soil Quality Guidelines by approximately 18 and 190 times (Figure 10) (Canadian Council of Ministers of the Environment 1998). The maximum concentrations for the soils in this study of Sb were approximately 740 mg kg^{-1} for Sb (profile 2) and 26377 mg kg^{-1} for Pb concentrations (profile 3) (Figure 10c and f). The soil profile with the

lowest total concentrations of Sb and Pb in the LFH horizon is profile 4 (TC_04) (Figure 10g-h), located approximately 4.1 km north and upwind of the smelter.

The concentrations of both Sb and Pb generally decreased with increasing depth in the soil profile, and are below Canadian Soil Quality Guidelines (< 20 and 140 mg kg^{-1} for Sb and Pb, respectively) in the C horizons, indicating an anthropogenic source of metal(loid)s (Figure 10). Surface horizons (LFH to 10 cm depths) with generally the highest Sb and Pb concentrations in total digests, phytoavailable, reducible, and oxidizable extracts (Profiles 1 and 2) were selected for more detailed analysis.

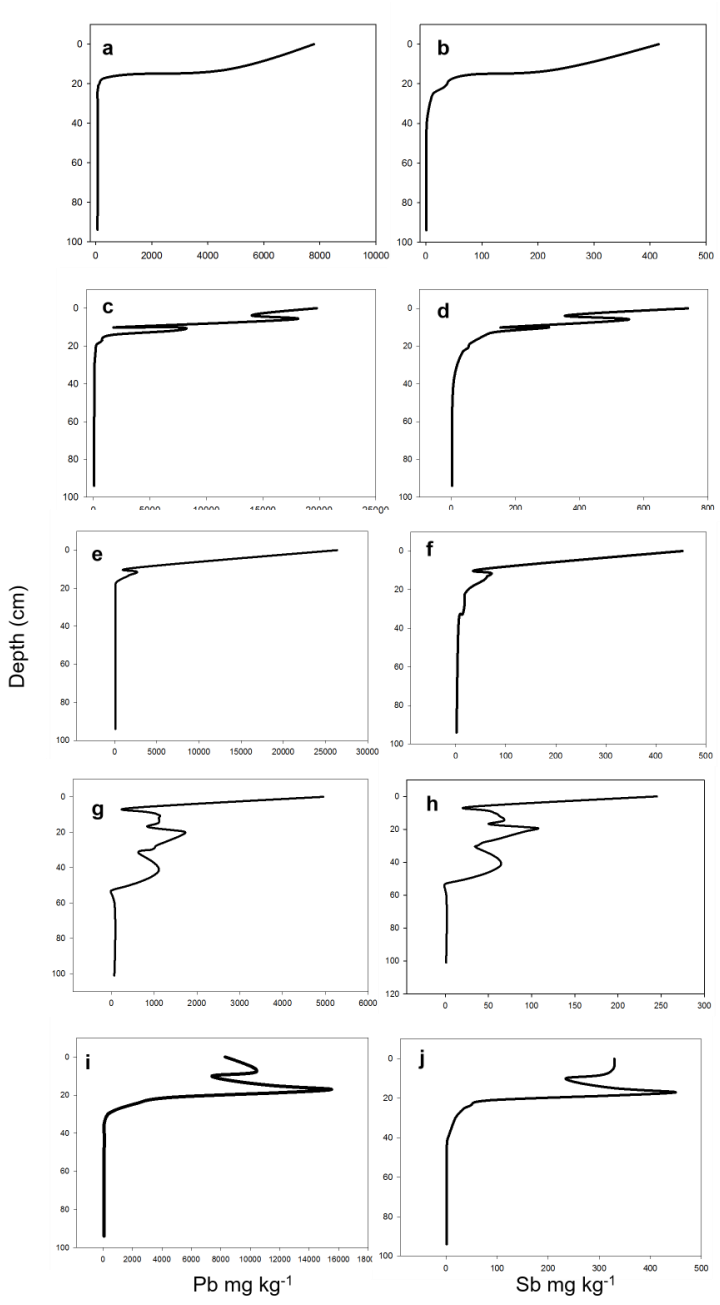

Figure 10. Total digest concentrations of Pb (left) and Sb (right) in mg kg^{-1} vs. depth (cm) for profiles 1 – 5. Each row represents a profile, beginning with profile 1 in the first row and ending with profile 5 in the last row.

The relative distribution of both Sb and Pb was similar with depth in all profiles, except for profile 5 (Figure 10i-j). The correlation coefficients between Pb vs. Sb being very strong (R^2 = 0.85), indicating a similar source. Both elements were enriched in surficial horizons, relatively depleted in the eluvial horizons relative to the LFH horizons, and enriched in the underlying Bm horizons relative to the concentrations measured in the C horizons. The presence of a charcoal layer in the Bm horizon, probably indicative of a pre-industrial forest fire, at the 10 to 12 cm depth in profile 2 (Figure 10c-d), demonstrates the adsorption capacity of charcoal for mobile phases of both Sb and Pb (53 and 44% higher in the charcoal relative to the mineral soil, respectively). The cumulic nature of profile 4 (Figure 10e-f) (TC_04), with periodic relative enrichments and depletions in Sb and Pb in buried diagenetic horizon depths in the soil profile, reflects several colluvial events during the lifetime of the Trail smelter complex.

5.5 Phytoavailable and Exchangeable Fractions

The potentially phytoavailable fraction ($LiNO_3$ extractable) of soil nutrient and metal(loid) contaminants represents the most labile and easily removed metal(loid)s available for plant uptake (Abedin et al. 2012). Potentially available Sb levels were below analytical detection limits for all profiles. Lead potential phytoavailability, below 0.1% of the total lead concentrations, is quantifiable in profiles 1, 2, 3 and 5, and below quantifiable limits in profile 4 (Appendix D). Profiles 1, 2 and 3 show approximately 8 – 11 mg kg^{-1} potentially phytoavailable Pb in the LFH horizons. Profiles 1 – 4 have phytoavailable Pb values < LOD for the mineral horizons, whereas Profile 5 has Pb values of approximately 7 – 5.5 mg kg^{-1} to 23 cm depth. Profile 5 shows the highest concentrations of Pb (7.2 – 6.6 mg kg^{-1}) associated with the Ae and Bm (8 – 21 cm) horizons whereas all other profiles have highest phytoavailable Pb in the LFH

horizons potentially a function of organic matter content in the soils as SEP show a strong association with the oxidizable fractions.

Metal(loid)s associated with the defined exchangeable fractions include elements in soil solution and those weakly sorbed by electrostatic interactions which can easily be exchanged by ion-exchange reactions, are considered to represent the most readily available metal(loid)s to the environment (Tessier et al. 1979, Filgueiras et al. 2002, Gleyzes et al. 2002, Bacon and Davidson 2008, Zimmerman and Weindorf 2010). Exchangeable Pb concentrations were generally highest in the surface horizons of the profiles (upper 10 cm), typically associated with the LFH and upper Ae horizons, with the exception of profile 4 (Figure 12d). The extractable concentrations in all horizons are generally low (max 39.85 mg kg^{-1}), with $CaCl_2$ extractable Pb not exceeding 0.4% of the total amounts (Appendix E), but more typically being < 0.3% $CaCl_2$ extractable. These concentrations were significantly below total Canadian Soil Quality Guidelines (Canadian Council of Ministers of the Environment 1998). Concentrations of Pb generally decreased with depth in the soil profile, with extractable Sb concentrations being below analytical detection limits (< 0.07 mg kg^{-1}) (Appendix E).

5.6 Reducible Fraction

Trace elements associated with reducible mineral phases, such as Fe- and Mn- (oxyhydr)oxides can be sequestered by co-precipitation, incorporation in the crystal lattice, ion exchange, complexation, and adsorption processes (Lintschinger et al. 1998, Filella et al. 2002, 2009a, Filgueiras et al. 2002, Van Vleek et al. 2011, Hockmann 2014). Destruction and/or reduction of these phases can lead to the release of trace elements into the surrounding environmental media

(Lintschinger et al. 1998, Filella et al. 2002, 2009a, Filgueiras et al. 2002, Van Vleek et al. 2011, Hockmann 2014).

Profiles 1 and 2 show depletions of Sb associated with the reducible phases in the LFH horizons and enrichments in the mineral horizons that subsequently decreased with increased depth in the profile. The amount of CD extractable Sb and Pb ranged from approximately 2 – 25% (Figure 11) and 0.5 – 10% (Figure 12), respectively. The highest CD extractable Sb concentrations (83.9 mg kg^{-1}) were associated with mineral horizons in profile 2, were lower in the LFH horizons for profiles 1, 2 and 5, and are higher in the LFH horizons for profiles 3 and 4 relative to the underlying mineral horizons (Ae and Bm) (Appendix F and Figure 11). Concentrations of CD extractable Pb were highest in the LFH horizons (183 – 380 mg kg^{-1}) in profiles 1 and 3, and highest in the mineral horizons for profiles 2, 4 and 5 (Appendix F). The concentrations of both elements decreased with depth in the profile to below < 1 mg kg^{-1} and < DL for Pb and Sb, respectively.

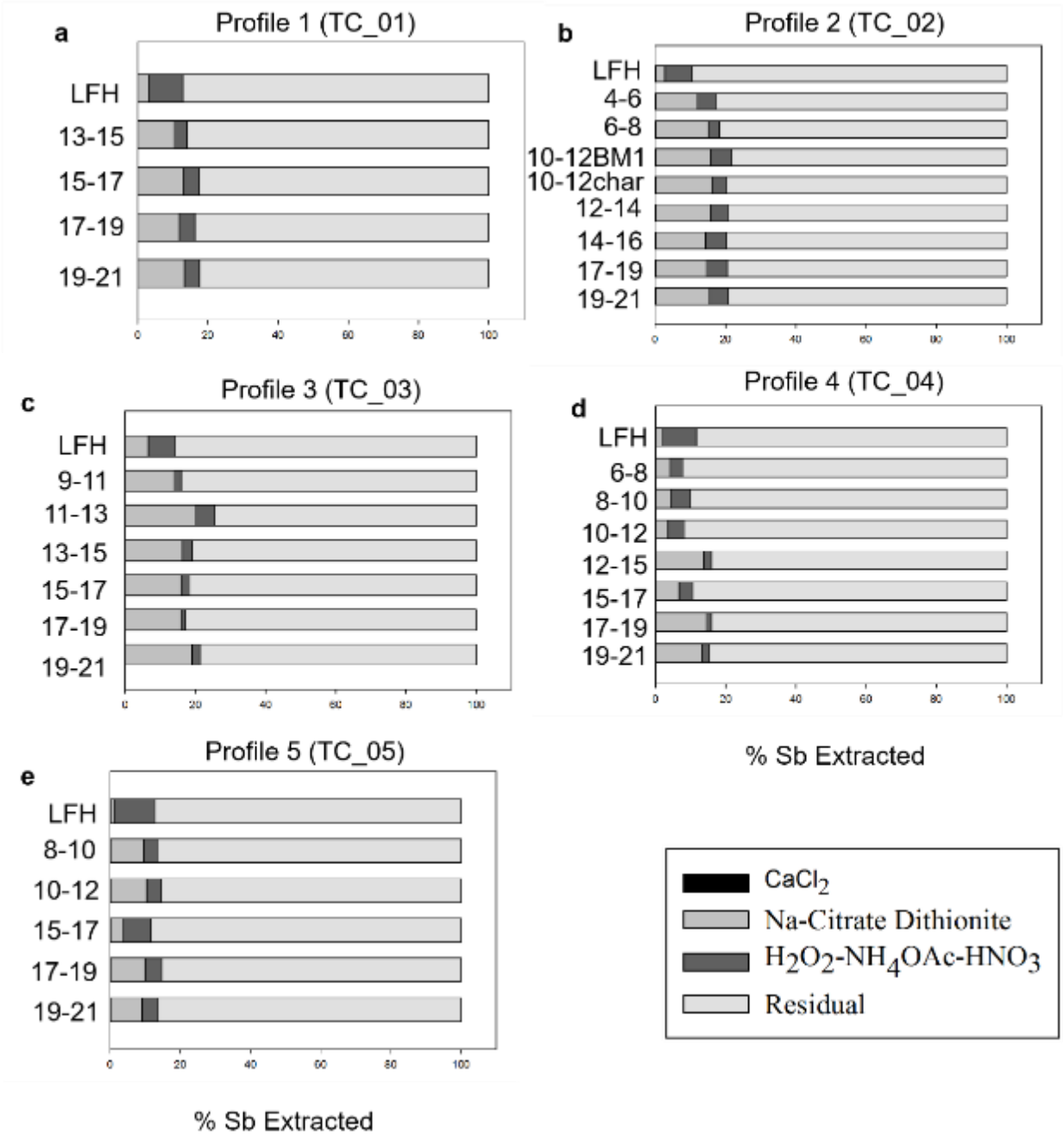

Figure 11. Percentage of Sb extracted for each extraction 1 method normalized to the total digest concentrations for profiles 1 – 5.

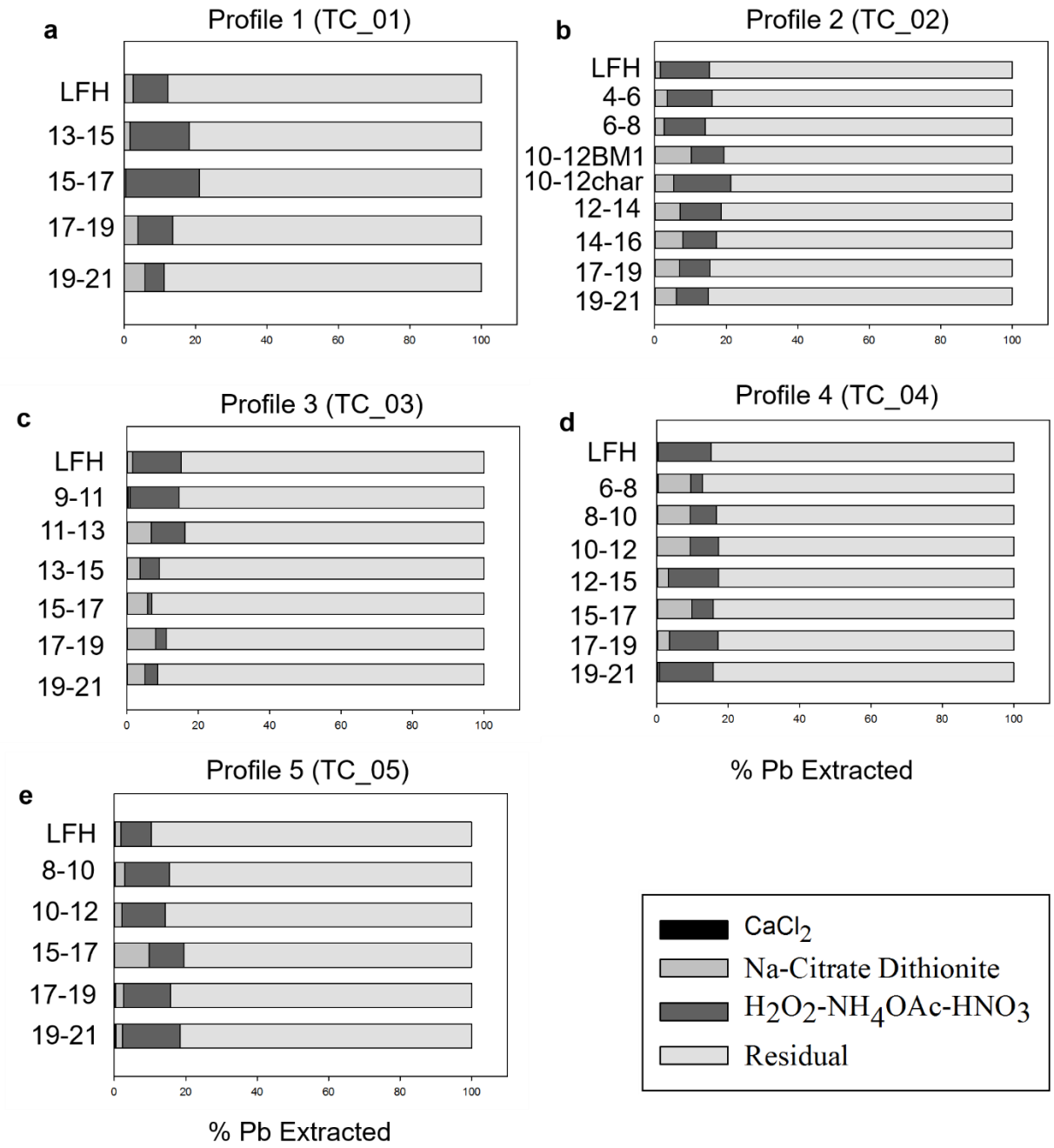

Figure 12. Percentage of Pb extracted for each extraction 1 method normalized to the total digest concentrations for profiles 1 – 5.

The highest CD extractable Sb concentrations were positively correlated ($R^2 = 0.76$) with the concentrations of CD extractable Fe in Profile 2 (Appendix F and Figure 13b) and showed a minor negative correlation with Profile 1 (Figure 13a). This apparent correlation could be due to the different behaviour of Sb in the organic and mineral horizons. For example, LFH horizons have lower concentrations of CD extractable Sb (13.2 mg kg^{-1}) and Fe (2750 mg kg^{-1}), the upper portion (13-15 cm depth) of the Ae horizon has higher CD extractable Sb (23.6 mg kg^{-1}) and Fe (3660 mg kg^{-1}), and concentrations of CD extractable Sb subsequently decrease with depth in the mineral horizon. Extractable Pb was not strongly related to levels of CD extractable Fe (Figure 13c and d), with R^2 values of 0.014 and 0.46 associated with profiles 1 and 2, respectively.

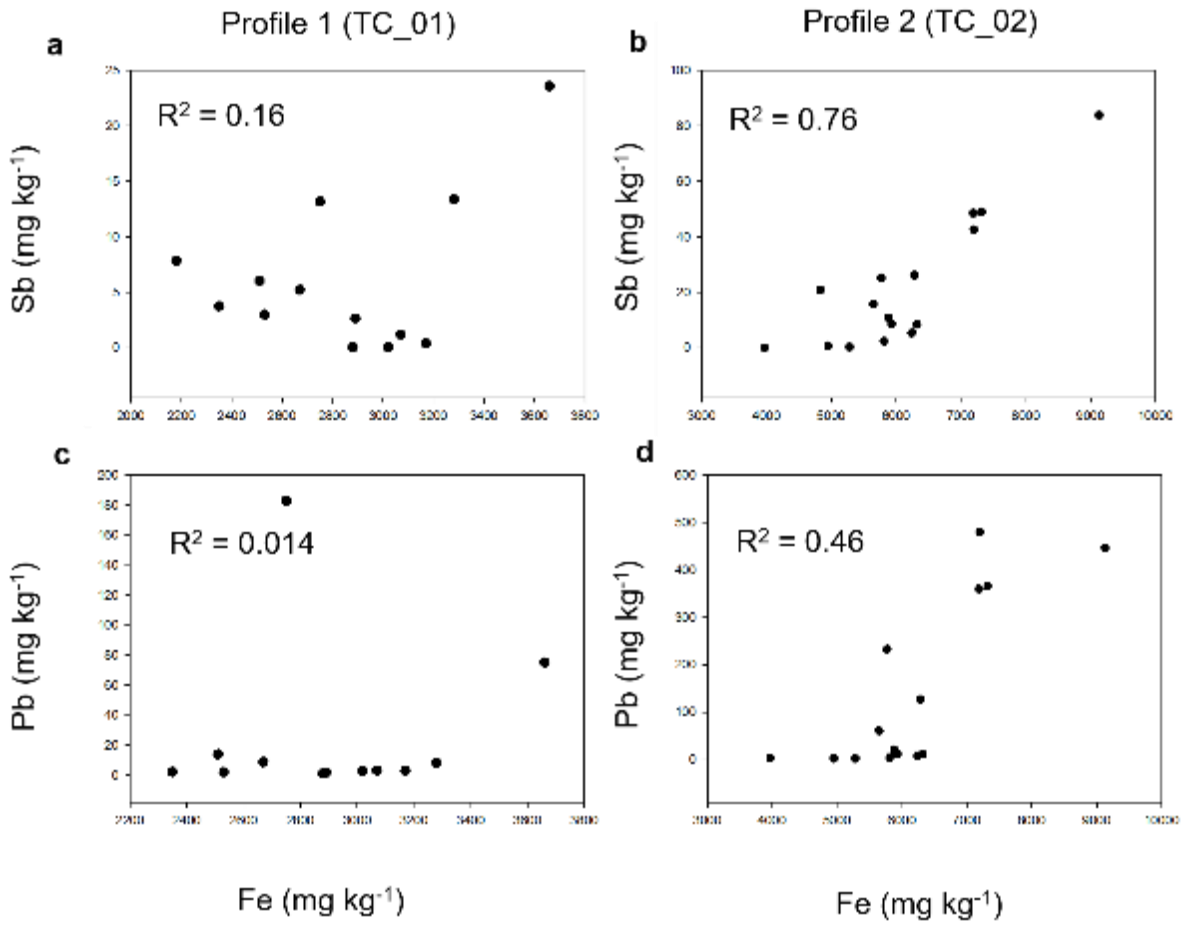

Figure 13. Plots comparing Na-citrate – Dithionite extractable concentrations of Fe (mg kg^{-1}) with concentrations of Sb (mg kg^{-1}) in a) profile 1, and b) profile 2, Pb (c-d) in c) profile 1 and d) profile 2.

5.7 Oxidizable Fraction

As trace elements associated in soils with oxidizable fractions are assumed to be dominantly complexed with humic substances and/or bound with sulfides, mobilization of trace elements can occur following decomposition or oxidation of these phases, an understanding of metal(loid)

association with this fraction is of paramount importance (Tessier et al. 1979, Hall et al. 1996b, Rauret et al. 1999, Filgueiras et al. 2002, Zimmerman and Weindorf 2010).

The tables of Appendix G show the H_2O_2-NH_4OAc-HNO_3 extraction results for Pb and Sb. The high Pb concentrations were associated with profile 3 (3590 mg kg^{-1}, LFH) > profile 2 (2710 mg kg^{-1}, LFH) > profile 5 (2060 mg kg^{-1}, 17-19 cm depth) > profile 1 (767 mg kg-1, 13-15 cm) > profile 4 (731 mg kg^{-1}, LFH) and were primarily restricted to the uppermost portion of the profile (>15 cm) (Figure 12). Peroxide extractable Pb proportions ranged from 20.5 – 1.8 % of the total Pb concentration in the upper 20 cm of the profile relative to the lower 60 cm of the profile, respectively (Figure 12 and Appendix G). The highest Sb concentrations were associated with the LFH horizons in all profiles (23.7 - 56.8 mg kg^{-1}), with < 10% extractable Sb associated with the oxidizable fraction (Appendix G and Figure 11).

Alkali pyrophosphate extractions have been shown to effectively attack colloidal organic matter (Hall et al. 1996a, 1996b). Antimony showed a minor association with the $Na_4P_2O_7$ extractable fractions (maximum 17.59%, commonly 1 – 6 %) (Appendix H and Figure 14). Pyrophosphate extractable concentrations of Sb reached a maximum of 35 mg kg^{-1} in profile 5 (17 - 19 cm) (Appendix H). Profiles 2 – 5 show higher pyrophosphate extractable Sb concentrations deeper in the profile relative to the Bm horizons (Figure 14b-e). The $Na_4P_2O_7$ extractable concentrations of Sb were generally lower in the LFH horizons, increased in the Ae horizons and peaked in the Bm horizons and then subsequently decreased with depth.

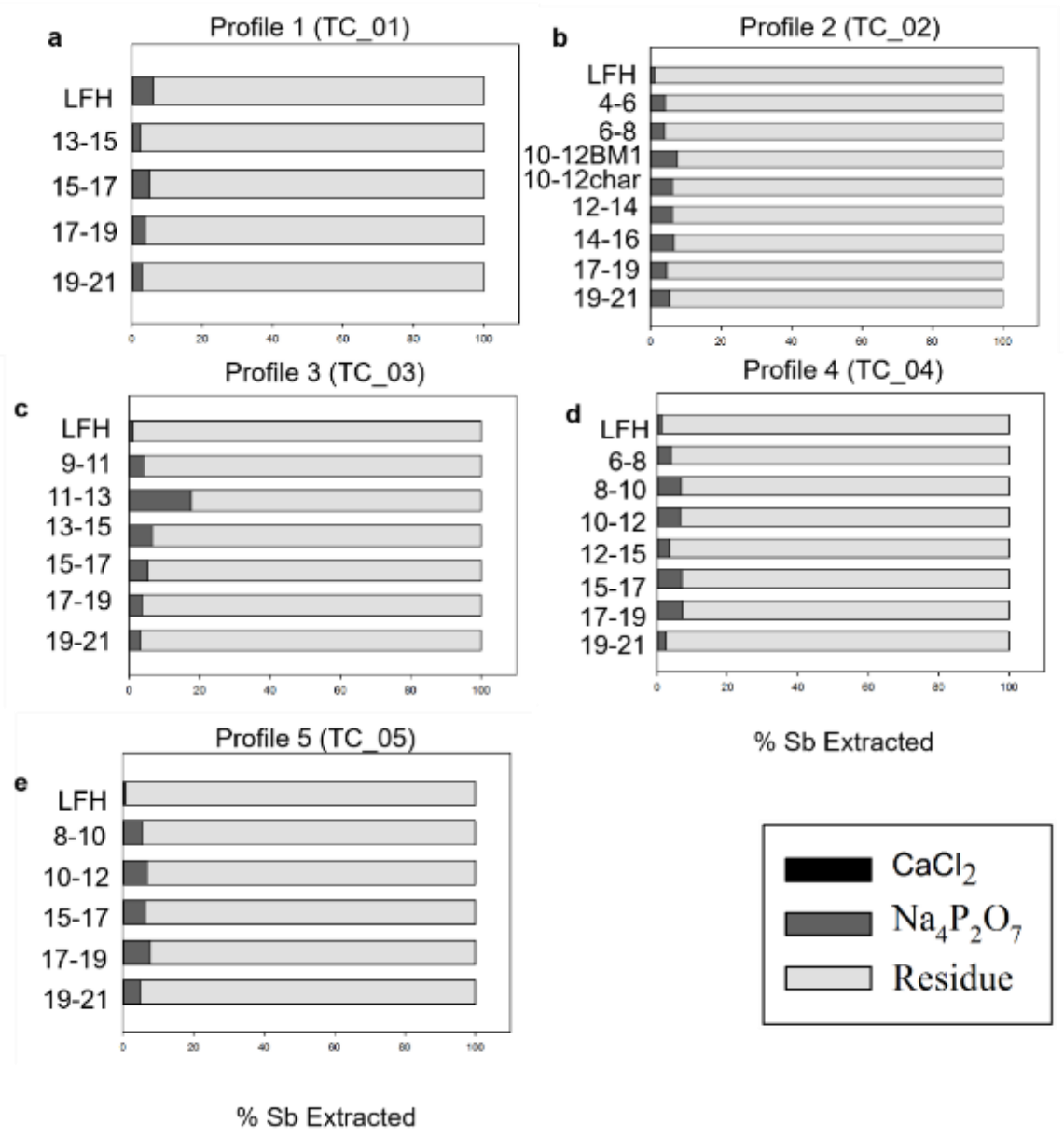

Figure 14. Percentage of Sb extracted for each extraction 2 method normalized to the total digest concentrations for profiles 1 – 5.

Lead concentrations associated with the organic matter extracted by the $Na_4P_2O_7$ extraction were high, with a maximum value of 2440 mg kg^{-1} at the 17 - 19 cm depth in profile 5 (Figure 15).

Profiles 1, 2, and 4 present the highest Pb extracted from the LFH horizons, with levels generally decreasing with depth, whereas profiles 3 and 5 show highest pyrophosphate extractable Pb (10.55 and 15.72% of total being extractable) accumulated deeper in the mineral horizons (Appendix H). Profile 2 displays the higher extractable Pb proportions associated with the charcoal layer, illustrating the effectiveness of charcoal at sequestering Pb relative to the Bm1 horizon (approximately 3% higher, Figure 15b). Pyrophosphate extractable Pb proportions range from 15.5 – 9 % of the total Pb level in the upper 10 cm of the profile (Appendix H and Figure 15), generally decreasing with depth. This result indicates maximum mobility of colloidal organic matter is restricted to the upper portion of the profile during pedogenesis.

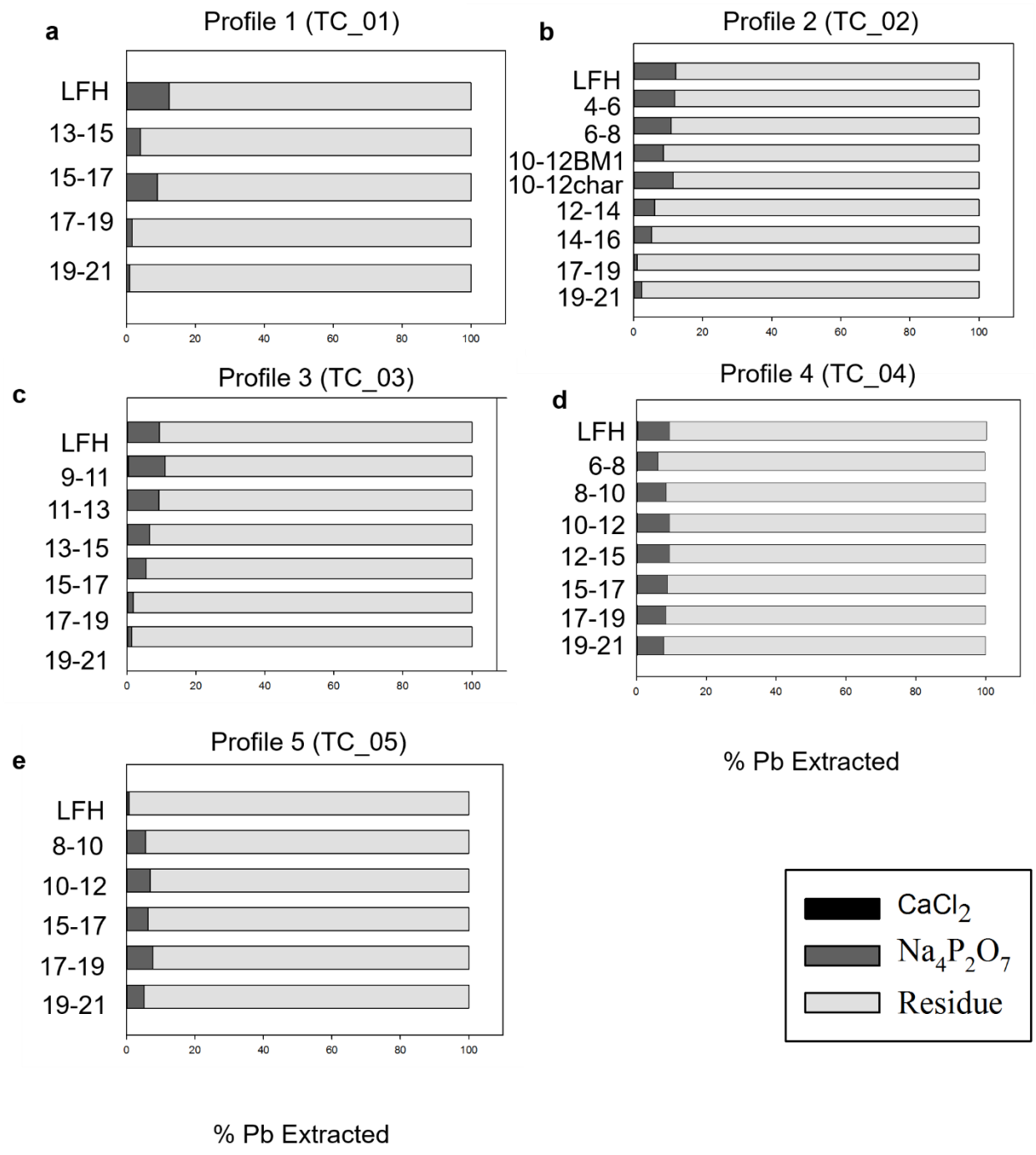

Figure 15. Percentage of Pb extracted for each extraction 2 method normalized to the total digest concentrations for profiles 1 – 5.

5.8 Optical Microscopy, Scanning Electron Microscopy, and Energy Dispersive Spectroscopy

Isolated magnetic grains showing spherical, oval, and aggregated morphologies were individually mounted on double-sided tape for further analysis by SEM-EDS. Particles with a reddish – orange hue, spherical and/or aggregated in morphology were selectively chosen for mounting on double-sided tape as sequential extraction data suggests the association of Sb with reducible phases and spherical particles may be smelter derived. Optical binocular microscope observations show heterogeneous soil aggregates having a reddish - orange to black hues, and spherical to ovoid particles having a black colouration. The analyzed soil particles ranged in size from < 10 – 750 µm along the long axis.

Particles enriched in Sb-, Pb-, and Sn- exhibit a variety of morphologies, sizes, and chemical compositions. A variety of particle types were identified ranging from Sn-, Sb-, and Pb-oxides, Sb-Pb oxides, Sb oxides, and Pb-sulfides/sulfates and are discussed in further detail below. The most dominant phases present were Sb – Sn – Pb oxides with varying proportions of Sb : Sn : Pb. Particles range from 2 to 10 µm in size (long axis), ovoid to angular massive particles which can be incorporated into the matrix material or adhering to the surfaces of Fe-(oxyhyr)oxide coatings, on and with phyllosilicates, and charcoal particles.

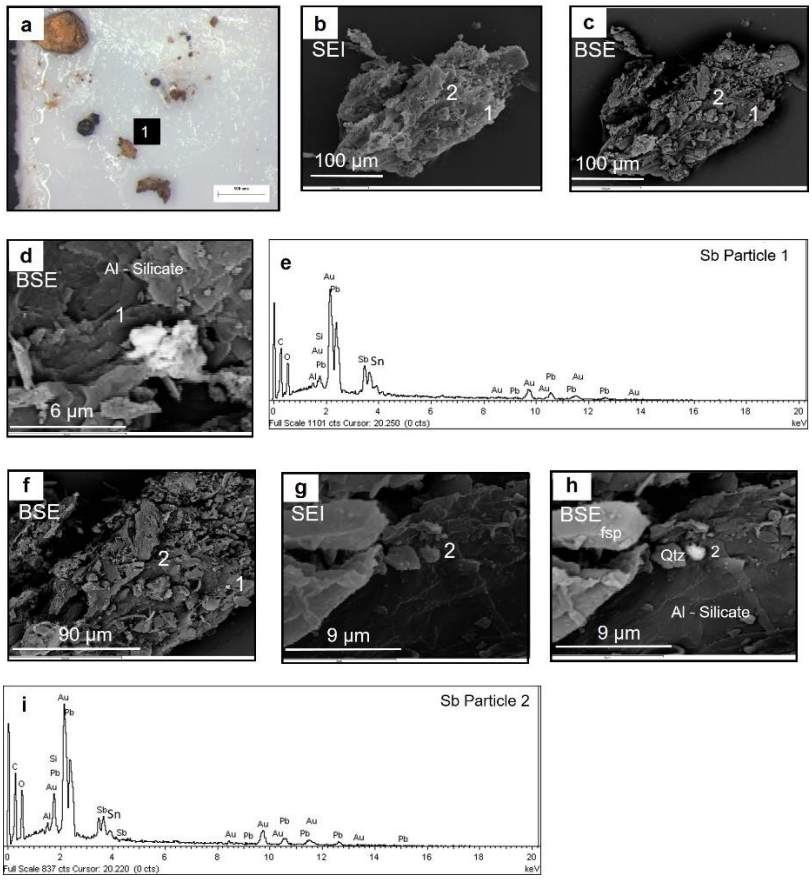

Figure 16. Images and SEM-EDS spectra for Sb – Pb – Sn- and Sb- Sn- Pb oxide particles in soil aggregates for Profile 1 (TC_01) a) binocular microscope image of the analyzed soil particle showing a red hue indicating the presence of Fe-(oxyhydr)oxides, b) secondary electron image (SEI) of the examined particle showing the variation in relief of the aggregate, c) backscattering electron (BSE) image of the aggregate with the particles of interest indicated by the numbers(1) and (2), d) BSE image of the Sb - Pb – Sn oxide particle with Sb : Pb : Sn ratios of 1 : 1.8 : 1.88, indicated by (1), e) SEM-EDS spectra of the particle, f-h) Sb- Sn – Pb oxide particle (2), with Sb : Sn : Pb ratios of 1 : 1.57 : 1.6, adhering to the surface of Fe-(oxyhydr)oxide coatings on Al-silicates, and i) SEM-EDS spectra for f.

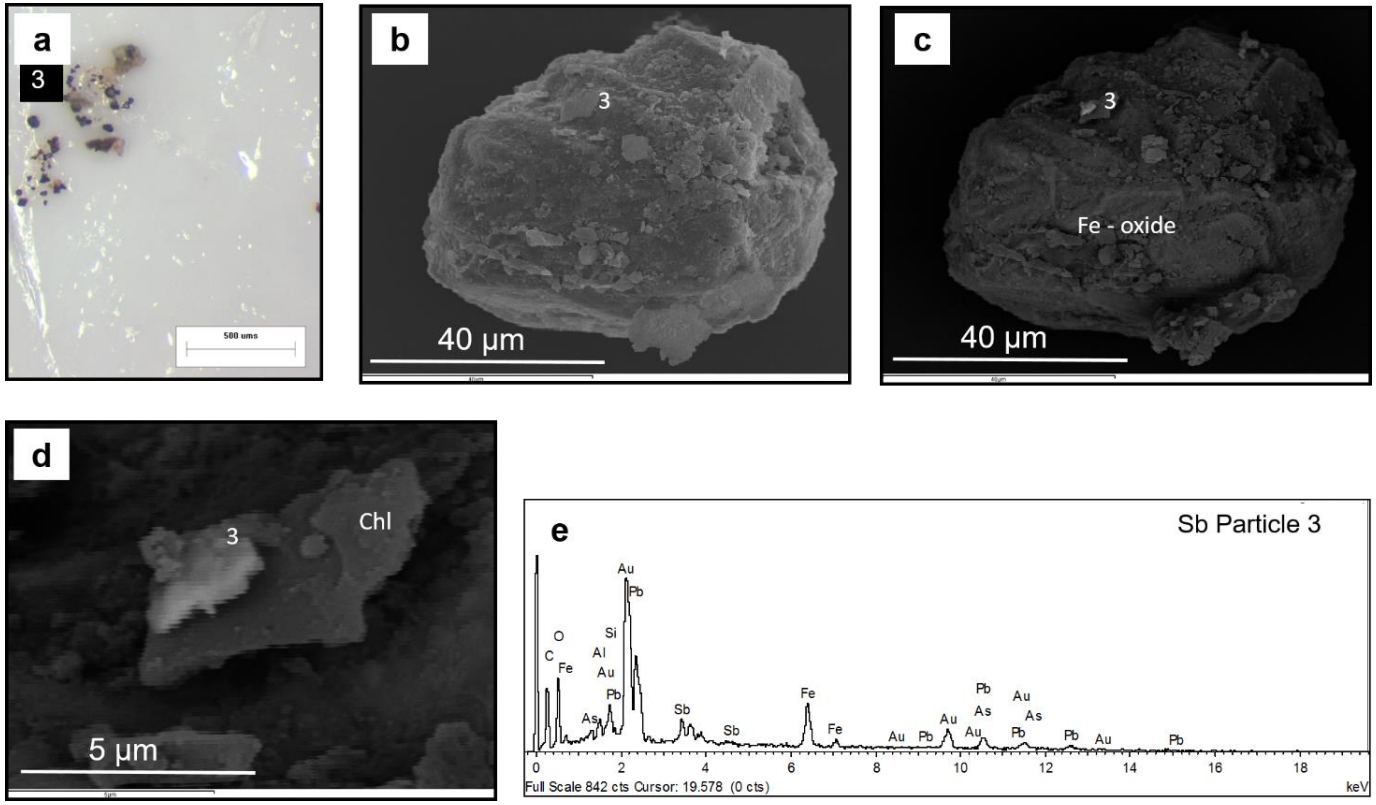

Figure 17. a) binocular microscope image of sub-rounded, black Fe-oxide particles, b) SE image of particle showing the Pb-Sb-As-oxide particle, with Pb : Sb : As ratios of 3 : 1 : 1.4, adhering onto the surfaces of chlorite, c) BSE image of b with the bright region indicating elements of higher atomic mass, d) BSE image of Pb-Sb particle (3) and e) Pb-Sb particle (3) SEM-ED spectra.

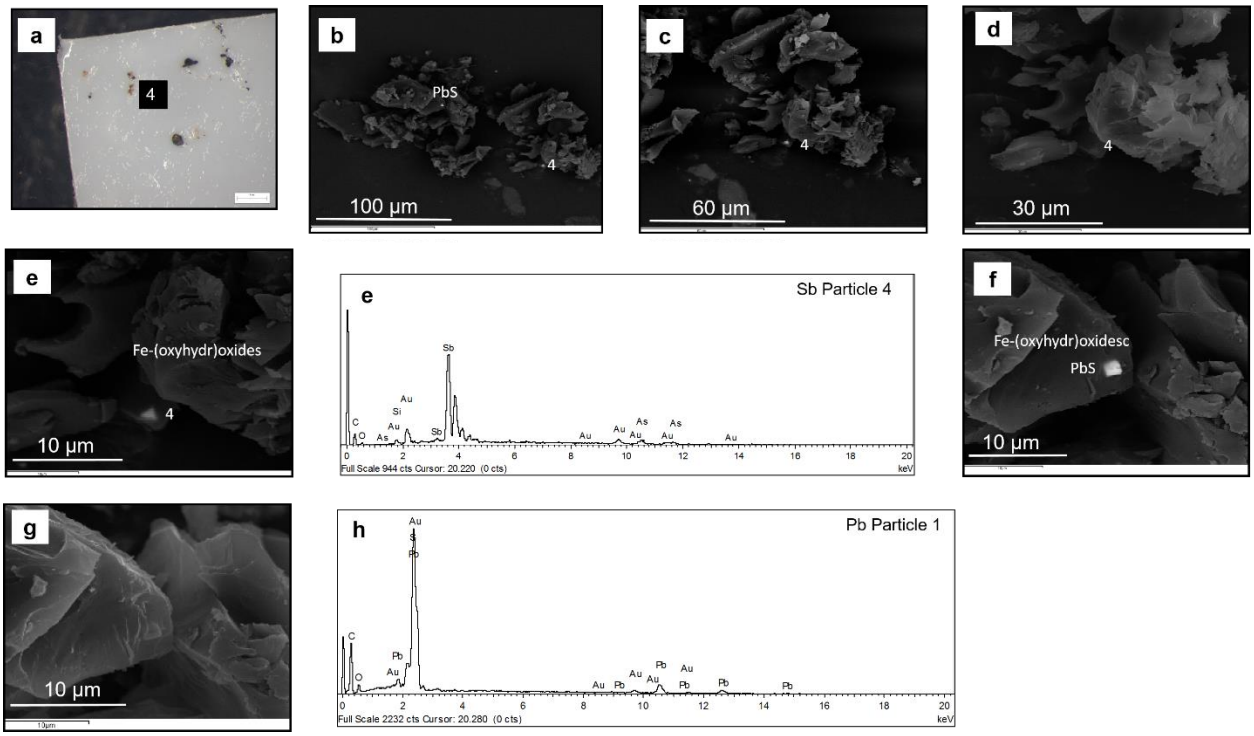

Figure 18. a) binocular optical image of the particles of interest for SEM-EDS analysis, b-c) shows the location of PbS and Sb particles analyzed (4), d) SE image of Sb particle showing the incorporation of the particle in the host-mineral, e) BSE image of triangular shaped Sb particle (4), e) ED spectra of the Sb particle, f) PbS particle in host-mineral showing a cubic morphology and composition similar to galena, g) morphology of the PbS mineral, and h) PbS particle ED spectra.

Four of ten metal – oxide particles analyzed were enriched in Sb, Pb and Sn, with variable ratios between the metal(loid)s. Subangular particles of average radius ~ 2.5 µm appeared to be adhering onto Fe-(oxyhydr)oxide coatings on Al-silicates as discrete oxide particles. Tin can be a major component of the particles (e.g. particles 1, 7, and 12) (Figure 16, Figure 20, and Figure 23). The ratios ranged from 1 : 1.8 : 1.88, 1 : 1.46 : 1.9, 1 : 1.57 : 1.6, and 1.3 : 1 : 1.47 for Sb-

Pb- Sn oxides (Figure 16d, Figure 20e and Figure 23d), and Sb- Sn- Pb- oxides (Figure 16h). Particle 6 (Figure 20c) had the lowest proportion of Sn and highest proportion of Sb, with Sn : Pb : Sb ratios of 1 : 1.95 : 4.38.

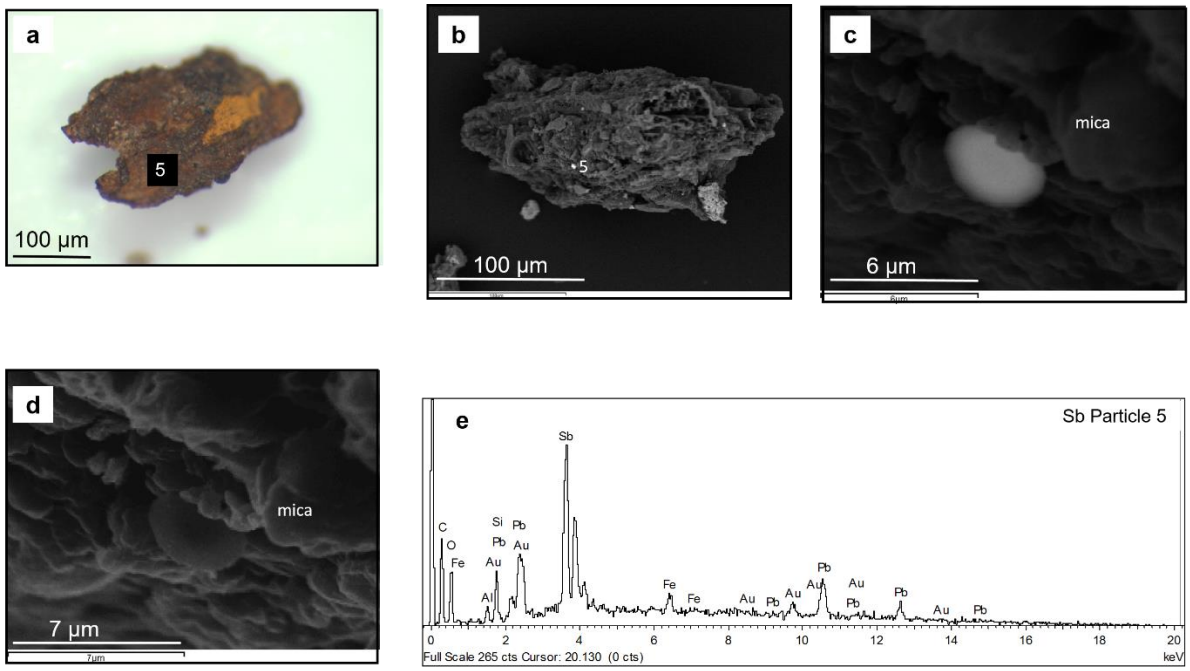

Figure 19. a) binocular optical microscope image of a soil particle of interest analyzed further for SEM-EDS analysis, b) BSE image of the soil particle showing the point of reference for the Pb-Sb particle of interest (5), c) ovoid Sb - Pb particle of interest with Sb : Pb ratios of 6 : 1, d) SE image of the particle in c indicating a platy texture and the adherence to the surface of the particle, and e) spectra for ED analysis of the particle.

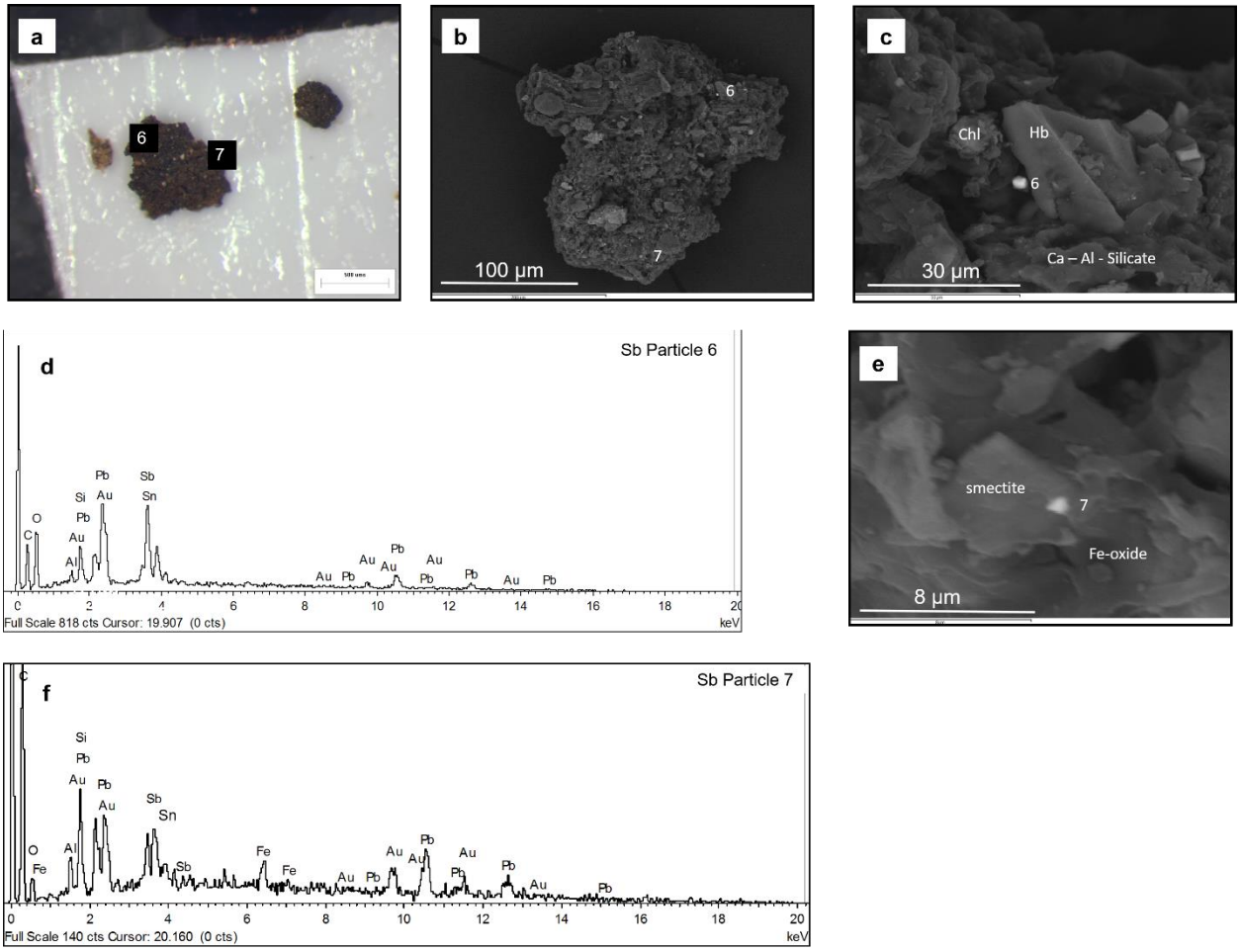

Figure 20. a) binocular optical microscope image of the particle of analysis with the analyzed regions indicated by the numbers 6 and 7, b) BSE image of the analyzed soil particle with individual particles analyzed indicated by numbers (6) and (7), c) discrete subrounded Sn – Pb – Sb oxide particle with Sn : Pb : Sb ratios of 1 : 1.95 : 4.38, d) ED spectra of particle (6), e) adhering angular Sb – Pb – Sn oxide particle with Sb : Pb : Sn ratios of 1.3 : 1 : 1.47, and f) ED spectra of particle (7).

Small (1 – 2 µm) euhedral Sb particles with a crystal habit and morphology consistent with cubic senarmontite (Sb_2O_3) were also present within the Fe-(oxyhydr)oxide matrix (Figure 18). The energy dispersive spectrum for Sb particle 4 did not suggest the presence of O, probably due to a combination of detector and electron beam orientation and the presence of Fe(oxyhydr)oxide particles blocking direct contact of the electron beam with the particle. Therefore, crystal morphology and mineral stability were the major identifying features of this particle (Figure 18). Discrete clusters of sub-rounded, fine (2 µm) antimony oxide particles were also present adhering to the surfaces of charcoal particle edges in the soil (Figure 21).

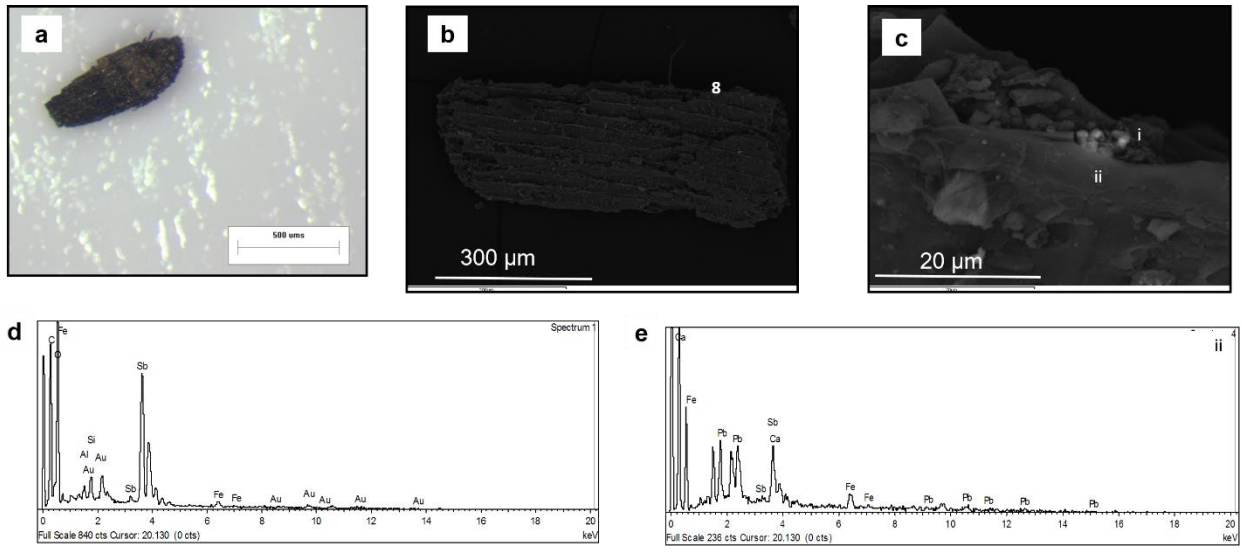

Figure 21. a) binocular image of a charcoal particle selected from TC_02, b) BSE image of the charcoal particle and Sb particles indicated by 8, c) BSE image of Sb particles (i) associated with edges of the charcoal particle and Pb – Sb rich regions indicated by (ii), d) ED spectra of Sb-particles (i), and e) EDS spectra of the Pb – Sb rich region (ii).

The presence of fine (2 µm) euhedral Pb-containing particles were indicated in Figure 18f-g showing an association within Fe-(oxyhydr)oxides. The chemical composition of the particle, crystal habit and morphology were consistent with cubic galena (PbS). Pb-sulfates (Figure 24), potentially anglesite ($PbSO_4$), were also rarely present. Pb can also be present as a component of 2 – 5 µm sub-rounded clusters of Pb-sulfates (Figure 24) adhering to the surfaces of Ca-Al silicate minerals (potentially epidote) as indicated by the SE image in Figure 24c.

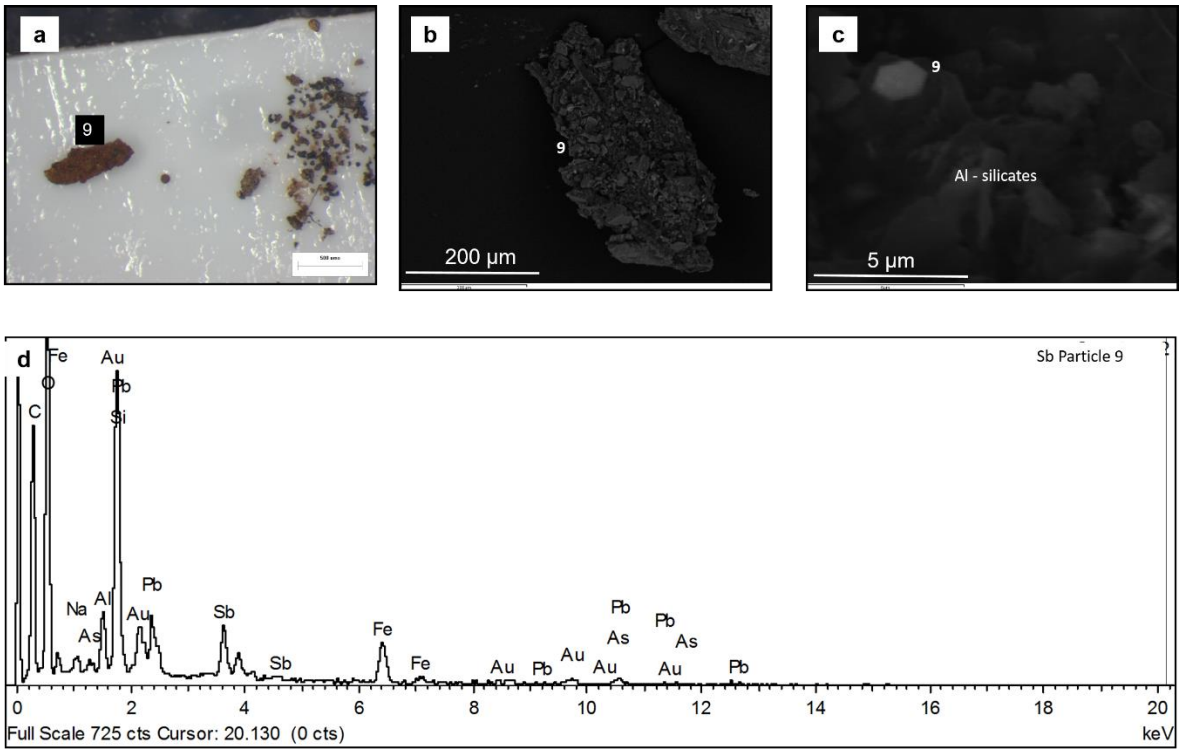

Figure 22. a) binocular microscope image of the particle of interest, b) general location of the Sb – particle of interest indicated by the number 9, c) euhedral nature of 2.5 µm Pb-Sb-oxide particles with Pb : Sb ratios of approximately 1 : 2 , consistent with rosiaite ($PbSb_2O_6$) showing the tabular habit along the basal face, associated with Fe-(oxyhydr)oxide coatings on Al -silicates, and d) ED spectra of rosiaite.

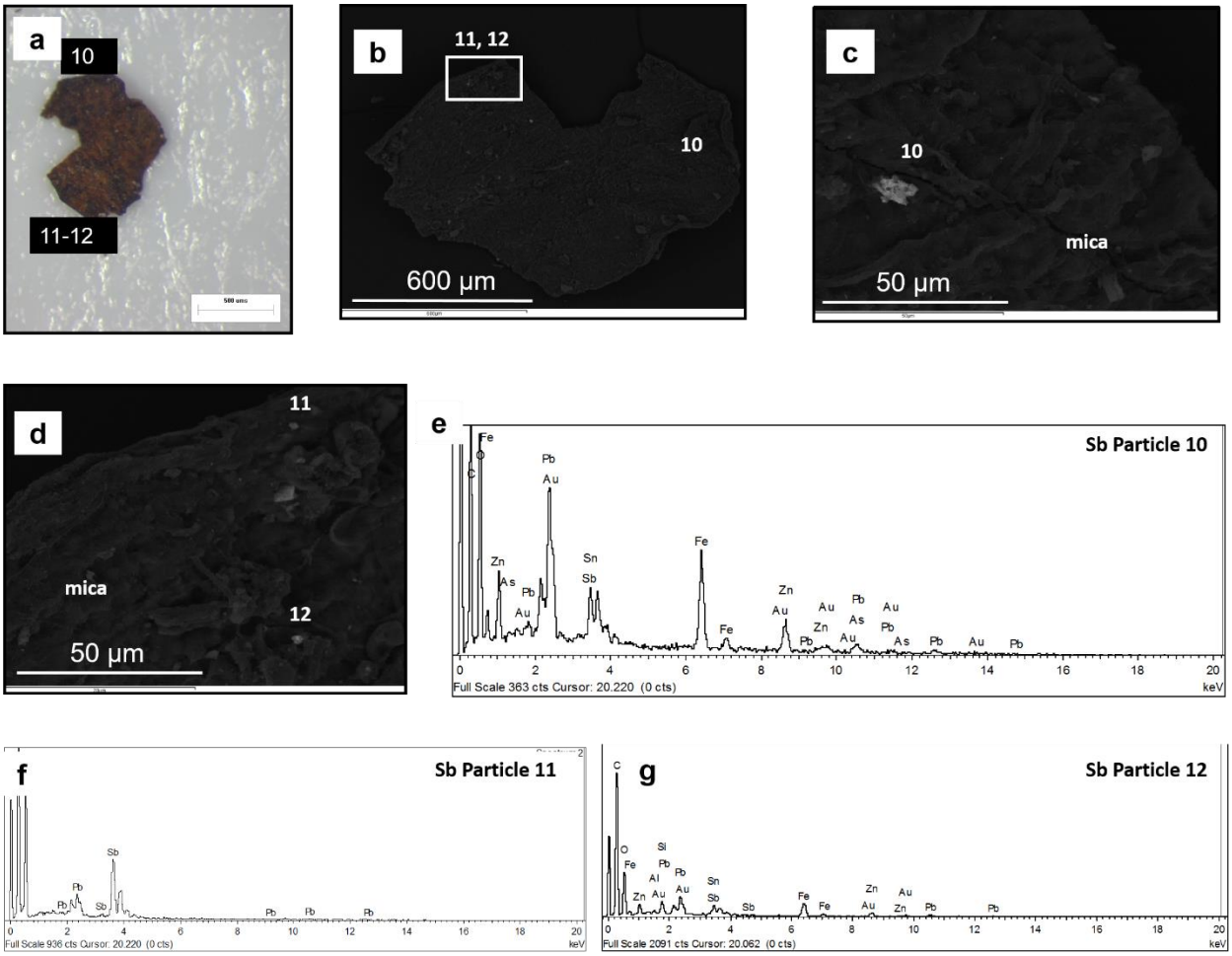

Figure 23. a) angular soil aggregates with a red hue (approximate particle location indicated by the numbers 10 to 12), b) approximate location of Sb particles 10-12, c) angular particle of Sb – Sn – Pb with Sb : Sn : Pb of 1 : 1.37 : 1.79 with minor amounts of As in the particle (~ 2 atm%), and Zn : Fe oxides with Zn : Fe ratios of 1 : 1.73 indicating Zn-rich spinels, d) discrete particles of Sb- Pb oxides (particle 11) with Sb : Pb ratios of 1 : 6.3 and Sb – Pb- Sn, and Zn - Fe oxide particles with Sb : Pb : Sn ratios of 1: 1:46 : 1.9 (particle 12) and Zn : Fe ratios of 1 : 1.97 indicating the presence of franklinite ($ZnFe_2O_3$), e-g) ED spectra of each particle analyzed.

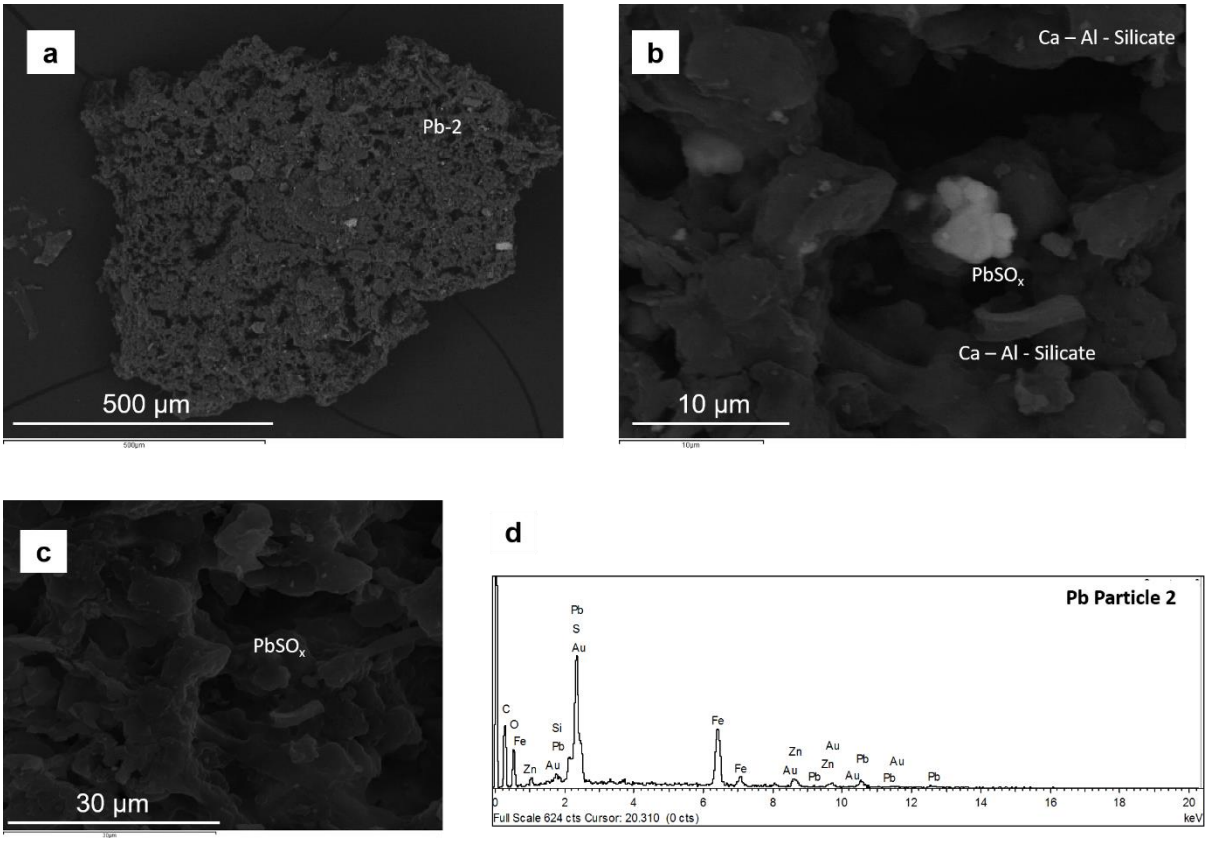

Figure 24. a) SEM BSE images of the region of interest of $PbSO_x$ particles adhering to the surface of soil aggregates, b) BSE image of subrounded morphology and clusters of $PbSO_x$ particles adhering to the surfaces of Ca Al – silicates, c) SE image showing the morphology and relief of the subrounded particles, and d) ED spectra of the $PbSO_x$ particles.

5.9 Powder X-Ray Diffraction

Powder X-Ray diffraction patterns were obtained for pre- and post-extraction residues, as well as for magnetic fractions extracted from LFH horizons for profiles 1 and 2, to gain an understanding of the mineralogy of the metal-endowed zones, and to provide insight into the potential dissolution loss of major mineral phases in the soil during the selective extractions

steps. Table 2 shows the major minerals in selected samples from profiles 1 and 2. Soil LFH horizons also have the presence of spinel group minerals (XY_2O_4, where X is octahedrally coordinated *[6]* divalent cations such as Mg, Fe(II), Zn, and Mn and Y is commonly tetrahedrally *[4]* coordinated trivalent cations, such as Al, Cr and Fe(III)), consistent with magnesioferrite ($MgFe_2O_4$) at the 2.54 Å d-spacing along 113. The mineralogy of the horizons within the soil profiles were dominated by quartz, feldspars, mica, chlorite group minerals and ± amphiboles. The XRD results obtained for horizon samples both pre-and post- extraction are similar, suggesting minimal attack of the major phases occurred during extraction 1 (exchangeable, reducible, and oxidizing extractants).

Table 2. Major mineral assemblages in selected samples (indicated by depth) from profiles 1 and 2 (TC_01 and TC_02) before extraction 1 and on the residue of the soil after extraction 1. Mineral abbreviations are as follows: qtz for quartz, fsp for feldspar, spl for spinel, chl for chlorite, amp for amphibole, verm for vermiculite, and mica for mica group minerals.

		Extraction 1	
Depth (cm)	Horizon	Pre-Extraction	Post-Extraction
		Profile 1	
0 – 13	LFH	qtz > fsp > mica > spl	qtz > fsp > mica > spl
13 – 15	Ae	qtz > fsp > mica > chl ~ amp	qtz > fsp > mica > chl ~ amp
15 – 17	Bm	qtz > fsp > mica > verm > amp ~ chl	qtz > fsp > mica > verm > amp ~ chl
50 – 60	BC	qtz > fsp > mica > chl	qtz > fsp > mica > chl

Profile 2			
0 – 4	LFH	fsp > qtz > mica > chl > spl	fsp > qtz > mica > chl > spl
4 – 6	Ae	fsp > qtz > mica > chl	fsp > qtz > mica > chl
6 – 8	Ae	qtz > fsp > mica > chl > amp	qtz > fsp > mica > chl > amp
10 - 12BM1	Bm1	fsp > qtz > mica > chl > amp	qtz > fsp > mica > chl > amp
10-12char	Charcoal	fsp > qtz > mica > chl	fsp > qtz > mica > chl

The major mineral assemblages for Profiles 3 and 5 (TC_03 and TC_05) for selected samples are listed in Table 3. The XRD results indicate that samples were dominated by feldspars, quartz, mica and chlorite group minerals, ± serpentine and amphiboles. Anhydrite ($CaSO_4$), identified in the pre-extraction LFH horizon for Profile 3 by the most intense 3.49 Å d-spacing, was not detected in the extraction residue suggesting possible breakdown of $CaSO_4$ phases during the extraction process. Positive identification of major clay minerals was not definitive in bulk samples because of the low angle limitations of the diffractometers used in this study, and also because of the low clay content of the soil horizon samples (< 4% in powder XRD results).

Table 3. Major mineral assemblages in selected samples (indicated by depth) from profiles 3 and 5 (TC_03 and TC_05) before extraction 2 and on the residue of the soil after extraction 2 (mineral abbreviations are as follows: qtz for quartz, fsp for feldspar, spl for spinel, chl for chlorite, amp for amphibole, serp for serpentine, mica for mica group minerals, and anhy for anhydrite).

		Extraction 2	
Depth (cm)	Horizon	Pre-Extraction	Post-Extraction
		Profile 3	
0 – 9	LFH	fsp > qtz > mica > anhy > amp	fsp > qtz > mica > amp
9 - 11	Ae	qtz > fsp > chl > amp	qtz > mica > fsp > chl> amp
13 - 15	Ae	fsp > qtz > chl ~ mica > amp	qtz > mica > fsp > chl > amp
15 - 17	Bm1	qtz > fsp > mica > chl > amp	fsp > qtz > mica > chl > amp
17- 19	Bm1	fsp > qtz > mica	qtz > fsp > mica > chl > amp
19 - 21	Bm1	fsp > qtz > chl ~ mica > amp	mica > fsp > qtz > chl > amp
		Profile 5	
0 – 8	LFH	fsp > qtz > mica > chl > spl > amp	fsp > qtz > mica > chl > spl > amp
8 - 10	Ahe	mica > fsp > qtz > chl > amp	mica > fsp > qtz > chl > amp
10 - 12	Ahe	fsp > qtz > mica > chl > amp	fsp > qtz > mica > amp> serp
15 - 17	Ahe	fsp > qtz > serp > amp	mica > fsp > qtz > chl > amp
17 - 19	Ahe	fsp > qtz > mica > chl > amp	mica > fsp > qtz > chl > amp
19 -21	Ahe	qtz > fsp > chl > amp	fsp > qtz > mica > serp > amp

The apparent lack of Fe- and/or Mn- (oxyhydr)oxides in the Powder XRD patterns, but association of metal(loid)s with Fe in the reducible fraction, red-hue of soil particles under binocular microscope suggests these low abundance phases are of short range order.

Samples with the highest extractable and phytoavailable Sb and Pb concentrations from profiles 1 and 2 (TC_01 and TC_02) were selectively chosen for detailed mineralogical analysis by powder XRD examination of the magnetic fractions as SEP data suggest an association with reducible phases (Table 4). The XRD results of the mineral assemblages suggest a high proportion of silicate minerals (feldspars, quartz, amphiboles) and minor oxides (spinel group minerals consistent with magnesioferrite).

Table 4. Mineral assemblage for the magnetic fractions of the LFH horizons for profiles 1 and 2.

Profile 1 (TC_01)	Profile 2 (TC_02)
Mineral Assemblage	Mineral Assemblage
fsp > qtz > amp > spl	fsp > qtz > amp > spl

Chapter 6

6.0 Discussion

6.1 Sb and Pb Mobility, and Potential Phytoavailability

Mobility factors (MF) for Sb and Pb were calculated for each horizon as a percentage of the exchangeable fraction (weakly bound and easily mobile) relative to the total amount of Sb and Pb in the soil using a modified calculation outlined by Kabala and Singh (2001) in equation 4 below:

$$MF_x = (\frac{X_{exch}}{X_{TD}}) \text{ x } 100 \quad [4]$$

where MF_x is the mobility factor in percent and the subscript is indicative of the element, X_{exch} is the concentration (mg kg^{-1}) of Sb or Pb extracted using the 0.1 M $CaCl_2$ extraction, X_{TD} is the concentration (mg kg^{-1}) of Sb or Pb in the total digest.

Antimony was <DL for all but four $CaCl_2$ extractions associated with profile 2 (LFH, 6 – 8 and 10-12 cm (charcoal) samples) and profile 3 (LFH) (Table 5) and <DL for all $LiNO_3$ extractions (Table 5). Samples with detectable Sb in the $CaCl_2$ extraction have a MF_{Sb} < 0.03% (Table 5) significantly less than leachable Sb in forested shooting range and mine soils in Poland with similar texture, and parental material to this studies soils (Lewińska et al. 2017). These values indicate that Sb is relatively immobile in the soils. Other investigators have also identified Sb as immobile in contaminated soils surrounding coal mines in China (Qi et al. 2011), shooting range soils (< 2% Sb leached from soils) (Lintschinger et al. 1998), and agricultural fields (Hammel et

al. 2000). The $LiNO_3$ extraction has been assumed to represent the most weakly bound fraction of the soils, thus being the concentrations of elements which can likely be easily released and/or taken up by biological processes (e.g., plants) (Abedin et al. 2012). The apparent lack of Sb associated with the $LiNO_3$ extraction suggests minimal potential phytoavailability of Sb to plants in the region. Hammel et al. (2000) showed Sb plant root and shoot uptake patterns to be similar at both contaminated coal mines in China and associated non-contaminated sites.

Table 5. Calculated mobility factors (MF, %) as a percentage of the exchangeable fraction relative to the total digest for soil samples. Samples that are not displayed in the table are < DL for both Pb and Sb in the $CaCl_2$ extraction.

Sample Number	Pb MF_{Pb} (%)	Sb MF_{Sb} (%)
Profile 1		
01_LFH_us_e1	0.02	<DL
01_13-15_e1	0.07	<DL
01_15-17_e1	0.04	<DL
01_17-19_e1	0.02	<DL
Profile 2		
02_LFH_e1	0.08	0.01
02_4-6_e1	0.14	<DL
02_6-8_e1	0.11	0.02
02_10-12 Bm1_e1	0.05	<DL
02_10-12 charcoal_e1	0.05	0.03
Profile 3		
03_LFH_e1	0.15	0.02
03_9-11_e1	0.38	<DL
03_11-13_e1	0.31	<DL
03_27-29_e1	0.00	<DL

Profile 4		
04_LFH_e1	0.16	<DL
04_6-8_e1	0.39	<DL
04_8-10_e1	0.22	<DL
04_10-12_e1	0.21	<DL
04_12-15_e1	0.26	<DL
04_15-17_e1	0.27	<DL
04_17-19_e1	0.30	<DL
04_19-21_e1	0.25	<DL
04_21-23_e1	0.25	<DL
04_26-28_e1	0.33	<DL
04_28-30_e1	0.37	<DL
04_30-32_e1	0.39	<DL
04_32-42_e1	0.19	<DL
04_42-52_e1	0.16	<DL
Profile 5		
05_LFH	0.15	<DL
05_8-10	0.18	<DL
05_10-12	0.16	<DL
05_15-17	0.10	<DL
05_17-19	0.10	<DL
05_19-21	0.12	<DL
05_21-23	0.10	<DL
05_23-25	0.13	<DL
05_25-27	0.13	<DL
05_30-40	0.08	<DL

Mobility factors (MF_{Pb}) calculated for Pb were higher than Sb, but all MF_{Pb} were typically < 0.4% (Table 5). Profile 4 has the most mobilizable Pb (indicated by MF_{Pb} deeper horizons relative to other profiles). For example, profile 4 shows an slight increase in MF_{Pb} from 21 – 52 cm depths which is also associated with higher extractable TOC in the supernatant (Appendix I) suggesting an association of Pb with easily solubilized organic substances (Tao and Lin 2000). In

profiles 1, 2, and 5 MF_{Pb} were highest in the surficial horizons (LFH and Ae) and are relatively inconsistent with depth (Table 5). Extractable TOC is lower for profile 1 and higher for profile 2. This immobility of Pb in soils is in agreement with observations from Pb contaminated shooting range soils and in soils examined near the Delta of the Guadalquivir River (Ramos et al. 1994, Lin et al. 1995). Lead in the $LiNO_3$ extractions ranged from 4.2 – 11. 2 mg kg^{-1}, though phytoavailable Pb levels are low these concentrations could cause deleterious effects on plants and toxicity is a function of metal interactions in the soil, nutritional status, age and mycorrhizal infection of the plant (Pahlsson 1989).

6.2 Role of Reducible Phases for Sb and Pb Sequestering

For profiles 1 and 2, higher concentrations of CD extractable Fe were associated with higher concentrations of Sb and Pb extracted in the reducible fraction (Appendix F and Figure 13) suggesting the Sb and Pb in the reducible fraction extracts could be associated with reducible phases (e.g., Fe-(oxyhydr)oxides (R^2 = 0.76, and 0.46, respectively). Antimony appears to show more affinity for the reducible fraction over the oxidizable fraction (Figure 11). The general association of Sb in the soils is residual > reducible > oxidizable > exchangeable and phytoavailable is suggestive of minimal potential impact on the surrounding environment. Adsorption onto amorphous Fe-(oxyhydr)oxides has been shown to be effective at immobilizing Sb in soils, and to be the dominant operationally-defined Sb species in soils (Lintschinger et al. 1998, Filella et al. 2002, 2009b, Wilson et al. 2010, Hernández-Nataren et al. 2011, Okkenhaug et al. 2011, Vithanage et al. 2013), with Sb (V) being strongly associated with amorphous $Fe(OH)_3$ (>95% adsorbed) and less strongly associated with soil humic acids (60%) under acidic

conditions (Tighe et al. 2005). The affinity of Sb for reducible Fe -(oxyhydr)oxides was also reported in an oxidized layer in lake sediments (Chen et al. 2003).

Lead, in comparison, shows a minor association with the reducible fraction (10.21 – 0.26%), most commonly around 4 – 5% extractable (Appendix F). This observation suggests reducible phases, while not the major sink for Pb, do have a slight affinity for lead as indicated by higher CD extractable Fe and Pb associated together in the mineral horizons (Appendix E).

6.3 Role of Organic Matter for Sb and Pb Sequestration

A majority of the organic matter in soils is assumed to be present as humic substances (Jones and Bryan 1998) which have a strong ability to aggregate together and behave similarly to colloidal materials in the presence of metal cations and acidic pH environments (Jones and Bryan 1998). The heterogeneous nature of humic substances provides a variety of potential binding sites that make humic components preferential materials for trace element sequestration (Jones and Bryan 1998, Ettler et al. 2005b).

The analytical results obtained from the peroxide extractions showed that Pb is strongly associated with the oxidizable fraction, ranging from 20.55 – 1.19 % (average = 10.81%) (Appendix G), being generally enriched in the subsurface horizons (10 – 20 cm depths). These fluctuations in extractable Pb appear to be associated with higher TOC in mineral samples (Figure 9, Appendix I, and Appendix J). The data from pyrophosphate extractions show a general decrease in extractable Pb concentrations with depth in the profile. The amount extractable ranged from 15.72 % - <DL (Appendix H), with the higher concentrations being from the LFH horizons for Profiles 1, 2, and 4 (Figure 15a, b and e), with depletions in the

underlying Ae horizons leading to re-enrichment in the underlying Bm1 horizons. Both extractions of organically bound materials indicate the association of Pb with residual > oxidizable > reducible > phytoavailable and exchangeable fractions. Organic matter has been shown to be effective at sequestering lead in other studies (Jones and Bryan 1998, Ettler et al. 2005b, Ahmed et al. 2013).

The pyrophosphate results suggest mobilization and translocation of colloidal organic material from the surface humus forms, with subsequent precipitation in the Bm horizons as $Na_4P_2O_7$ extractions are shown to be very effective for selectively extracting colloidal organic matter (Hall et al. 1996b). Profiles 3 and 5 show levels of $Na_4P_2O_7$ extractable Pb with depth to be relatively constant (Figure 15c-e). The results of peroxide extractions suggest a strong association of Pb with the LFH horizons, with a significant decrease in extractability from the mineral horizons (Figure 12). The differences in extractable elemental concentrations between the two data sets could be due to a variety of factors: the pyrophosphate extraction has been shown to be more effective at selectively dispersing only the colloidal organic materials (Bremner and Lees 1949; Hall et al. 1996a), whereas the peroxide extraction has also been shown to both break down organic matter and attack sulfides and silicates, thus potentially liberating higher concentrations of metals (Hall et al. 1996a, Gleyzes et al. 2002). The presence of galena grains in the LFH horizons was confirmed by SEM-EDS analysis (Figure 18f).

The low concentrations of Sb with the peroxide and sodium pyrophosphate extractions relative to the reducible and residual extractions ranged from 11.67 - <DL and 17.59 - <DL, respectively (Appendix G and Appendix H), and suggests a weak tendency for Sb to be complexed with organic matter. High proportions of Sb (17.59% $Na_4P_2O_7$ extractable) in profile 3 (TC_03_11-

13) at 11-13 cm depths suggest the precipitation of colloidal Sb in the base of the Ae horizon, which also is the layer of Fe-(oxyhydr)oxide precipitation. Antimony (V) adsorption in floodplain soils was shown to be less strongly associated with soil humic acids (60%) in the presence of $Fe(OH)_3$ in acidic conditions (Tighe et al. 2005). The results of the SEM-EDS analysis on edges of charcoal particles labelled Sb-8ii (Figure 21c) also suggests adsorption of Sb and Pb.

6.4 Association of Sb and Pb with Refractory Phases

The proportions of both Sb and Pb in the residual fractions (Figure 11 and Figure 12) ranged from approximately 75 – 85 and 80 – 90% of the total elemental content, respectively, in Extraction 1. Extraction 2 showed a maximum of 99 – 82 Pb and 80 - >99% Sb associated with the residual fractions (Figure 14 and Figure 15). These results suggest that Sb and Pb are both associated with more refractory phases, potentially oxides and some silicates, and also indicate very little potential mobility in the soils in the region. These results are in agreement with studies on Pb-contaminated agricultural soils and surface sediments in the Hara Bioreserve in Iran (Filella et al. 2009a, Ettler et al. 2010, Nowrouzi et al. 2014).

6.5 Association of Pb and Sb with TOC in exchangeable and CD fractions

Organic matter content is important for the control of the availability of metal(loid)s in soils as a majority of metals can be bound as metal – organic complexes (Jones and Bryan 1998, Sauve et al. 2000), therefore factors that influence organic matter solubility will in turn affect metal solubility (Sauve et al. 2000). For example, the presence of competing ions can influence the

adsorption and/or desorption of metal(loid)s onto organic molecules, their solubility, or could promote coagulation of organic matter (Sauve et al. 2000).

The results obtained from the $CaCl_2$ extractions showed weak positive correlations between Pb and extractable TOC content for profiles 1, 2, 3, and 5, whereas profile 4 (clustering of data) shows an apparent lack of correlation (Figure 25a). These results suggest that, in profiles 1 – 3, and 5 Pb was associated with $CaCl_2$ soluble organic matter. Additionally, a lack of correlation between Pb and extractable TOC values in the CD extractions suggest that the major portion of Pb extracted was associated with reducible phases and not with the OC extracted during the SEP (Figure 25b).

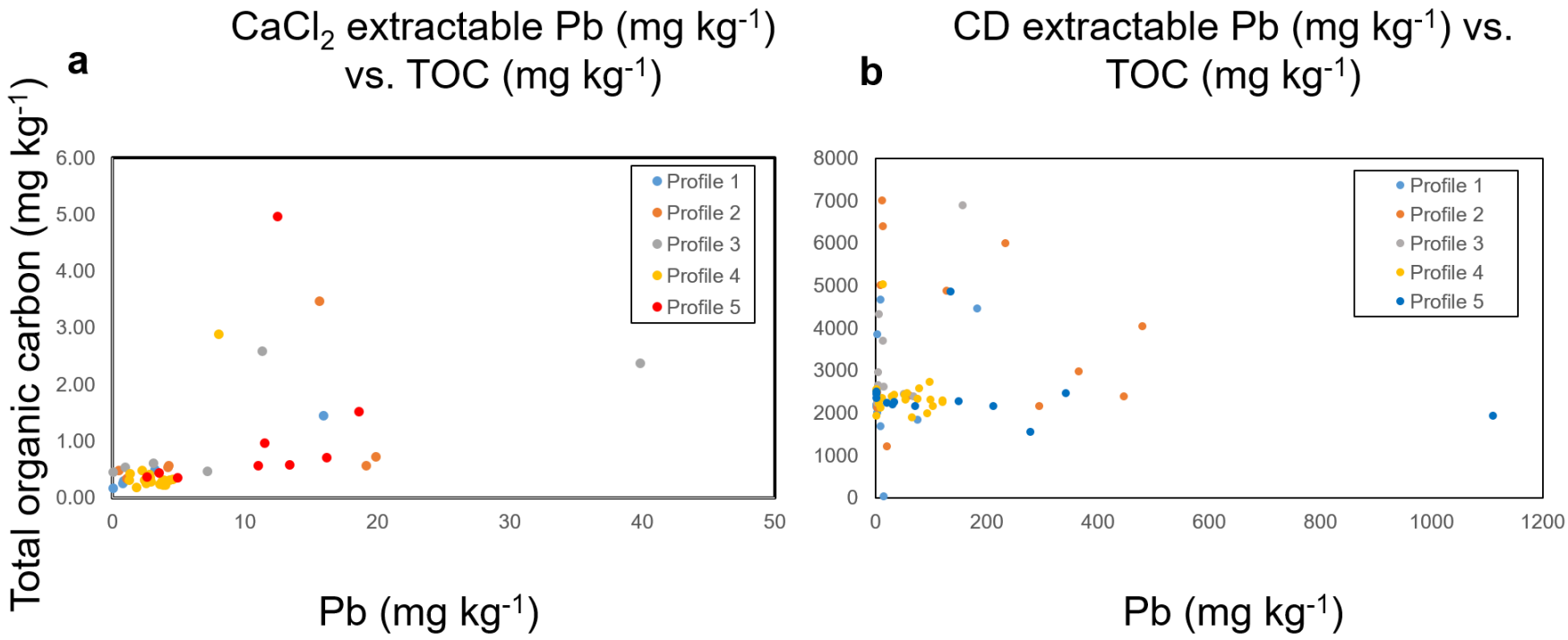

Figure 25. Concentration of Pb (mg kg^{-1}) vs. total organic carbon content (mg kg^{-1}) for the a) $CaCl_2$ and b) CD extractions for each profile. Separate profiles are indicated by coloured dots <DL are not displayed.

Comparison of the extractable TOC content with depth in the soil profiles 1 and 2 indicates zones of irregular enrichment and depletions in the profiles (Figure 9), suggestive of the mobilization of colloidal organic matter in the humus form and subsequent deposition in the mineral horizons, potentially associated with mineral surfaces. Percolation of colloidal OC downwards in the profile is the likely source of higher extractable TOC values in the lower profiles (Neagoe et al. 2012). The subsequent decrease in extractable TOC is proportional to the significant decrease in total digest and sequential extraction Sb and Pb concentrations in profiles 1 and 2 (Figure 9 and Figure 10), a result indicating that the 27 to 30 cm depths are maximum depths of percolation for colloidal materials in the studied soils.

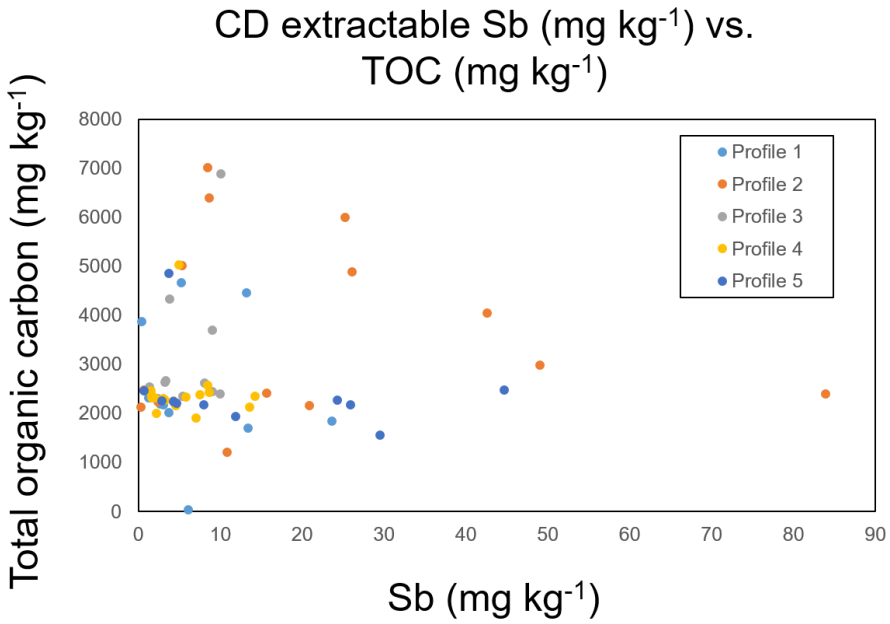

Figure 26. Lack of correlations between CD extractable Sb (mg kg^{-1}) vs. TOC (mg kg^{-1}) content in the CD extraction for each soil profile (indicated by colour of dots).

A significant amount of organic carbon was also dissolved from the soil matrix during the extraction with the CD solutions (38 – 7018 mg kg^{-1}) (Appendix J). Antimony levels, however, have little to no correlation with the extractable TOC content in the CD extraction (Figure 26), a result indicating that Sb is probably not complexed with the extractable TOC.

6.6 Potential Origin of Pb and Sb-bearing Phases

Powder X-Ray diffractograms confirm the presence of major soil minerals (feldspars, phyllosilicates, quartz, and amphiboles) with minor amounts of spinel group minerals and, in one sample, anhydrite (TC_05_LFH). Spinel group minerals are known to form from high temperature processes, such as smelting (Knight and Henderson 2006, Lanteigne et al. 2012, Mantha et al. 2012a, 2012b, Schindler and Kyser 2012, Caplette et al. 2015, Ettler et al. 2016). Anhydrite has recently been observed in trace amounts as a secondary mineral in contaminated surface soils surrounding a historical Zn-Pb mining site (Cabala et al. 2009).

Three major populations of particles were identified based on a combination of morphology and chemical composition, namely, discrete angular – subangular, anhedral and massive particles of stoichiometrically complex Sn – Sb and – Pb- oxides, oval Pb-oxide particles, and euhedral particles of Sb- and Pb-oxides and Pb-sulfides. The morphology and stability of the particulate materials suggest geogenic-anthropogenic and anthropogenic sources.

Table 6. Sb- and Pb-particles describing their respective location, morphology, and approximate size in µm.

Particle		Location	Morphology	Size (µm)
Sb-1		Figure 16d	angular, anhedral, massive	4
Sb-2		Figure 16h	subrounded, anhedral, massive	3
Sb-3		Figure 17d	subangular, anhedral, massive	3
Sb-4		Figure 18d	euhedral, cubic	2
Sb-5		Figure 19c	rounded, ovoid	4
Sb-6		Figure 20c	subrounded, anhedral, massive	4
Sb-7		Figure 20e	angular, triangular	2
Sb-8	i	Figure 21c	subangular – subrounded	2
	ii	Figure 21c	NA	NA
Sb-9		Figure 22c	euhedral, trigonal hexagonal scalenohedral	3.5
Sb-10		Figure 23c	angular, anhedral, massive	10
Sb-11		Figure 23d	angular, anhedral, massive	~ 5
Sb-12		Figure 23d	angular, anhedral, massive	~ 5

Particle	Location	Morphology	Size (μm)
Pb-1	Figure 18f	euhedral, cubic	3
Pb-2	Figure 24b	subangular - subrounded, massive clusters	5 – 2

The incorporation of PbS and Sb-oxides in Fe-(oxyhydr)oxides (Figure 18) suggests that the minerals galena and valentinite were present pre- or syn- matrix formation. Euhedral smelter derived sphalerite was observed in soils surrounding a Zn-smelter, confirming that euhedral metal particles can be emitted by anthropogenic sources (Xie et al. 2005). Monitoring stations using moss-bags set-up in the Trail, British Columbia region by the MITE project showed the presence of PbS in airborne particulate matter (Goodarzi et al. 2001a). Goodarzi et al.(2001a) suggested that PbS was similar in composition, and likely sourced, from the ore materials. Metallic Sb and Sb- oxides have also regularly been observed to be emitted from smelting activities and fugitive emissions (Bloch et al. 1983, Ainsworth and Cooke 1991, Takaoka et al. 2005).

The observation of particles adhering to mineral surfaces are suggestive of a post-matrix formation. Lead sulfates have been observed in both smelter derived particulate matter (Xie et al. 2005, Choël et al. 2006, Jung et al. 2012), and formed *in situ* under acidic conditions (Vitkova et al. 2009, Caplette et al. 2015). The clustering, or aggregation of, $PbSO_x$ (potentially anglesite, $PbSO_4$) particles of subangular to subrounded morphology (Figure 24b) suggests smelter origin

(Bloch et al. 1983, Choël et al. 2006, Romo-Kröger 2006), and is associated with airborne particulate matter in studies in soils in the vicinity of Pb smelters in China (Choël et al. 2006, Romo-Kröger 2006). Both Pb- and Zn- particles have been observed to be subjected to physical coagulation shortly after emission from the smelter (Choël et al. 2006). Smelter-derived $PbSO_4$, PbO, and PbO-$PbSO_4$ have also been previously observed to be emitted from the Trail smelter (Goodarzi et al. 2003). Spherical and oval shaped particles are postulated to be formed during the smelting processes owing to the exhalation of molten droplets and quench cooling of these droplets in the air (Xie et al. 2005, Knight and Henderson 2006, Romo-Kröger 2006, Suzuki 2006, Lanteigne et al. 2012, Mantha et al. 2012a, 2012b, Caplette et al. 2015, Ettler et al. 2016). Oval Sb - Pb oxides with Sb : Pb ratios of 6 : 1 are assumed to be emitted from the smelter (Figure 19c). Airborne particulate matter in the Trail region in 1980 revealed a maximum concentration of 2140 mg kg^{-1} and 28 100 mg kg^{-1}, of Sb and Pb respectively. The airborne particulate matter was significantly more enriched in these two elements relative to the soil, further indicating an anthropogenic origin (Lynch et al. 1980). Both the total digest and extraction results are also suggestive in identifying the anthropogenic source of Sb and Pb in the soils.

The majority of the anthropogenic particles in the humus forms were fine, (sub)-angular massive discrete oxide particles enriched in Sn – Sb -and Pb, with variable proportions of these trace elements and were stoichiometrically complex. This study is in agreement with Miler and Gosar (2013) who found angular anthropogenically derived oxide particles composed of Sn- Sb- and Pb in snow particulate matter surrounding a Pb-processing region in Slovenia. Morphologically, the ± (Sn)- Sb- Pb- oxides were consistent with SEM-EDS analysis on wet deposited metal oxides in

Brazil (Migliavacca et al. 2009). Vitrification of fly ash products in Japan and particulate matter in Slovenia were also discovered to contain considerable amounts of Sn, Sb and Pb created by the volatilization of these elements during high temperature processing (Izumikawa 1996, Miler and Gosar 2013). Airborne particulate matter in Trail humus forms had an enrichment factor 17.7 and 43.7 of Pb and Sb, respectively, relative to the surface soils and was dominated by an angular massive morphology suggesting these elements are released by anthropogenic sources (Lynch et al. 1980, Goodarzi et al. 2003). Tin levels were not examined in these studies.

Tabular euhedral rosiaite along the basal face (0001) was also found to be present in the soils associated with Al-silicates (Figure 21c). Rosiaite is an oxidized secondary Sb mineral (Roper et al. 2015) and has been observed in mining regions associated with valentinite (Sb_2O_3), bindheimite ($Pb_2Sb_2O_6(O,OH)$), and triphyuite (Bassoi et al. 1996; Roper et al. 2015). Formation of rosiaite is generally dependent upon mineralization style (Bassoi et al. 1996, Roper et al. 2015), and can be stable under circumneutral oxidizing conditions, with euhedral rosiaite also having been observed in particulate matter in snow adjacent to a Pb-processing area in Slovenia (Miler and Gosar 2013). Acidic conditions of the study region soils suggest that rosiaite is unlikely to form *in situ*, and is potentially anthropogenically derived.

SEM-EDS analysis of grain mounts (profiles 1 and 2) with reddish-orange to black hues selected from soil humus forms indicated the presence of two major origins of particles. Particles range in morphology from fine angular massive, oval or euhedral ±(Sn)- Sb- Pb oxide, Sb- oxide, Pb-sulfides and sulfates particles. Optical microscopy suggests that particles are dominantly present as discrete metal- oxide particles adhering to the surfaces of aluminosilicates and Fe-(oxyhydr)oxide coatings (indicated by red-hue under the binocular microscope) associated with

aluminosilicates. An examination of mineral stability suggests two major sources of Sb- and Pb-particles. Particles are likely to be anthropogenically derived (*i.e.*, smelting complex) or geogenically-anthropogenically derived (e.g. galena is similar to the ore composition).

6.5 Future Work

This study has identified the association of Sb and Pb bearing phases to be strongly associated with operationally-defined refractory phases. Antimony and lead are associated with operationally-defined reducible and oxidizable fractions, respectively, indicating reduction, oxidation and decomposition of soil phases are of major concern for Sb and Pb release in the soils. Sequential extraction procedures alone cannot define the bioavailable fraction of metal(loid)s due to different uptake mechanisms of individual plants and species, therefore a detailed study assessing the bioavailability of Sb and Pb using plant extraction and soil extraction methods together would strongly compliment this study. A detailed SEM-EDS analysis on the residual fractions of the soils would advance our understanding of Sb and Pb mineralogy in operationally-defined immobile, "stable" phases. These analyses, in turn, will provide an understanding of potential long-term solubility and mobilization of metal(loid)s in Trail, B.C. Additionally, complimenting this study with additional moss or snow particulate matter studies would be beneficial to better categorize smelter and/or fugitive dust derived particulates in the region. Using *in situ* techniques (e.g. XANES, EXAFS) in conjunction with SEP would help to confirm the Sb- and Pb- speciation (e.g. binding mechanisms) in the separate soil fractions and their potential for mobilization. Additional research in the region is required to understand the impact Pb-Zn smelting activities are having on the ecosystem in the region.

7.0 Conclusion

Antimony and lead are both strongly enriched in the uppermost horizons in the soil profile (0 – 27 cm depths), with total concentrations in the soils reaching a maximum of 737 and 26377 mg kg^{-1}, respectively. Phytoavailability and mobility in the Trail, British Columbia region has been assessed using $LiNO_3$ and $CaCl_2$ extractants. Lead mobility and phytoavailability was determined to be significantly higher than that of antimony in the soil profiles, but levels were considerably lower than Canadian Soil Quality Guidelines. Antimony concentrations in the phytoavailable and exchangeable fractions was below analytical detection limits indicating little to no lability in the soils, and thus minimal potential uptake by biota. Sequential extraction results for Sb showed the concentrations in the operationally-defined fractions as residual (silicates and oxides) > reducible (hydrous-oxide bound) > oxidizable (organic matter and sulfide bound) > available fractions, whereas Pb showed residual > oxidizable > reducible > available fractions.

Morphological and chemical analysis using SEM-EDS indicated the dominant phases in magnetically separated particles in LFH horizons were associated with discrete particles that are adhering to the surfaces of Fe-(oxyhydr)oxides and/or aluminosilicates. Two major source populations were identified: anthropogenically derived, stoichiometrically complex ± (Sn)- Sb-Pb oxides, Pb- and Sb-oxides, Pb-sulfates, and geogenic-anthropogenic derived PbS (galena). Particle morphology is a function of source, with angular massive to subrounded (oval) particulates dominantly derived from anthropogenic sources (*i.e.* smelter) and euhedral PbS being likely sourced from a geological-anthropogenic source.

References

Abdullah, A.H., Noor, N.H.M., Ramli, I., and Hashim, M. 2008. Effect of precipitation route on the properties of antimony trioxide. Materials Chemistry and Physics, **111**: 201–204. doi:10.1016/j.matchemphys.2008.04.041.

Abedin, J., Beckett, P., and Spiers, G. 2012. An evaluation of extractants for assessment of metal phytoavailability to guide reclamation practices in acidic soilscapes in northern regions. Canadian Journal of Soil Science, **92**: 253–268. doi:10.4141/cjss2010-061.

Abollino, O., Aceto, M., Malandrino, M., and C. Sarzaninia, E.M. 2003. Adsorption of heavy metals on Na-montmorillonite. Effect of pH and organic substances. Water Research, **37**: 1619–1627. doi:10.1016/S0043-1354(02)00524-9.

Agg, M.. 2004. Trail ecological risk assessment. Teck Cominco Metals Ltd., Trail British Columbia,: 16. Trail British Columbia.

Ahmed, I.M., Helal, A.A., El Aziz, N.A., Gamal, R., Shaker, N.O., and Helal, A.A. 2013. Influence of some organic ligands on the adsorption of lead by agricultural soil. Arabian Journal of Chemistry,. King Saud University. doi:10.1016/j.arabjc.2015.03.012.

Ainsworth, N., and Cooke, J.A. 1991. Biological significance of antimony in contaminanted grassland. Water, Air, & Soil Pollution, **57**: 193–199. doi:10.1007/BF00282882.

Álvarez-Ayuso, E., Otones, V., Murciego, A., and García-Sánchez, A. 2013. Evaluation of different amendments to stabilize antimony in mining polluted soils. Chemosphere, **90**:

2233–2239. doi:10.1016/j.chemosphere.2012.09.086.

Archibold, O.W. 1978. Vegetation recovery following pollution control at Trail, British Columbia. Canadian Journal of Botany, **56**: 1625–1637.

Bacon, J.R., and Davidson, C.M. 2008. Is there a future for sequential chemical extraction? The Analyst, **133**: 25–46. doi:10.1039/b711896a.

Barbosa, F.J., Tanus-Santos, J.E., Gerlach, R.F., and Parsons, P.J. 2005. A critical review for biomarkers used for monitoring human exposure to lead: advantages, limitations and future needs. environmental health, **113**: 1669–1674. doi:10.1289/ehp.7917.

Bassoi, R., Lucchettii, G., Palenzona, A., Europa, C., and Genova, U. 1996. Rosiaite , PbSb206 , a new mineral from the Cetine mine , Siena , Italy. European Journal of Mineralogy, **8**: 487–492.

Bloch, P., Vanderborght, B., Adams, F., and Vanlanduyt, J. 1983. Investigation of the Emissions of an Antimony Metallurgical Factory With Transmission Electron-Microscopy. International Journal of Environmental Analytical Chemistry, **14**: 257–274. doi:10.1080/03067318308071624.

Bremner, J.M., and Lees, H. 1949. Studies on soil organic matter: Part II. The extraction of organic matter from soil by neutral reagents. doi:10.1017/S0021859600004214.

Brugger, J., Giere, R., and Graeser, S. 1997. The crystal chemistry of romeite. Contribution to Mineral Petrology, **127**: 136–146. doi:10.1007/s004100050271.

Cabala, J., Krupa, P., and Misz-Kennan, M. 2009. Heavy metals in mycorrhizal rhizospheres contaminated by Zn-Pb mining and smelting around olkusz in Southern Poland. Water, Air, and Soil Pollution, **199**: 139–149. doi:10.1007/s11270-008-9866-x.

Canadian Council of Ministers of the Environment. 1998. Canadian Environmental Quality Guidelines. Available from http://st-ts.ccme.ca/en/index.html?chems=8&chapters=4 [accessed 4 November 2016].

Caplette, J.N., Schindler, M., and Kyser, T.K. 2015. The black rock coatings in Rouyn-Noranda, Québec: fingerprints of historical smelter emissions and the local ore. Canadian Journal of Earth Sciences,: 1–14. NRC Research Press. doi:10.1139/cjes-2015-0064.

Choël, M., Deboudt, K., Flament, P., Lecornet, G., Perdrix, E., and Sobanska, S. 2006. Fast evolution of tropospheric Pb- and Zn-rich particles in the vicinity of a lead smelter. Atmospheric Environment, **40**: 4439–4449. doi:10.1016/j.atmosenv.2006.04.027.

Courtin-Nomade, A., Rakotoarisoa, O., Bril, H., Grybos, M., Forestier, L., Foucher, F., and Kunz, M. 2012. Weathering of Sb-rich mining and smelting residues: Insight in solid speciation and soil bacteria toxicity. Chemie der Erde - Geochemistry, **72**: 29–39. Elsevier GmbH. doi:10.1016/j.chemer.2012.02.004.

Dousova, B., Buzek, F., Herzogova, L., Machovic, V., and Lhotka, M. 2015. Effect of organic matter on arsenic(V) and antimony(V) adsorption in soils. European Journal of Soil Science, **66**: 74–82. doi:10.1111/ejss.12206.

Ettler, V., Johan, Z., Baronnet, A., Jankovský, F., Gilles, C., Mihaljevič, M., Šebek, O., Strnad,

L., and Bezdička, P. 2005a. Mineralogy of air-pollution-control residues from a secondary lead smelter: Environmental implications. Environmental Science and Technology, **39**: 9309–9316. doi:10.1021/es0509174.

Ettler, V., Johan, Z., Kříbek, B., Veselovský, F., Mihaljevič, M., Vaněk, A., Penížek, V., Majer, V., Sracek, O., Mapani, B., Kamona, F., and Nyambe, I. 2016. Composition and fate of mine- and smelter-derived particles in soils of humid subtropical and hot semi-arid areas. Science of the Total Environment, **563**–**564**: 329–339. doi:10.1016/j.scitotenv.2016.04.133.

Ettler, V., Legendre, O., Bodenan, F., and Touray, J.-C. 2001. Primary Phases and Natural Weathering of Old Lead Zinc Pyrometallurgical Slag From Pribram, Czech Republic. The Canadian Mineralogist, **39**: 873–888. doi:10.2113/gscanmin.39.3.873.

Ettler, V., Mihaljevic, M., Sebek, O., and Nechutný, Z. 2007. Antimony availability in highly polluted soils and sediments - a comparison of single extractions. Chemosphere, **68**: 455–63. doi:10.1016/j.chemosphere.2006.12.085.

Ettler, V., Mihaljevic, M., Sebek, O., Valigurova, R., and Klementova, M. 2012. Differences in antimony and arsenic releases from lead smelter fly ash in soils. Chemie der Erde - Geochemistry, **72**: 15–22. doi:10.1016/j.chemer.2012.01.004.

Ettler, V., Tejnecký, V., Mihaljevič, M., Šebek, O., Zuna, M., and Vaněk, A. 2010. Antimony mobility in lead smelter-polluted soils. Geoderma, **155**: 409–418. doi:10.1016/j.geoderma.2009.12.027.

Ettler, V., Vaněk, A., Mihaljevič, M., and Bezdička, P. 2005b. Contrasting lead speciation in

forest and tilled soils heavily polluted by lead metallurgy. Chemosphere, **58**: 1449–1459. doi:10.1016/j.chemosphere.2004.09.084.

Filella, M., Belzile, N., and Chen, Y.-W. 2002. Antimony in the environment: a review focused on natural waters I. Earth-Science Reviews, **57**: 125–176. doi:10.1016/S0012-8252(01)00070-8.

Filella, M., Williams, P.A., and Belzile, N. 2009a. Antimony in the environment: Knowns and unknowns. Environmental Chemistry, **6**: 95–105. doi:10.1071/EN09007.

Filella, M., Williams, P. a., and Belzile, N. 2009b. Antimony in the environment: Knowns and unknowns. Environmental Chemistry, **6**: 95–105. doi:10.1071/EN09007.

Filgueiras, A. V, Lavilla, I., and Bendicho, C. 2002. Chemical sequential extraction for metal partitioning in environmental solid samples. Analytical and Bioanalytical Chemistry, **374**: 103–108. doi:10.1007/s00216-002-1427-3.

Flynn, H.C., Meharg, A.A., Bowyer, P.K., and Paton, G.I. 2003. Antimony bioavailability in mine soils. Environmental Pollution, **124**: 93–100. doi:10.1016/S0269-7491(02)00411-6.

Fox, C., and Tarnocai, C. 2011. Organic soils of Canada: Part 2. Upland Organic soils. Canadian Journal of Soil Science, **91**: 823–842. doi:10.4141/cjss10032.

Fu, Z., Wu, F., Mo, C., Deng, Q., Meng, W., and Giesy, J.P. 2016a. Comparison of arsenic and antimony biogeochemical behavior in water, soil and tailings from Xikuangshan, China. Science of The Total Environment, **539**: 97–104. Elsevier B.V. doi:10.1016/j.scitotenv.2015.08.146.

Fu, Z., Zhang, G., Li, H., Chen, J., Liu, F., and Wu, Q. 2016b. Influence of reducing conditions on the release of antimony and arsenic from a tailings sediment. Journal of Soils and Sediments, **16**: 2471–2481. Journal of Soils and Sediments. doi:10.1007/s11368-016-1484-4.

Gál, J., Hursthouse, A.S., and Cuthbert, S.J. 2006. Chemical availability of arsenic and antimony in industrial soils. Environmental Chemistry Letters, **3**: 149–153. doi:10.1007/s10311-005-0022-1.

van Gestel, C.A.M. 2008. Physico-chemical and biological parameters determine metal bioavailability in soils. Science of the Total Environment, **406**: 385–395. Elsevier B.V. doi:10.1016/j.scitotenv.2008.05.050.

Gleyzes, C., Tellier, S., and Astruc, M. 2002. Fractionation studies of trace elements in contaminated soils and sediments : a review of sequential extraction procedures. Trends in Analytical Chemistry, **21**: 451–467. doi:10.1016/S0165-9936(02)00603-9.

Goodarzi, F., Sanei, H., and Duncan, W.. 2003. Deposition of trace elements in the Trail region, British Columbia; An assessment of the environmental effect of a base metal smelter on land. Geological Survey of Canada, **Bull 573**: 1–58. doi:10.1126/science.ns-6.149S.521-a.

Goodarzi, F., Sanei, H., and Duncan, W.F. 2001a. Monitoring the distribution and deposition of trace elements associated with a zinc-lead smelter in the Trail area, British Columbia, Canada. Journal of environmental monitoring : JEM, **3**: 515–525. doi:10.1039/b105940h.

Goodarzi, F., Sanei, H., Garrett, R.G., and Duncan, W.F. 2002a. Accumulation of trace elements

on the surface soil around the trail smelter, British Columbia, Canada. Environmental Geology, **43**: 29–38. doi:10.1007/s00254-002-0634-8.

Goodarzi, F., Sanei, H., Garrett, R.G., and Duncan, W.F. 2002b. Accumulation of trace elements on the surface soil around the Trail smelter, British Columbia, Canada. Environmental Geology, **43**: 29–38. doi:10.1007/s00254-002-0634-8.

Goodarzi, F., Sanei, H., and Klassen, P. 2001b. Preliminary Assessment of Background Concentrations of Elements in Soil From the Trail Area. Trail British Columbia.

Goodarzi, F., Sanei, H., Labonté, M., and Duncan, W.F. 2002c. Sources of lead and zinc associated with metal smelting activities in the Trail area, British Columbia, Canada. Journal of environmental monitoring, **4**: 400–407. doi:10.1039/b200787h.

Goyer, R.A. 1993. Lead Toxicity : Current Concerns. Environmental health perspectives, **100**: 177–187.

Hall, G.E.M., Gauthier, G., Pelchat, J.-C., Pelchat, P., and Vaive, J.E. 1996a. Application of a sequential extraction scheme to ten geological certified reference materials for the determination of 20 elements. Journal of Analytical Atomic Spectrometry, **11**: 787. doi:10.1039/ja9961100787.

Hall, G.E.M., Vaive, J.E., and MacLaurin, a. I. 1996b. Analytical aspects of the application of sodium pyrophosphate reagent in the specific extraction of the labile organic component of humus and soils. Journal of Geochemical Exploration, **56**: 23–36. doi:10.1016/0375-6742(95)00046-1.

Hammel, W., Debus, R., and Steubing, L. 2000. Mobility of antimony in soil and its availability to plants. Chemosphere, **41**: 1791–1798. doi:10.1016/S0045-6535(00)00037-0.

Heiri, O., Lotter, A.F., and Lemcke, G. 2001. Loss on ignition as a method for estimating organic and carbonate content in sediments: reproducibility and comparability of results. Journal of Paleolimnology, **25**: 101–110. doi:10.1023/A.

Hernández-Nataren, E., Sahuquillo, A., Rubio, R., and López-Sánchez, J.F. 2011. Solid-phase extraction (SPE) assays to ascertain the mechanisms of retention of antimony species in several stationary phases. Microchemical Journal, **97**: 74–77. doi:10.1016/j.microc.2010.05.008.

Hettiarachchi, G.M., and Pierzynski, G.M. 2004. Soil lead bioavailability and in situ remediation of lead-contaminated soils: A review. Environmental Progress, **23**: 78–93. doi:10.1002/ep.10004.

Hilts, S.R., Bock, S.E., Oke, T.L., Yates, C.L., and Copes, R.A. 1998. Effect of interventions on children's blood lead levels. Environmental health perspectives, **106**: 79–83. doi:10.2307/3433782.

Hockmann, K. 2014. Antimony leaching from contaminated soil under changing redox conditions. ETH Zurich.

Hoy, T., and Andrew, K.P.E. 1991. Geology of the Rossland Area, Southeastern British Columbia. Trail British Columbia.

Intrinsik environmental sciences, I., delphinium holdings, I., swanson environmental strategies,

I., and teck cominco metals, L. 2008. Terrestrial Ecological Risk Assessment for the Teck Cominco Smelter at Trail , BC .

Izumikawa, C. 1996. Metal recovery from fly ash generated from vitrification process for MSW ash. Waste Management, **16**: 501–507. doi:10.1016/S0956-053X(96)00092-X.

Jones, M.N., and Bryan, N.D. 1998. Colloidal properties of humic substances. Advances in Colloid and Interface Science, **78**: 1–48. doi:10.1016/S0001-8686(98)00058-X.

Jung, H., Song, Y., Liu, X., Li, Y., and Ro, C. 2012. Single-particle Characterization of Aerosol Particles Collected Nearby a Lead Smelter in China. **6**: 83–95. doi:10.5572/ajae.2012.6.2.083.

Kabala, C., and Singh, B.R. 2001. Fractionation and mobility of copper, lead, and zinc in soil profiles in the vicinity of a copper smelter. Journal of environmental quality, **30**: 485–492. doi:10.2134/jeq2001.302485x.

Klimko, T., Lalinská, B., Majzlan, J., Chovan, M., Kučerová, G., and Paul, C. 2011. Chemical composition of weathering products in neutral and acidic mine tailings from stibnite exploitation in Slovakia. Journal of Geosciences, **56**: 327–340. doi:10.3190/jgeosci.104.

Knight, R.D., and Henderson, P.J. 2006. Smelter dust in humus around Rouyn-Noranda, Quebec. Geochemistry: Exploration, Environment, Analysis, **6**: 203–214. doi:10.1144/1467-7873/05-087.

Lanteigne, S., Schindler, M., McDonald, A.M., Skeries, K., Abdu, Y., Mantha, N.M., Murayama, M., Hawthorne, F.C., and Hochella, M.F. 2012. Mineralogy and weathering of

smelter-derived spherical particles in soils: Implications for the mobility of Ni and Cu in the surficial environment. Water, Air, and Soil Pollution, **223**: 3619–3641. doi:10.1007/s11270-012-1135-3.

Leverett, P., Reynolds, J.K., Roper, A.J., and Williams, P.A. 2012. Tripuhyite and schafarzikite: two of the ultimate sinks for antimony in the natural environment. Mineralogical Magazine, **76**: 891–902. doi:10.1180/minmag.2012.076.4.06.

Lewińska, K., Karczewska, A., Siepak, M., Gałka, B., Stysz, M., and Kaźmierowski, C. 2017. recovery and leachability of antimony from mine- and shooting range soils. journal of elementology, **22**: 79–90. doi:10.5601/jelem.2016.21.1.1115.

Lin, Z., Comet, B., Qvarfort, U., and Herbert, R. 1995. The chemical and mineralogical behavior of lead in shooting range soils from central Sweden. Environmental Pollution, **89**: 303–309.

Lintschinger, J., Michalke, B., Schulte-hostede, S., and Schramel, P. 1998. Studies on Speciation of Antimony in Soil Contaminated by Industrial Activity. International Journal of Environmental Analytical Chemistry, **72**: 11–25. doi:10.1080/03067319808032641.

Little, H. 1982. Geology of the Rossland-Trail map-area British Columbia. Ottawa.

Lynch, A.J., McQuaker, N.R., and Brown, D.F. 1980. ICP/AES Analysis and the Composition of Airborne and Soil Materials in the Vicinity of A Lead/Zinc Smelter Complex. Journal of the Air Pollution Control Association, **30**: 257–260. doi:10.1080/00022470.1980.10465943.

Magrisso, S., Belkin, S., and Erel, Y. 2009. Lead bioavailability in soil and soil components. Water, Air, and Soil Pollution, **202**: 315–323. doi:10.1007/s11270-009-9978-y.

Maiz, I., Esnaola, M., and Millfin, E. 1997. Evaluation of heavy metal availability in contaminated soils by a short sequential extraction procedure. The Science of the Total Environment, **206**: 107–115. doi:10.1016/S0048-9697(97)80002-2.

Manceau, A., Boisset, M.C., Sarret, G., Hazemann, J.L., Mench, M., Cambier, P., and Prost, R. 1996. Direct determination of lead speciation in contaminated soils by EXAFS spectroscopy. Environmental Science and Technology, **30**: 1540–1552. doi:10.1021/es9505154.

Mantha, N.M., Schindler, M., and Kyser, T.K. 2012a. Silica- and sulfate-bearing rock coatings in smelter areas: Part II. Forensic tools for atmospheric metal(loid)- and sulfur-isotope compositions. Geochimica et Cosmochimica Acta, **90**: 221–241. Elsevier Ltd. doi:10.1016/j.gca.2012.05.013.

Mantha, N.M., Schindler, M., Murayama, M., and Hochella, M.F. 2012b. Silica- and sulfate-bearing rock coatings in smelter areas: Products of chemical weathering and atmospheric pollution I. Formation and mineralogical composition. Geochimica et Cosmochimica Acta, **85**: 254–274. doi:10.1016/j.gca.2012.01.033.

Migliavacca, D.M., Teixeira, E.C., Gervasoni, F., Conceição, R.V., and Rodriguez, M.T.R. 2009. Characterization of wet precipitation by X-ray diffraction (XRD) and scanning electron microscopy (SEM) in the metropolitan area of Porto Alegre, Brazil. Journal of Hazardous Materials, **171**: 230–240. doi:10.1016/j.jhazmat.2009.05.135.

Miler, M., and Gosar, M. 2013. assessment of metal pollution sources by SEM/EDS analysis of

solid paricles in snow: a case study of Zerjav, Slovenia. Microscopy and Microanalysis, **19**: 1606–1619.

Mitsunobu, S., Harada, T., and Takahashi, Y. 2006. Comparison of antimony behavior with that of arsenic under various soil redox conditions. Environmental Science and Technology, **40**: 7270–7276. doi:10.1021/es060694x.

Mitsunobu, S., Takahashi, Y., Utsunomiya, S., Marcus, M. a., Terada, Y., Iwamura, T., and Sakata, M. 2011. Identifcation and characterization of nanosized tripuhyite in soil near Sb mine tailings. American Mineralogist, **96**: 1171–1181. doi:10.2138/am.2011.3651.

Neagoe, A., Iordache, V., and Fa, I.C. 2012. Bio-Geo Interactions in Metal-Contaminated Soils. **31**. doi:10.1007/978-3-642-23327-2.

Nowrouzi, M., Pourkhabbaz, A., and Rezaei, M. 2014. Sequential extraction analysis of metals in sediments from the Hara Biosphere Reserve of Southern Iran. Chemical Speciation and Bioavailability, **26**: 273–277. doi:10.3184/095422914X14141630849689.

Okkenhaug, G., Zhu, Y.G., Luo, L., Lei, M., Li, X., and Mulder, J. 2011. Distribution, speciation and availability of antimony (Sb) in soils and terrestrial plants from an active Sb mining area. Environmental Pollution, **159**: 2427–2434. doi:10.1016/j.envpol.2011.06.028.

Ontario Geoscience Laboratories. 2016. PSA : Method Code PSA-100 Procedure for the Determination of Particle Size Analysis by Laser with the Microtrac S3500 System.

Pahlsson, A.-M.B. 1989. Toxicity of heavy metals (Zn, Cu, Cd, Pb) to vascular plants. Water, Air, and Soil Pollution, **47**: 287–319. doi:10.1007/BF00279329.

Patterson, C.C. 1971. Lead in the environment. Connecticut Medicine, **35**: 347–352. doi:10.1016/0013-9327(73)90048-7.

Qi, C., Liu, G., Kang, Y., Lam, P.K.S., and Chou, C.-L. 2011. Assessment and distribution of antimony in soils around three coal mines, Anhui, China. Journal of the Air and Waste Management Association, **61**: 850–857. doi:10.3155/1047-3289.61.8.850.

Ramos, L., Hernandez, L.M., and Gonzalez, M.J. 1994. Sequential fraction of copper, lead, cadmium and zinc in soils from or near Donana National Park. Journal of Environmental Quality, **23**: 50–57. doi:10.2134/jeq1994.00472425002300010009x.

Rauret, G., López-Sánchez, J.F., Sahuquillo, A., Rubio, R., Davidson, C., Ure, A., and Quevauviller, P. 1999. Improvement of the BCR three step sequential extraction procedure prior to the certification of new sediment and soil reference materials. Journal of environmental monitoring, **1**: 57–61. doi:10.1039/a807854h.

Romo-Kröger, C.M. 2006. A qualitative study of atmospheric aerosols and particles deposited on flat membrane surfaces by microscopy and other techniques. Powder Technology, **161**: 235–241. doi:10.1016/j.powtec.2005.10.014.

Roper, A.J., Leverett, P., Murphy, T.D., and Williams, P. a. 2015. Stabilities of byströmite, MgSb2O6, ordoñezite, ZnSb2O6 and rosiaite, PbSb2O6, and their possible roles in limiting antimony mobility in the supergene zone. Mineralogical Magazine, **79**: 537–544. doi:10.1180/minmag.2015.079.3.03.

Roper, A.J., Williams, P. a., and Filella, M. 2012. Secondary antimony minerals: Phases that

control the dispersion of antimony in the supergene zone. Chemie der Erde - Geochemistry, **72**: 9–14. Elsevier GmbH. doi:10.1016/j.chemer.2012.01.005.

Ryan, P.C., Wall, A.J., Hillier, S., and Clark, L. 2002. Insights into sequential chemical extraction procedures from quantitative XRD: A study of trace metal partitioning in sediments related to frog malformites. Chemical Geology, **184**: 337–357. doi:10.1016/S0009-2541(01)00390-4.

Sanborn, P., Lamontagne, L., and Hendershot, W. 2011. Brunisolic soils of Canada: Gensis, distribution, and classification. Canadian Journal of Soil Science, **91**: 843–880. doi:10.4141/cjss10024.

Sanderson, P., Bolan, N., Bowman, M., and Ravi, N. 2010. Distribution and availability of metal contaminants in shooting range soils around Australia. Journal Of Plant Nutrition And Soil Science,: 65–67.

Sanei, H., Goodarzi, F., and Hilts, S. 2007. Site-specific natural background concentrations of metals in topsoil from the Trail region, British Columbia, Canada. Geochemistry: Exploration, Environment, Analysis, **7**: 41–47. doi:10.1144/1467-7873/06-114.

Sauve, S., Hendershot, W., and Allen, H.E. 2000. solid solution partitioning of metals in contaminated soils: dependence on pH, Total Metal Burden and Organic Matter. Environmental Science & Technology, **34**: 1125–1131. doi:10.1021/es9907764.

Sauve, S., Mcbride, M.B., and Hendershot, W.H. 1997. Soil Solution Speciation of Lead (II): Effects of Organic Matter and pH. Soil science society of america, **63**: 618–621.

doi:10.2136/sssaj1998.03615995006200030010x.

Scheinost, A.C., Rossberg, A., Vantelon, D., Xifra, I., Kretzschmar, R., Leuz, A.K., Funke, H., and Johnson, C.A. 2006. Quantitative antimony speciation in shooting-range soils by EXAFS spectroscopy. Geochimica et Cosmochimica Acta, **70**: 3299–3312. doi:10.1016/j.gca.2006.03.020.

Schindler, M., and Kyser, K.T. 2012. Shining light on black rock coatings in smelter impacted areas. Journal of the Geological Association of Canada, **39**: 148–157.

Schmitt, N., J.J, P., A.A., L., and M, H. 1979. surface soil as a potential source of lead exposure for young children. Canadian Medical Association Journal, **121**: 1474–1478.

Simony, P.S. 1979. Pre-Carboniferous basement near Trail, British Columbia. Canadian Journal of Earth Sciences, **16**: 1–11. doi:10.1139/e79-001.

Simony, P.S., Sevigny, J.H., Mortensen, J.K., and Roback, R.C. 2006. age and origin of trail gneiss complex: Basement to Quesnel terrane near Trail, southeastern British Columbia. Paleozoic Evolution and Metallogeny of Pericratonic Terranes at the Ancient Pacific Margin of North America, Canadian and Alaskan Cordillera: Geological Association of Canada, Special Paper, **45**: 50–15.

Smichowski, P. 2008. Antimony in the environment as a global pollutant: A review on analytical methodologies for its determination in atmospheric aerosols. Talanta, **75**: 2–14. doi:10.1016/j.talanta.2007.11.005.

Smith, K.S. 1999. Metal Sorption on Mineral Surfaces: An Overview with Examples Relating to

Mineral Deposits. Review in Economic Geology, **6A**–**6B**: 161–182.

Sundar, S., and Chakravarty, J. 2010. Antimony Toxicity. International Journal of Environmental Research and Public Health, **7**: 4267–4277. doi:10.3390/ijerph7124267.

Suzuki, K. 2006. Characterisation of airborne particulates and associated trace metals deposited on tree bark by ICP-OES, ICP-MS, SEM-EDX and laser ablation ICP-MS. Atmospheric Environment, **40**: 2626–2634. doi:10.1016/j.atmosenv.2005.12.022.

Swanson, S. 2007. Summary report of aquatic ecological risk. Trail British Columbia.

Tai, Y., McBride, M.B., and Li, Z. 2013. Evaluating specificity of sequential extraction for chemical forms of lead in artificially-contaminated and field-contaminated soils. Talanta, **107**: 183–188. doi:10.1016/j.talanta.2013.01.008.

Takaoka, M., Fukutani, S., Yamamoto, T., Horiuchi, M., Satta, N., Takeda, N., Oshita, K., Yoneda, M., Morisawa, S., and Tanaka, T. 2005. Determination of chemical form of antimony in contaminated soil around a smelter using X-ray absorption fine structure. Analytical sciences : the international journal of the Japan Society for Analytical Chemistry, **21**: 769–73. doi:10.2116/analsci.21.769.

Takeno, N. 2005. Atlas of Eh-pH diagrams Intercomparison of thermodynamic databases. National Institute of Advanced Industrial Science and Technology Tokyo,: 285. Available from http://scholar.google.com/scholar?hl=en&btnG=Search&q=intitle:Atlas+of+Eh-pH+diagrams+Intercomparison+of+thermodynamic+databases#0.

Tao, S., and Lin, B. 2000. Water soluble organic carbon and its measurement in soil and

sediment. Water Research, **34**: 1751–1755. doi:10.1016/S0043-1354(99)00324-3.

Tessier, A., Campbell, P.G.C., and Bisson, M. 1979. Sequential Extraction Procedure for the Speciation of Particulate Trace Metals. Analytical Chemistry, **51**: 844–851. doi:10.1021/ac50043a017.

Tighe, M., Lockwood, P., and Wilson, S. 2005. Adsorption of antimony(V) by floodplain soils, amorphous iron(III) hydroxide and humic acid. Journal of environmental monitoring : JEM, **7**: 1177–1185. doi:10.1039/b508302h.

United States Department of agriculture. 1996. Soil Survey Laboratory Methods Manual. doi:10.1021/ol049448l.

Vink, B.W. 1996. Stability relations of antimony and arsenic compounds in the light of revised and extended Eh-pH diagrams. Chemical Geology, **130**: 21–30. doi:10.1016/0009-2541(95)00183-2.

Vithanage, M., Rajapaksha, A.U., Dou, X., Bolan, N.S., Yang, J.E., and Ok, Y.S. 2013. Surface complexation modeling and spectroscopic evidence of antimony adsorption on iron-oxide-rich red earth soils. Journal of Colloid and Interface Science, **406**: 217–224. Elsevier Inc. doi:10.1016/j.jcis.2013.05.053.

Vitkova, M., Ettler, V., Sebek, O., Mihaljevic, M., Grygar, T., and Rohovec, J. 2009. The pH-dependent leaching of inorganic contaminants from secondary lead smelter fly ash. Journal of Hazardous Materials, **167**: 427–433. doi:10.1016/j.jhazmat.2008.12.136.

Van Vleek, B., Amarasiriwardena, D., and Xing, B. 2011. Investigation of distribution of soil

antimony using sequential extraction and antimony complexed to soil-derived humic acids molar mass fractions extracted from various depths in a shooting range soil. Microchemical Journal, **97**: 68–73. doi:10.1016/j.microc.2010.05.015.

Wilson, N.J., Craw, D., and Hunter, K. 2004. Antimony distribution and environmental mobility at an historic antimony smelter site, New Zealand. Environmental Pollution, **129**: 257–266. doi:10.1016/j.envpol.2003.10.014.

Wilson, S.C., Lockwood, P. V., Ashley, P.M., and Tighe, M. 2010. The chemistry and behaviour of antimony in the soil environment with comparisons to arsenic: A critical review. Environmental Pollution, **158**: 1169–1181. doi:10.1016/j.envpol.2009.10.045.

Xie, R.K., Seip, H.M., Leinum, J.R., Winje, T., and Xiao, J.S. 2005. Chemical characterization of individual particles (PM10) from ambient air in Guiyang City, China. Science of the Total Environment, **343**: 261–272. doi:10.1016/j.scitotenv.2004.10.012.

Zänker, H., Moll, H., Richter, W., Brendler, V., Hennig, C., Reich, T., Kluge, A., and Hüttig, G. 2002. The colloid chemistry of acid rock drainage solution from an abandoned Zn-Pb-Ag mine. Applied Geochemistry, **17**: 633–648. doi:10.1016/S0883-2927(01)00126-3.

Zimdahl, R.L., and Skogerboe, R.K. 1977. Behavior of Lead in Soil. Environmental Science & Technology, **11**: 1202–1207. doi:10.1021/es60136a004.

Zimmerman, A.J., and Weindorf, D.C. 2010. Heavy metal and trace metal analysis in soil by sequential extraction: a review of procedures. International journal of analytical chemistry, **2010**: 387803. doi:10.1155/2010/387803.

Appendices

Appendix A. Summary of profile horizons (relative to depth interval sampling) dominant site vegetation, wet and dry Munsell colours, and soil texture.

Sample ID	Depth		Site vegetation	Boundary Description	Colour		Texture
	start	end			dry	wet	
Profile 1							
LFH	0	13		sharp irregular			dominantly pine, minor poplar coarse - medium twig
Ae	13	19	dominantly pine, minor birch	sharp irregular discontinuous	10 YR 5/4 yellowish brown	10 YR 3/2 very dark greyish brown	sand
Bm1	19	27		distinct wavy	10 YR 5/6 yellowish brown	10 YR 3/4 dark yellowish brown	sand
Bm2-Bm3	30	40		diffuse smooth	10 YR 5/6 brownish yellow	10 YR 3/6 dark yellowish brown	sand
Bm3-BC	40	50		diffuse smooth	10 YR 7/6 yellow	10 YR 4/4 dark yellowish brown	sand

BC	50	60		*NA*	10 YR 6/6 brownish yellow	10 YR 4/4 dark yellowish brown	sand
BC-C	60	94		*NA*	10 YR 7/6 yellow	10 YR 4/4 dark yellowish brown	sand

Profile 2

LFH	0	9		distinct wavy			dominantly birch, minor pine, fine - medium twigs
Ae	2	12		distinct wavy discontinuous	10 YR 4/3 brown	10 YR 3/3 dark brown	loamy sand
Bm1	10	20		diffuse smooth	10 YR 5/6 yellowish brown	10 YR 3/6 dark yellowish brown	loamy sand
Bm2	20	30	dominantly birch, minor pine and acacia	diffuse smooth	10 YR 5/6 yellowish brown	10 YR 3/6 dark yellowish brown	loamy sand
Bm3	30	40		diffuse - sharp smooth	10 YR 5/6 yellowish brown	10 YR 3/6 dark yellowish brown	loamy sand
Bm4	40	50		abrupt smooth	10 YR 6/6 brownish yellow	7.5 YR 4/6 strong brown	loamy sand
BC	50	60		*NA*	10 YR 6/6 brownish yellow	10 YR 4/6 dark yellowish brown	loamy sand
IIC	60	94		*NA*	10 YR 6/4 light yellowish brown	10 YR 4/4 dark yellowish brown	loamy sand

Profile 3

LFH	0	9		sharp wavy			dominantly birch and minor pine needles
Ae	9	14		sharp wavy discontinuous	10 YR 7/1 light grey	10 YR 4/1 dark grey	loamy sand
Bm1	14	24	dominantly birch and minor pine	diffuse wavy	10 YR 5/4 yellowish brown	10 YR 4/4 dark yellowish brown	loamy sand
Bm2	24	33		sharp to diffuse smooth	10 YR 6/4 light yellowish brown	10 YR 4/4 dark yellowish brown	loamy sand
BC	33	39		diffuse smooth - wavy	10 YR 6/4 light yellowish brown	11 YR 4/4 dark yellowish brown	loamy sand
IIC	39	60		*NA*	10 YR 7/6 yellow	10 YR 5/6 yellowish brown	loamy sand
IIC	60	94		*NA*	10 YR 6/6 brownish yellow	10 YR 4/6 dark yellowish brown	loamy sand

Profile 4

LFH	0	8		sharp smooth			dominantly birch leaves, minor needles, abundant fine twigs, minor coarse twigs
Ae	8	12		sharp smooth	10 YR 6/4 light yellowish brown	10 YR 5/3 brown	sand
Bm1	12	20		sharp smooth	10 YR 6/3 pale brown	10 YR 5/4 brown	sand
Ahj	20	23	dominantly birch and minor pine and ferns	sharp - diffuse smooth - wavy	10 YR 6/4 light yellowish brown	10 YR 4/4 dark yellowish brown	sand
2Bm	23	33		diffuse smooth	10 YR 6/4 light yellowish brown	10 YR 4/3 brown	sand
3Ae&3Bm	33	42		diffuse smooth	10 YR 6/3 pale brown	10 YR 4/3 brown	sand
3Bm	42	52		sharp smooth	10 YR 6/3 pale brown	10 YR 4/3 brown	sand
4Bm	52	60		sharp smooth	10 YR 6/4 light yellowish brown	10 YR 4/6 dark yellowish brown	sand

4Bmi	60	67		*NA*	10 YR 6/6 brownish yellow	10 YR 4/6 dark yellowish brown	sand
4C	67	101		*NA*	10 YR 6/6 brownish yellow	10 YR 4/6 dark yellowish brown	sand

Profile 5

LFH	0	8		sharp smooth			dominantly maple leaves
Ahe	8	21		sharp wavy	10 YR 4/3 brown	10 YR 3/2 very dark grayish brown	sand
Bm1	21	31	abundant maple, poplar rare	diffuse smooth	10 YR 5/4 yellowish brown	10 YR 4/4 dark yellowish brown	sand
Bm2	31	43		diffuse smooth	10 YR 6/4 light yellowish brown	10 YR 4/6 dark yellowish brown	sand
BC	43	60		*NA*	10 YR 6/6 brownish yellow	10 YR 4/4 dark yellowish brown	sand
C	60	94		*NA*	10 YR 6/4 light yellowish brown	10 YR 5/4 yellowish brown	sand

Appendix B. Textural analysis of the < 2 mm fractions of selection soil horizons from Profiles 1 and 2.

Sample ID	% Sand	% Silt	% Clay
	Profile 1		
01_13-15	85.08	14.92	0.000
01_13-15	88.66	11.34	0.000
01_15-17	88.36	11.64	0.000
01_17-19	91.40	8.60	0.000
01_19-21	93.55	6.450	0.000
01_21-23	93.30	6.700	0.000
01_23-25	93.24	6.760	0.000
01_25-27	92.67	7.330	0.000
01_30-40	93.76	6.240	0.000
01_40-50	95.50	4.500	0.000
01_40-50	95.44	4.560	0.000
01_50-60	95.43	4.570	0.000
01_BC-C	96.32	3.680	0.000

Profile 2			
02_4-6	76.78	23.22	0.000
02_6-8	69.54	30.46	0.000
02_10-12 Bm1	73.22	26.78	0.000
02_10-12 char	69.30	30.70	0.000
02_10-12 char_DUP	68.88	31.12	0.000
02_12-14	71.43	28.57	0.000
02_14-16	71.97	28.03	0.000
02_17-19	72.10	27.90	0.000
02_17-19	72.89	27.11	0.000
02_19-21_DUP	71.72	28.28	0.000
02_21-23	71.62	28.38	0.000
02_23-27	72.38	27.62	0.000
02_30-40	73.96	26.04	0.000
02_40-50	74.52	25.48	0.000
02_BC	74.90	25.10	0.000
02_IIC	77.87	22.13	0.000

Appendix C. Soil pH (H_2O and $CaCl_2$) using a 1:2 and 1:4 (w:v) ratio for mineral and organic soils, respectively, soil reduction-oxidation potential (Eh in mV), soil conductivity (EC in µS) and loss on ignition (LOI, % OM) for all samples.

	Depth		pH		Eh	Conductivity	LOI
Sample ID	from	To	H_2O	$CaCl_2$	(+) mV	(µs) unless indicated	(% OM)
			Profile 1				
01_LFH	0	13	4.97	3.92	557.8	66.8	39.3
01_13-15	13	15	4.41	4.09	634.4	52.9	6.70
01_15-17	15	17	4.65	4.27	659.4	79.2	3.19
01_15-17_DUP							3.57
01_17-19	17	19	4.92	4.57	609.6	49.3	2.79
01_19-21	19	21	5.08	4.68	574.7	23.4	2.17
01_21-23	21	23	5.05	4.68	642.2	52.8	2.49
01_23-25	23	25	4.98	4.48	556	57.9	2.02
01_25-27	25	27	4.95	4.4	646.9	44.5	1.76
01_30-40	30	40	5.05	4.48	593.6	31.2	1.59

01_40-50	40	50	5.17	4.5	595.5	26.8	1.06
01_50-60	50	60	5.38	4.73	592.3	36.1	1.02
01_BC-C	60	94	5.29	4.53	579.1	30.8	1.00
01_BC-C_DUP	60	94	5.28	4.51	592.3	27.4	

Profile 2

02_LFH	0	9	4.2	4.08	670.2	669	58.7
02_4-6	4	6	4.36	3.85	500.7	137	9.30
02_6-8	6	8	4.46	4.1	504.5	123	8.51
02_10-12 Bm1	10	12	4.78	4.46	677	73.3	8.05
02_10-12 char	10	12	4.75	4.29	621.9	97.1	5.74
02_10-12 char_DUP	10	12					6.07
02_12-14	12	14	4.99	4.5	650.8	82.2	4.54
02_14-16	14	16	4.93	4.49	626.6	73.8	4.81
02_17-19	17	19	4.91	4.52	611.3	54.2	4.34
02_19-21	19	21	4.94	4.57	584.1	54.5	4.35
02_21-23	21	23	4.87	4.6	569.5	65.0	4.06
02_23-27	23	27	4.83	4.6	570.4	71.8	3.86
02_23-27_DUP	23	27	4.86	4.59	565.5	66.1	
02_30-40	30	40	5.2	4.88	541.8	65.5	3.48
02_40-50	40	56	5.03	4.83	546.4	59.4	3.07

02_BC	50	60	4.58	4.62	734.8	51.2	2.88
02_IIC	60	94	4.63	4.1	733.3	53.5	1.82

Profile 3

03_LFH	0	9	4.07	4.30	631.4	556	45.0
03_9-11	9	11	4.14	3.50	522.4	68.6	2.66
03_13-15	13	15	4.31	3.80	527.4	66.1	3.52
03_15-17	15	17	4.32	3.96	514.1	88.1	3.65
03_17-19	17	19	4.57	4.08	487.6	83.1	2.84
03_19-21	19	21	4.63	4.18	531.2	65.5	2.44
03_19-21_DUP	19	21	4.67	4.21	534.3	69.1	
03_21-23	21	23	4.67	4.26	531.3	63.3	2.22
03_11-13	11	13	4.19	3.75	521.5	87.8	2.63
03_25-27	25	27	4.71	4.27	527.8	62.4	1.95
03_27-29	27	29	4.7	4.32	524.4	57.4	1.80
03_27-29_DUP	27	29					1.91
03_BC	33	39	4.72	4.32	523.5	47.7	1.30
03_IIC	39	60	4.94	4.39	546.0	34.9	0.940
03_60-94	60	94	5.56	4.80	531.2	29.9	0.860

Profile 4

04_LFH	0	8	4.14	3.92	630.3	130	25.6
04_6-8	6	8	4.45	3.73	511.7	52.7	1.85
04_8-10	8	10	4.37	3.84	503.8	62.7	1.82
04_10-12	10	12	4.45	3.84	511.1	46.7	1.91
04_12-15	12	15	4.53	3.88	514.8	41.4	1.97
04_12-15_DUP	12	15	4.53	3.86	510.7	42.0	2.06
04_15-17	15	17	4.55	3.94	510.0	40.1	1.94
04_17-19	17	19	4.49	3.88	510.4	40.4	1.60
04_19-21	19	21	4.52	3.99	511.7	35.6	1.97
04_19-21_DUP	19	21					2.01
04_21-23	21	23	4.48	3.92	507.8	43.4	1.54
04_21-23_DUP	21	23					1.78
04_26-28	26	28	4.37	3.85	699.6	34.6	1.26
04_28-30	28	30	4.50	3.80	722.7	33.1	1.28
04_30-32	30	32	4.41	3.98	700.8	36.3	1.12

04_32-42	32	42	4.83	4.08	704.4	24.9	1.15
04_42-52	42	52	4.75	4.11	681.6	19.5	1.32
04_4Bm	52	60	4.83	4.68	695.7	53.7	2.04
04_4Bmi	60	67	5.00	4.50	672.0	57.8	1.81
04_4Bmi_DUP	60	67					1.85
04_4C	67	101	5.30	4.42	648.8	22.4	0.710
04_4C_DUP	67	101	5.18	4.39	647.5	25.8	

Profile 5

05_LFH	0	8	3.75	3.30	661.2	264	84.9
05_8-10	8	10	3.60	3.11	552.6	239	22.6
05_10-12	10	12	3.71	3.22	545.6	180	13.8
05_15-17	15	17	3.83	3.36	558.5	104	19.5
05_17-19	17	19	3.80	3.42	488.8	126	25.4
05_19-21	19	21	3.84	3.44	575.0	109	18.9
05_21-23	21	23	4.17	3.70	549.2	83.2	8.38
05_23-25	23	25	4.15	3.76	577.5	79.4	6.03
05_23-25_DUP	23	25	4.13	3.77	573.3	79.6	
05_25-27	25	27	4.20	3.80	575.4	73.6	4.75
05_30-40	30	40	4.31	4.11	585.9	65.9	3.35
05_40-50	40	50	4.46	4.04	591.4	71.5	2.00
05_50-60	50	60	4.39	3.82	594.0	70.4	1.64
05_C	60	94	4.84	3.96	610.1	42.0	2.06

Appendix D. Concentrations of $LiNO_3$ extractable (phytoavailable fraction) Pb and Sb concentrations in mg kg^{-1}, measured by ICP-MS (analytical detection limits are indicated by bold underneath Pb and Sb concentration columns), and amount extracted normalized to total Pb and Sb for all depth intervals in profiles 1 – 5.

Sample Number	Pb LiNO3	Sb LiNO3	Pb ICP-MS	Sb TD-ICPMS	Pb %Extracted	Sb %Extracted
	4	**2.9**				
			Profile 1			
01_LFH_us_e3	8.50	<DL	7790.02	415.60	0.11	<DL
01_13-15_e3	<DL	<DL	4630.70	228.48	<DL	<DL
01_15-17_e3	<DL	<DL	1747.05	102.81	<DL	<DL
01_17-19_e3	<DL	<DL	361.65	50.94	<DL	<DL
01_19-21_e3	<DL	<DL	150.46	39.36	<DL	<DL
01_21-23_e3	<DL	<DL	87.71	35.13	<DL	<DL
01_23-25_e3	<DL	<DL	75.74	24.38	<DL	<DL
01_25-27_e3	<DL	<DL	59.04	12.99	<DL	<DL
01_30-40_e3	<DL	<DL	72.52	7.25	<DL	<DL
01_40-50_e3	<DL	<DL	72.50	1.67	<DL	<DL
01_50-60_e3	<DL	<DL	67.66	1.20	<DL	<DL

01_BC-C_e3	<DL	<DL	65.53	0.90	<DL	<DL

Profile 2

02_LFH_e3	11.19	<DL	19777.16	737.97	0.06	<DL
02_4-6_e3	4.26	<DL	14058.23	353.66	0.03	<DL
02_6-8_e3	5.22	<DL	17609.57	553.19	0.03	<DL
02_10-12 Bm1_e3	<DL	<DL	2282.42	160.76	<DL	<DL
02_10-12 char_e3	<DL	<DL	7048.78	303.08	<DL	<DL
02_10-12 char_e3_DUP	<DL	<DL	6905.80	302.25	<DL	<DL
02_12-14_e3	<DL	<DL	1791.46	166.33	<DL	<DL
02_14-16_e3	<DL	<DL	776.99	108.69	<DL	<DL
02_17-19_e3	<DL	<DL	299.87	74.39	<DL	<DL
02_19-21_e3	<DL	<DL	209.15	56.25	<DL	<DL
02_21-23_e3	<DL	<DL	188.61	51.57	<DL	<DL
02_23-27_e3	<DL	<DL	139.96	35.67	<DL	<DL
02_30-40_e3	<DL	<DL	100.22	18.04	<DL	<DL
02_40-50_e3	<DL	<DL	87.11	6.50	<DL	<DL

02_BC_e3	<DL	<DL	74.09	2.32	<DL	<DL
02_IIC_e3	<DL	<DL	117.82	<DL	<DL	<DL

Profile 3

03_LFH_e3	8.22	<DL	26376.77	453.48	0.03	<DL
03_9-11_e3	4.20	<DL	2945.04	64.78	0.14	<DL
03_11-13_e3	<DL	<DL	2304.80	62.11	<DL	<DL
03_13-15_e3	<DL	<DL	1792.27	62.77	<DL	<DL
03_15-17_e3	<DL	<DL	885.92	56.38	<DL	<DL
03_17-19_e3	<DL	<DL	180.79	42.15	<DL	<DL
03_19-21_e3	<DL	<DL	115.10	29.14	<DL	<DL
03_21-23_e3	<DL	<DL	89.68	21.32	<DL	<DL
03_25-27_e3	<DL	<DL	102.57	17.39	<DL	<DL
03_27-29_e3	<DL	<DL	93.72	17.68	<DL	<DL
03_27-29_e3_DUP	<DL	<DL	96.43	17.72	<DL	<DL
03_BC_e3	<DL	<DL	74.90	12.20	<DL	<DL
03_IIC_e3	<DL	<DL	80.94	5.21	<DL	<DL
03_60-94_e3	<DL	<DL	83.35	1.55	<DL	<DL

Profile 4

04_LFH_e3	<DL	<DL	4949.61	245.17	<DL	<DL
04_6-8_e3	<DL	<DL	621.09	36.56	<DL	<DL
04_8-10_e3	<DL	<DL	582.59	37.77	<DL	<DL
04_10-12_e3	<DL	<DL	1080.89	56.27	<DL	<DL
04_12-15_e3	<DL	<DL	1107.57	62.84	<DL	<DL
04_12-15_e3_DUP	<DL	<DL	1143.05	65.77	<DL	<DL
04_15-17_e3	<DL	<DL	1081.10	66.74	<DL	<DL
04_17-19_e3	<DL	<DL	848.85	51.60	<DL	<DL
04_19-21_e3	<DL	<DL	1500.93	102.80	<DL	<DL
04_19-21_e3_DUP	<DL	<DL	1555.03	105.82	<DL	<DL
04_21-23_e3	<DL	<DL	1695.45	94.75	<DL	<DL
04_21-23_e3_DUP	<DL	<DL	1713.26	93.21	<DL	<DL
04_26-28_e3	<DL	<DL	1208.83	60.18	<DL	<DL
04_28-30_e3	<DL	<DL	1030.39	43.57	<DL	<DL

04_30-32_e3	<DL	<DL	906.41	36.95	<DL	<DL
04_32-42_e3	<DL	<DL	644.44	39.33	<DL	<DL
04_42-52_e3	<DL	<DL	1103.56	63.92	<DL	<DL
04_4Bm52-60_e3	<DL	<DL	110.21	8.23	<DL	<DL
04_4Bm_e3	<DL	<DL	73.98	1.12	<DL	<DL
04_4Bm_e3_DUP	<DL	<DL	71.70	1.16	<DL	<DL
04_4C_e3	<DL	<DL	70.72	0.83	<DL	<DL

Profile 5

05_LFH	<DL	<DL	8287.02	329.61	<DL	<DL
05_8-10	7.18	1.59	10344.96	308.72	0.07	0.51
05_10-12	4.62	<DL	7398.99	234.04	0.06	<DL
05_15-17	4.73	<DL	11506.73	334.29	0.04	<DL
05_17-19	5.47	<DL	15523.08	449.63	0.04	<DL
05_19-21	6.56	<DL	11218.61	284.13	0.06	<DL
05_21-23	<DL	<DL	5012.01	87.08	<DL	<DL
05_23-25	<DL	<DL	2823.95	50.83	<DL	<DL
05_25-27	<DL	<DL	1966.71	35.60	<DL	<DL
05_30-40	<DL	<DL	331.56	18.24	<DL	<DL
05_40-50	<DL	<DL	78.78	3.88	<DL	<DL
05_50-60	<DL	<DL	72.03	1.57	<DL	<DL
05_C	<DL	<DL	71.51	1.27	<DL	<DL

Appendix E. Concentrations of $CaCl_2$ extractable (exchangeable fraction) Pb and Sb concentrations in mg kg^{-1}, measured by ICP-MS (analytical detection limits are indicated in bold underneath Pb and Sb concentration columns), and amount extracted normalized to total Pb and Sb in the soil in all depth intervals in soil profiles 1 – 5.

Sample Number	Pb	Sb	Pb	Sb
	mg kg^{-1}	mg kg^{-1}	% Extracted	% Extracted
	0.06	**0.07**		
		Profile 1		
01_LFH_us_e1	15.95	<DL	0.20	<DL
01_13-15_e1	3.25	<DL	0.07	<DL
01_15-17_e1	0.77	<DL	0.04	<DL
01_15-17_e1_DUP	0.84	<DL		
01_17-19_e1	0.07	<DL	0.02	<DL
01_19-21_e1	<DL	<DL	<DL	<DL
01_21-23_e1	<DL	<DL	<DL	<DL
01_23-25_e1	<DL	<DL	<DL	<DL
01_25-27_e1	<DL	<DL	<DL	<DL
01_30-40_e1	<DL	<DL	<DL	<DL
01_40-50_e1	<DL	<DL	<DL	<DL
01_50-60_e1	<DL	<DL	<DL	<DL
01_BC-C_e1	<DL	<DL	<DL	<DL

Profile 2

02_LFH_e1	15.60	0.08	0.08	<DL
02_4-6_e1	19.90	<DL	0.14	<DL
02_6-8_e1	19.15	0.09	0.11	0.02
02_10-12 Bm1_e1	1.07	<DL	0.05	<DL
02_10-12 charcoal_e1	4.25	0.08	0.06	0.03
02_10-12 charcoal_e1_DUP	4.21	0.08	0.06	0.03
02_12-14_e1	<DL	<DL	<DL	<DL
02_14-16_e1	<DL	<DL	<DL	<DL
02_17-19_e1	<DL	<DL	<DL	<DL
02_19-21_e1	<DL	<DL	<DL	<DL
02_21-23_e1	<DL	<DL	<DL	<DL
02_23-27_e1	<DL	<DL	<DL	<DL
02_30-40_e1	<DL	<DL	<DL	<DL
02_40-50_e1	<DL	<DL	<DL	<DL
02_BC_e1	<DL	<DL	<DL	<DL
02_IIC_e1	<DL	<DL	<DL	<DL

Profile 3				
03_LFH_e1	39.85	0.08	0.15	0.02
03_9-11_e1	11.33	<DL	0.38	<DL
03_11-13_e1	7.16	<DL	0.31	<DL
03_13-15_e1	3.07	<DL	<DL	<DL
03_15-17_e1	<DL	<DL	<DL	<DL
03_17-19_e1	<DL	<DL	<DL	<DL
03_19-21_e1	<DL	<DL	<DL	<DL
03_21-23_e1	<DL	<DL	<DL	<DL
03_25-27_e1	<DL	<DL	<DL	<DL
03_27-29_e1	0.08	<DL	0.00	<DL
03_27-29_e1_DUP	<DL	<DL	<DL	<DL
03_BC_e1	<DL	<DL	<DL	<DL
03_IIC_e1	<DL	<DL	<DL	<DL
03_60-94_e1	<DL	<DL	<DL	<DL

Profile 4

04_LFH_e1	8.02	<DL	0.16	<DL
04_6-8_e1	2.40	<DL	0.39	<DL
04_8-10_e1	1.31	<DL	0.22	<DL
04_10-12_e1	2.23	<DL	0.21	<DL
04_12-15_e1	2.88	<DL	0.26	<DL
04_12-15_e1_DUP	2.81	<DL	0.25	<DL
04_15-17_e1	2.91	<DL	0.27	<DL
04_17-19_e1	2.56	<DL	0.30	<DL
04_19-21_e1	3.76	<DL	0.25	<DL
04_19-21_e1_DUP	3.89	<DL	0.25	<DL
04_21-23_e1	4.56	<DL	0.27	<DL
04_21-23_e1_DUP	4.32	<DL	0.25	<DL
04_26-28_e1	4.01	<DL	0.33	<DL
04_28-30_e1	3.82	<DL	0.37	<DL
04_30-32_e1	3.56	<DL	0.39	<DL
04_32-42_e1	1.25	<DL	0.19	<DL
04_42-52_e1	1.82	<DL	0.16	<DL
04_4Bm52-60_e1	<DL	<DL	<DL	<DL
04_4Bm_e1	<DL	<DL	<DL	<DL
04_4Bm_e1_DUP	<DL	<DL	<DL	<DL
04_4C_e1	<DL	<DL	<DL	<DL

Profile 5

05_LFH	12.45	<DL	0.15	<DL
05_8-10	18.60	<DL	0.18	<DL
05_10-12	11.50	<DL	0.16	<DL
05_15-17	11.00	<DL	0.10	<DL
05_17-19	16.20	<DL	0.10	<DL
05_19-21	13.35	<DL	0.12	<DL
05_21-23	4.89	<DL	0.10	<DL
05_23-25	3.55	<DL	0.13	<DL
05_25-27	2.58	<DL	0.13	<DL
05_30-40	0.25	<DL	0.08	<DL
05_40-50	<DL	<DL	<DL	<DL
05_50-60	<DL	<DL	<DL	<DL
05_C	<DL	<DL	<DL	<DL

Appendix F. Concentrations of Na-Citrate – Dithionite (CD) extractable (reducible fraction) Pb and Sb concentrations in mg kg^{-1}, measured by ICP-MS (analytical detection limits are indicated in bold underneath Pb and Sb concentration columns), and amount extracted normalized to total Pb and Sb in the soil in all depth intervals in soil profiles 1 – 5.

Sample Number	Fe ($mg\ kg^{-1}$)	Pb ($mg\ kg^{-1}$)	Sb ($mg\ kg^{-1}$)	Pb ($mg\ kg^{-1}$)	Sb ($mg\ kg^{-1}$)	Pb	Sb
	CD	CD	CD	TD ICP-MS	TD ICP-MS	% Extracted	% Extracted
	1	**0.06**	**0.07**				
			Profile 1				
01_LFH_us_e1	2750.00	183.00	13.20	7790.02	415.60	2.35	3.18
01_13-15_e1	3660.00	75.20	23.60	4630.70	228.48	1.62	10.33
01_15-17_e1	3280.00	8.63	13.40	1747.05	102.81	0.49	13.03
01_17-19_e1	2510.00	14.10	6.04	361.65	50.94	3.90	11.86
01_19-21_e1	2670.00	8.83	5.23	150.46	39.36	5.87	13.29
01_21-23_e1	2350.00	2.27	3.75	87.71	35.13	2.59	10.67

01_23-25_e1	2530.00	2.13	3.01	75.74	24.38	2.81	12.35
01_25-27_e1	2890.00	1.97	2.66	59.04	12.99	3.34	20.47
01_30-40_e1	3070.00	3.27	1.22	72.52	7.25	4.51	16.82
01_40-50_e1	3170.00	3.15	0.40	72.50	1.67	4.34	23.67
01_50-60_e1	3020.00	3.09	<DL	67.66	1.20	4.57	<DL
01_BC-C_e1	2880.00	1.31	<DL	65.53	0.90	2.00	<DL

Profile 2

02_LFH_e1	4830.00	294.00	20.90	19777.16	737.97	1.49	2.83
02_4-6_e1	7200.00	480.00	42.60	14058.23	353.66	3.41	12.05
02_6-8_e1	9130.00	447.00	83.90	17609.57	553.19	2.54	15.17
02_10-12 Bm1_e1	5770.00	233.00	25.20	2282.42	160.76	10.21	15.68
02_10-12 char_e1	7320.00	366.00	49.00	7048.78	303.08	5.19	16.17
02_10-12 char_e1_DUP	7190.00	360.00	48.60	6905.80	302.25	5.21	16.08
02_12-14_e1	6280.00	127.00	26.10	1791.46	166.33	7.09	15.69
02_14-16_e1	5650.00	60.70	15.70	776.99	108.69	7.81	14.44
02_17-19_e1	5880.00	20.60	10.80	299.87	74.39	6.87	14.52
02_19-21_e1	5930.00	12.70	8.67	209.15	56.25	6.07	15.41
02_21-23_e1	6320.00	11.30	8.44	188.61	51.57	5.99	16.37
02_23-27_e1	6240.00	8.61	5.32	139.96	35.67	6.15	14.92
02_30-40_e1	5810.00	4.49	2.41	100.22	18.04	4.48	13.36
02_40-50_e1	4950.00	2.36	0.71	87.11	6.50	2.71	10.90

02_BC_e1	5280.00	2.18	0.32	74.09	2.32	2.94	13.62
02_IIC_e1	3970.00	3.39	<DL	177.82	<DL	1.91	<DL

Profile 3

03_LFH_e1	4750.00	380.00	29.50	26376.77	453.48	1.44	6.51
03_9-11_e1	1520.00	13.30	9.03	2945.04	64.78	0.45	13.94
03_11-13_e1	3240.00	156.00	10.10	2304.80	62.11	6.77	16.26
03_13-15_e1	6920.00	68.00	10.00	1792.27	62.77	3.79	15.93
03_15-17_e1	7280.00	51.10	8.98	885.92	56.38	5.77	15.93
03_17-19_e1	7850.00	14.50	8.05	180.79	42.15	8.02	19.10
03_19-21_e1	6430.00	5.83	5.47	115.10	29.14	5.07	18.77
03_21-23_e1	5660.00	3.43	4.29	89.68	21.32	3.82	20.12
03_25-27_e1	5270.00	5.40	3.84	102.57	17.39	5.26	22.09
03_27-29_e1	4500.00	4.86	3.26	93.72	17.68	5.19	18.44
03_27-29_e1_DUP	4770.00	4.52	3.38	96.43	17.72	4.69	19.08
03_BC_e1	3990.00	2.39	2.40	74.90	12.20	3.19	19.67
03_IIC_e1	2930.00	2.65	1.32	80.94	5.21	3.27	25.36
03_60-94_e1	2850.00	4.30	<DL	83.35	1.55	5.16	<DL

Profile 4

04_LFH_e1	2290.00	12.90	4.97	4949.61	245.17	0.26	2.03
04_6-8_e1	174.00	57.20	1.51	621.09	36.56	9.21	4.13
04_8-10_e1	149.00	53.10	1.63	582.59	37.77	9.11	4.32
04_10-12_e1	185.00	99.10	2.03	1080.89	56.27	9.17	3.61
04_12-15_e1	3930.00	33.20	8.60	1107.57	62.84	3.00	13.68
04_12-15_e1_DUP	240.00	92.10	2.17	1143.05	65.77	8.06	3.30
04_15-17_e1	534.00	103.00	4.53	1081.10	66.74	9.53	6.79
04_17-19_e1	3740.00	28.50	7.50	848.85	51.60	3.36	14.53
04_19-21_e1	4370.00	8.06	13.60	1500.93	102.80	0.54	13.23
04_19-21_e1_DUP	4260.00	11.80	14.20	1555.03	105.82	0.76	13.42
04_21-23_e1	128.00	120.00	3.25	1695.45	94.75	7.08	3.43
04_21-23_e1_DUP	245.00	121.00	3.10	1713.26	93.21	7.06	3.33
04_26-28_e1	3220.00	77.90	8.44	1208.83	60.18	6.44	14.03
04_28-30_e1	3150.00	64.60	7.02	1030.39	43.57	6.27	16.11

04_30-32_e1	3270.00	75.50	5.81	906.41	36.95	8.33	15.72
04_32-42_e1	36.00	52.50	1.40	644.44	39.33	8.15	3.56
04_42-52_e1	222.00	96.80	2.68	1103.56	63.92	8.77	4.19
04_4Bm52-60_e1	<DL	5.60	<DL	110.21	8.23	5.08	<DL
04_4Bm_e1	<DL	1.53	<DL	73.98	1.12	2.07	<DL
04_4Bm_e1_DUP	<DL	1.46	<DL	71.70	1.16	2.04	<DL
04_4C_e1	<DL	0.82	<DL	70.72	0.83	1.16	<DL

Profile 5

05_LFH	1470.00	135.00	3.74	8287.02	329.61	1.63	1.13
05_8-10	10900.00	278.00	29.50	10344.96	308.72	2.69	9.56
05_10-12	9150.00	150.00	24.30	7398.99	234.04	2.03	10.38
05_15-17	2300.00	1110.00	11.90	11506.73	334.29	9.65	3.56
05_17-19	10900.00	342.00	44.70	15523.08	449.63	2.20	9.94
05_19-21	7730.00	211.00	25.90	11218.61	284.13	1.88	9.12
05_21-23	5630.00	71.10	7.98	5012.01	87.08	1.42	9.16
05_23-25	5170.00	30.00	4.65	2823.95	50.83	1.06	9.15
05_25-27	5970.00	20.40	4.31	1966.71	35.60	1.04	12.11
05_30-40	5080.00	33.80	2.87	331.56	18.24	10.19	15.74
05_40-50	5060.00	1.58	0.64	78.78	3.88	2.01	16.49
05_50-60	5090.00	1.48	<DL	72.03	1.57	2.05	<DL
05_C	3370.00	1.81	<DL	71.51	1.27	2.53	<DL

Appendix G. Concentrations of H_2O_2-NH_4OAc-HNO_3 extractable (oxidizable fraction) Pb and Sb concentrations in mg kg^{-1}, measured by ICP-MS (analytical detection limits are indicated in bold underneath Pb and Sb concentration columns), and amount extracted normalized to total Pb and Sb in the soil in all depth intervals in soil profiles 1 – 5.

Sample Number	Pb mg kg^{-1} H_2O_2-NH_4OAc-HNO_3 **0.06**	Sb mg kg^{-1} H_2O_2-NH_4OAc-HNO_3 **0.07**	Pb mg kg^{-1} TD-ICP-MS	Sb mg kg^{-1} TD-ICPMS	Pb % Extracted	Sb % Extracted
			Profile 1			
01_LFH_us_e1	759.00	40.10	7790.02	415.60	9.74	9.65
01_13-15_e1	767.00	8.54	4630.70	228.48	16.56	3.74
01_15-17_e1	359.00	4.55	1747.05	102.81	20.55	4.43
01_17-19_e1	34.90	2.28	361.65	50.94	9.65	4.48
01_19-21_e1	8.04	1.72	150.46	39.36	5.34	4.37
01_21-23_e1	4.11	1.09	87.71	35.13	4.69	3.10
01_23-25_e1	1.55	0.53	75.74	24.38	2.05	2.17
01_25-27_e1	2.27	0.17	59.04	12.99	3.85	1.29

01_30-40_e1	2.65	0.31	72.52	7.25	3.65	4.28
01_40-50_e1	2.02	<DL	72.50	1.67	2.79	<DL
01_50-60_e1	2.11	<DL	67.66	1.20	3.12	<DL
01_BC-C_e1	1.21	<DL	65.53	0.90	1.85	<DL

Profile 2

02_LFH_e1	2710.00	56.80	19777.16	737.97	13.70	7.70
02_4-6_e1	1750.00	18.30	14058.23	353.66	12.45	5.17
02_6-8_e1	2020.00	17.40	17609.57	553.19	11.47	3.15
02_10-12 Bm1_e1	208.00	9.63	2282.42	160.76	9.11	5.99
02_10-12 char_e1	1130.00	12.70	7048.78	303.08	16.03	4.19
02_10-12 char_e1_DUP	1020.00	12.50	6905.80	302.25	14.77	4.14
02_12-14_e1	206.00	8.11	1791.46	166.33	11.50	4.88
02_14-16_e1	73.10	6.30	776.99	108.69	9.41	5.80
02_17-19_e1	25.70	4.43	299.87	74.39	8.57	5.96
02_19-21_e1	18.50	3.01	209.15	56.25	8.85	5.35
02_21-23_e1	14.90	2.38	188.61	51.57	7.90	4.62
02_23-27_e1	10.30	1.88	139.96	35.67	7.36	5.27
02_30-40_e1	6.76	1.22	100.22	18.04	6.75	6.76
02_40-50_e1	5.94	0.32	87.11	6.50	6.82	4.84
02_BC_e1	3.08	<DL	74.10	2.32	4.16	2.13
02_IIC_e1	4.46	<DL	177.82	<DL	2.51	<DL

Profile 3

03_LFH_e1	3590.00	33.80	26376.77	453.48	13.61	7.45
03_9-11_e1	404.00	1.34	2945.04	64.78	13.72	2.07
03_11-13_e1	214.00	1.65	2304.80	62.11	9.29	2.66
03_13-15_e1	96.00	1.54	1792.27	62.77	5.36	2.45
03_15-17_e1	10.70	0.72	885.92	56.38	1.21	1.27
03_17-19_e1	5.46	0.92	180.79	42.15	3.02	2.18
03_19-21_e1	4.07	0.37	115.10	29.14	3.54	1.28
03_21-23_e1	174.00	1.14	89.68	21.32	194.03	5.35
03_25-27_e1	4.08	0.38	102.57	17.39	3.98	2.17
03_27-29_e1	4.70	0.36	93.72	17.68	5.02	2.06
03_27-29_e1_DUP	4.53	0.22	96.43	17.72	4.70	1.24
03_BC_e1	3.24	0.32	74.90	12.20	4.33	2.62
03_IIC_e1	2.53	<DL	80.94	5.21	3.13	<DL
03_60-94_e1	0.99	<DL	83.35	1.55	1.19	<DL

Profile 4

04_LFH_e1	731.00	23.70	4949.61	245.17	14.77	9.67
04_6-8_e1	19.80	1.35	621.09	36.56	3.19	3.69
04_8-10_e1	42.90	2.14	582.59	37.77	7.36	5.67
04_10-12_e1	85.90	2.59	1080.89	56.28	7.95	4.60
04_12-15_e1	156.00	1.40	1107.57	62.84	14.09	2.23
04_12-15_e1_DUP	89.40	3.34	1143.05	65.77	7.82	5.08
04_15-17_e1	64.40	2.51	1081.10	66.74	5.96	3.76
04_17-19_e1	115.00	0.72	848.85	51.60	13.55	1.39
04_19-21_e1	226.00	2.23	1500.93	102.80	15.06	2.17
04_19-21_e1_DUP	232.00	2.37	1555.03	105.82	14.92	2.24
04_21-23_e1	126.00	4.82	1695.45	94.75	7.43	5.09
04_21-23_e1_DUP	140.00	4.45	1713.26	93.21	8.17	4.77
04_26-28_e1	104.00	1.18	1208.83	60.18	8.60	1.96
04_28-30_e1	92.10	1.03	1030.39	43.57	8.94	2.36
04_30-32_e1	63.50	0.71	906.41	36.95	7.01	1.92
04_32-42_e1	49.80	2.03	644.44	39.33	7.73	5.16

04_42-52_e1	98.80	3.60	1103.56	63.92	8.95	5.63
04_4Bm52-60_e1	5.89	0.80	110.21	8.23	5.34	9.67
04_4Bm_e1	2.15	<DL	73.98	1.13	2.91	<DL
04_4Bm_e1_DUP	2.07	<DL	71.70	1.16	2.89	<DL
04_4C_e1	2.13	<DL	70.72	0.83	3.01	<DL

Profile 5

05_LFH	715.00	38.30	8287.02	329.61	8.63	11.62
05_8-10	1310.00	11.80	10344.96	308.72	12.66	3.82
05_10-12	899.00	9.89	7398.99	234.04	12.15	4.23
05_15-17	1120.00	27.00	11506.73	334.29	9.73	8.08
05_17-19	2060.00	21.80	15523.08	449.63	13.27	4.85
05_19-21	1800.00	13.10	11218.61	284.13	16.05	4.61
05_21-23	842.00	4.93	5012.01	87.08	16.80	5.66
05_23-25	558.00	3.21	2823.95	50.83	19.76	6.32
05_25-27	404.00	2.51	1966.71	35.60	20.54	7.05
05_30-40	17.80	0.84	331.56	18.24	5.37	4.59
05_40-50	4.10	<DL	78.78	3.88	5.20	<DL
05_50-60	2.46	<DL	72.03	1.57	3.42	<DL
05_C	2.70	<DL	71.51	1.27	3.78	<DL

Appendix H. Concentrations of $Na_4P_2O_7$ extractable (organic matter fraction) Pb and Sb concentrations in mg kg^{-1}, measured by ICP-MS (analytical detection limits are indicated by bold underneath Pb and Sb concentration columns), and amount extracted normalized to total Pb and Sb for all depth intervals in profiles 1 – 5.

Sample Number	Pb	Sb	Pb	Sb	Pb	Sb
	mg kg^{-1}	mg kg^{-1}	mg kg^{-1}	mg kg^{-1}	% Extracted	% Extracted
	0.27	**1.11**	TD-ICP-MS	TD-ICP-MS		
			Profile 1			
01_LFH_us_e1	954.44	25.23	7790.02	415.60	12.25	6.07
01_13-15_e1	183.60	5.68	4630.70	228.48	3.96	2.49
01_15-17_e1	157.29	5.13	1747.05	102.81	9.00	4.99
01_17-19_e1	6.00	1.89	361.65	50.94	1.66	3.70
01_19-21_e1	1.33	<DL	150.46	39.36	0.88	<DL
01_21-23_e1	<DL	1.61	87.71	35.13	<DL	4.58
01_23-25_e1	2.00	1.21	75.74	24.38	2.64	4.97
01_25-27_e1	0.85	<DL	59.04	12.99	1.45	<DL
01_30-40_e1	0.37	<DL	72.52	7.25	0.51	<DL

01_40-50_e1	0.45	<DL	72.50	1.67	0.62	<DL
01_50-60_e1	0.36	<DL	67.66	1.20	0.54	<DL
01_BC-C_e1	425.31	5.43	65.53	0.90	649.00	601.73

Profile 2

02_LFH_e1	2409.36	8.77	19777.16	737.97	12.18	1.19
02_4-6_e1	1660.16	14.77	14058.23	353.66	11.81	4.18
02_6-8_e1	1899.24	22.15	17609.57	553.19	10.79	4.00
02_10-12 Bm1_e1	196.61	12.16	2282.42	160.76	8.61	7.57
02_10-12 charcoal_e1	806.43	18.87	7048.78	303.08	11.44	6.23
02_12-14_e1	108.52	10.17	1791.46	166.33	6.06	6.12
02_14-16_e1	40.31	7.27	776.99	108.69	5.19	6.69
02_17-19_e1	3.19	3.43	299.87	74.39	1.06	4.61
02_19-21_e1	4.82	3.06	209.15	56.25	2.31	5.44
02_21-23_e1	3.02	3.12	188.61	51.57	1.60	6.05
02_23-27_e1	1.51	1.99	139.96	35.67	1.08	5.59
02_30-40_e1	<DL	<DL	100.22	18.04	<DL	<DL
02_40-50_e1	<DL	<DL	87.11	6.50	<DL	<DL
02_BC_e1	<DL	<DL	74.09	2.32	<DL	<DL

02_IIC_e1	0.51	<DL	177.82	<DL	0.29	<DL

Profile 3

03_LFH_e1	2416.91	4.71	26376.77	453.48	9.16	1.04
03_9-11_e1	310.76	2.63	2945.04	64.78	10.55	4.05
03_11-13_e1	209.45	3.75	2304.80	21.32	9.09	17.59
03_13-15_e1	116.49	4.10	1792.27	62.11	6.50	6.60
03_15-17_e1	49.19	3.42	885.92	62.77	5.55	5.45
03_17-19_e1	3.26	2.05	180.79	56.38	1.80	3.63
03_19-21_e1	1.51	1.41	115.10	42.15	1.31	3.34
03_21-23_e1	0.64	<DL	89.68	29.14	0.71	0.85
03_25-27_e1	0.70	<DL	102.57	17.39	0.68	<DL
03_27-29_e1	0.00	<DL	93.72	17.68	0.00	<DL
03_BC_e1	0.29	<DL	74.90	12.20	0.39	<DL
03_IIC_e1	0.65	<DL	80.94	5.21	0.81	<DL
03_60-94_e1	<DL	<DL	83.35	1.55	<DL	<DL

Profile 4

04_LFH_e1	447.43	3.25	4949.61	245.17	9.04	1.32
04_6-8_e1	36.68	1.40	621.09	36.56	5.91	3.84
04_8-10_e1	48.20	2.60	582.59	37.77	8.27	6.89
04_10-12_e1	98.58	3.72	1080.89	56.27	9.12	6.61
04_12-15_e1	100.72	2.29	1107.57	62.84	9.09	3.64
04_15-17_e1	91.46	4.66	1081.10	66.74	8.46	6.98
04_17-19_e1	69.12	3.68	848.85	51.60	8.14	7.14
04_19-21_e1	113.28	2.56	1500.93	102.80	7.55	2.49
04_21-23_e1	105.36	2.45	1695.45	94.75	6.21	2.59
04_26-28_e1	107.08	2.55	1208.83	60.18	8.86	4.23
04_28-30_e1	70.32	2.12	1030.39	43.57	6.82	4.86
04_30-32_e1	65.05	1.55	906.41	36.95	7.18	4.19
04_32-42_e1	50.44	3.23	644.44	39.33	7.83	8.22
04_42-52_e1	84.80	3.48	1103.56	63.92	7.68	5.44
04_4Bm52-60_e1	1.32	<DL	110.21	8.23	1.20	<DL

04_4Bm_e1	<DL	<DL	73.98	1.12	<DL	<DL
04_4C_e1	<DL	<DL	70.72	0.83	<DL	<DL

Profile 5

05_LFH	927.85	2.35	8287.02	329.61	11.20	0.71
05_8-10	1603.85	17.07	10344.96	308.72	15.50	5.53
05_10-12	1081.44	16.03	7398.99	234.04	14.62	6.85
05_15-17	1612.46	20.78	11506.73	334.29	14.01	6.22
05_17-19	2439.80	34.64	15523.08	449.63	15.72	7.70
05_19-21	1581.32	14.25	11218.61	284.13	14.10	5.02
05_21-23	505.65	3.20	5012.01	87.08	10.09	3.68
05_23-25	298.68	2.52	2823.95	50.83	10.58	4.96
05_25-27	168.78	1.54	1966.71	35.60	8.58	4.32
05_30-40	12.09	<DL	331.56	18.24	3.64	<DL
05_40-50	<DL	<DL	78.78	3.88	<DL	<DL
05_50-60	<DL	<DL	72.03	1.57	<DL	<DL
05_C	0.90	<DL	71.51	1.27	1.26	<DL

Appendix I. Total organic carbon (TOC) measured in mg kg^{-1} analysis on $CaCl_2$ extract solutions for all profiles. Sample duplicates are indicated by "DUP" at the end of each sample ID, standards (~ 10 ppm organic C solution) and blanks (Milli-Q water) were also run approximately every 10 samples.

$CaCl_2$ Extractable TOC (mg kg^{-1})

Extraction Number	Sample Number	TOC mg kg^{-1}
	Profile 1	
1	blank	0.15
2	standard	11.57
18	01_LFH_us_e1	1.45
3	01_13-15_e1	0.50
4	01_15-17_e1	0.25
5	01_15-17_e1_DUP	0.30
6	01_17-19_e1	0.18
7	01_19-21_e1	8.12
8	01_21-23_e1	0.35
9	01_23-25_e1	0.28
10	01_25-27_e1	0.31
11	01_30-40_e1	0.24
12	01_40-50_e1	0.20
13	01_40-50_e1	0.19

16	01_50-60_e1	0.22
17	01_BC-C_e1	0.24

Profile 2

19	02_LFH_e1	3.47
20	02_4-6_e1	0.73
21	02_6-8_e1	0.57
22	02_10-12 Bm1_e1	0.34
23	02_10-12 charcoal_e1	0.57
24	02_10-12 charcoal_e1_DUP	0.54
25	02_12-14_e1	0.49
26	02_12-14_e1_DUP	0.47
27	blank	-0.90
28	standard	11.78
29	02_14-16_e1	0.49
30	02_17-19_e1	0.48
31	02_19-21_e1	0.43
32	02_21-23_e1	0.47
33	02_23-27_e1	0.45
34	02_30-40_e1	0.35
35	02_40-50_e1	0.34
36	02_BC_e1	0.22
37	02_IIC_e1	0.35

Profile 3

38	03_LFH_e1	2.38
39	03_LFH_e1_DUP	2.59
40	blank	-0.90
41	standard	11.37
42	03_9-11_e1	0.61
43	03_13-15_e1	0.54
44	03_15-17_e1	0.65
45	03_17-19_e1	0.47
46	03_19-21_e1	0.45
47	03_21-23_e1	0.47
48	03_11-13_e1	0.65
49	03_25-27_e1	0.46
50	03_27-29_e1	0.44
51	03_27-29_e1_DUP	0.40
52	03_27-29_e1_DUP	0.40
53	blank	-0.90
54	standard	11.38
55	03_BC_e1	0.41
56	03_IIC_e1	0.36
57	03_60-94_e1	0.29

Profile 4

58	04_LFH_e1	2.89
59	04_6-8_e1	0.32
60	04_8-10_e1	0.43
61	04_10-12_e1	0.48
62	04_12-15_e1	0.36
63	04_12-15_e1_DUP	0.41
65	blank	0.10
66	standard	11.38
67	04_15-17_e1	0.28
68	04_17-19_e1	0.25
69	04_19-21_e1	0.29
70	04_19-21_e1_DUP	0.32
71	04_21-23_e1	0.32
72	04_21-23_e1_DUP	0.31
73	04_26-28_e1	0.24
74	04_28-30_e1	0.23
75	04_30-32_e1	0.25
76	04_30-32_e1	0.23
77	blank	-0.90
78	standard	11.19
4	04_32-42_e1	0.31
5	04_42-52_e1	0.19

6	04_4Bm52-60_e1	0.29
7	04_4Bm_e1	0.17
8	04_4Bm_e1_DUP	0.25
9	04_4C_e1	0.26

Profile 5

10	05_LFH	4.96
11	05_8-10	1.52
12	05_10-12	0.96
13	05_10-12	0.87
14	blank	-0.90
15	standard	11.27
16	05_15-17	0.58
17	05_17-19	0.72
18	05_19-21	0.58
19	05_21-23	0.36
20	05_23-25	0.44
21	05_25-27	0.37
22	05_30-40	0.46
23	05_40-50	0.23
24	05_50-60	0.22
25	05_C	0.26
26	05_C	0.33
27	blank	-0.90
28	standard	11.52

Appendix J. Total organic carbon (TOC) measured in mg kg^{-1} analysis on Na-Citrate – Dithionite extract solutions for all profiles. Sample duplicates are indicated by "DUP" at the end of each sample ID, standards (~ 10 ppm organic C solution) and blanks (Milli-Q water) were also run approximately every 10 samples.

Na-Citrate Dithionite TOC (mg kg^{-1})

Extraction ID	Sample Number	TOC mg kg^{-1}
	Profile 1	
Blank		-0.90
Standard		11.49
44	01_LFH	4462
29	01_13-15	1844
30	01_15-17	1701
32	01_17-19	37.88
33	01_19-21	4666
34	01_21-23	2014
35	01_23-25	2177
37	01_25-27	2197
38	01_30-40	2313
39	01_40-50	3866
Blank		1.02
Standard		12.08

42	01_50-60	2164
43	01_BC-C	2146

Profile 2

45	02_LFH	2159
46	02_4-6	4052
47	02_6-8	2397
48	02_10-12 Bm1	5998
49	02_10-12 charcoal	2986
52	02_12-14	4882
Blank		1.42
Standard		11.53
55	02_14-16	2422
56	02_17-19	1208
57	02_19-21	6397
58	02_21-23	7018
59	02_23-27	5007
60	02_30-40	2238
61	02_40-50	2482
62	02_BC	2132
63	02_IIC	2198
64	02_IIC_DUP	2187
Blank		0.41
Standard		11.23

Profile 3

67	03_9-11	3700
73	03_11-13	6887
68	03_13-15	2395
69	03_15-17	2446
70	03_17-19	2626
71	03_19-21	2347
72	03_21-23	2251
74	03_25-27	4326
75	03_27-29	2630
Blank		0.75
Standard		11.40
3	03_27-29_DUP	2669
4	03_BC	2300
5	03_IIC	2538
6	03_60-94	2962

Profile 4

7	04_LFH	5026
8	04_6-8	2468
9	04_8-10	2316
10	04_10-12	2315
11	04_12-15	2432
12	04_12-15_DUP	2002
Blank		0.42
Standard		11.42
16	04_15-17	2168
17	04_17-19	2388
18	04_19-21	2131
19	04_19-21_DUP	2350
20	04_21-23	2265
21	04_21-23_DUP	2304
22	04_26-28	2576
23	04_28-30	1905
24	04_30-32	2331
25	04_32-42	2423
Blank		0.24
Standard		11.51
29	04_42-52	2730
30	04_4Bm52-60	2227

31	04_4Bm	2562
32	04_4Bm_DUP	2519
33	04_4C	1931

Profile 5

34	05_LFH	4858
35	05_8-10	1552
36	05_10-12	2273
37	05_15-17	1937
38	05_17-19	2474
42	05_19-21	2169
43	05_21-23	2173
44	05_23-25	2213
45	05_25-27	2243
46	05_30-40	2257
47	05_40-50	2457
48	05_50-60	2508
49	05_C	2353